
The University Of Sheffield.

# Zebrafish as model for human ciliopathies

by

Eleni Leventea

A thesis submitted in partial fulfillment of the requirements for the Doctor of Philosophy Degree in Biomedical Science of the University of Sheffield

September 2016

**Acknowledgements**

First I would like to thank my supervisor; Dr. Jarema Malicki for his guidance throughout my postgraduate research. I would also like to express my sincere gratitude to my advisors, Dr. Freek van Eeden and Prof. David Strutt for their support and valuable advice.

Thanks to all the Malicki lab members, it has been a pleasure working with you!

Lastly, I would like to thank the Aquarium staff for their assistance with zebrafish maintenance and Chris Hill for the SEM and microtome training.

# ABSTRACT

Ciliopathies are a family of rare pleiotropic disorders associated with cilia defects. They display a wide variability of phenotypes but are also characterized by common manifestations. A typical example includes mutations in the *CEP290* gene, which result in a widely variable severity of phenotypes ranging from retina disorders (e.g. Leber Congenital Amaurosis) to perinatal lethality (Meckel Gruber Syndrome). Aiming to characterise a wide spectrum of human ciliopathy phenotypes using the zebrafish model, we studied mutant alleles for *bbs2* and *bbs9*, *cep290*, *alms1*, *rab23* and *tubby*. In the course of this work, we sought to characterise the relevance of zebrafish mutant phenotypes to human manifestations of ciliopathy syndromes. Both *bbs* genes analysed exhibit skeletal morphogenesis defects during early juvenile stages, while only *bbs9* but not *bbs2* homozygous mutants are characterised by retinal degeneration. *Cep290* homozygous mutants do not display obvious external defects, they are however characterised by high frequency of ectopic otoliths during larval stages, and hyperactivity both during larval and adult developmental stages. This behavioural defect led us to the observation of planar cell polarity and otolith crystal structural defects in one of the three ear chambers. Proteomic analysis additionally revealed differences between the protein content of *cep290*$^{-/-}$ mutant and non-mutant sibling otoliths, suggesting that Cep290 has a role in otolith biomineralisation. *Alms1*$^{-/-}$ mutants exhibit curly body axis, ciliogenesis defects and opsin mislocalization. Homozygous mutants are also characterised by cardiac defects. Lastly, *rab23*$^{-/-}$ mutants exhibit curly body axis, ciliogenesis and laterality defects while *tub*$^{-/-}$ are characterised by opsin trafficking defects in the retina. Collectively, this survey of zebrafish cilia mutants revealed new functions for genes involved in human ciliopathies. Zebrafish proved to be an excellent model to investigate these novel functions further.

# ABBREVIATIONS

| | |
|---|---|
| BBS | Bardet-Biedl Syndrome |
| GPCR | G Protein Coupled Receptor |
| SSTR3 | Somatostatin Receptor 3 |
| MCHR1 | Melanin Concentrating Receptor 1 |
| DR | Dopamine Receptor |
| 5-HTR | 5-Hydroxytryptamine receptor |
| CEP290 | Centrosomal Protein 290 |
| JBTS | Joubert Syndrome |
| MKS | Meckel Gruber Syndrome |
| IFT | Intraflagellar Transport |
| Kif | Kinesin family member |
| KV | Kuppfer's Vesicle |
| LCA | Leber's Congenital Amaurosis |
| NPHP | Nephronopthisis |
| WT | Wild type |
| PCP | Planar Cell Polarity |
| Hh | Hedgehog signaling |
| SEM | Scanning Electron Microscopy |
| ENU | N-Ethyl-N-Nitrosourea |
| PCNA | Proliferating Cell Nuclear Antigen |
| ALMS | Alstrom Syndrome |
| aa | Amino acids |
| AMOT | Angiomotin |
| Lats | Large Tumor Suppressor |
| Birc2 | Baculoviral IAP Repeat Containing 2 |
| Mst1 | Macrophage Stimulating 1 |

# TABLE OF CONTENTS

**INTRODUCTION** ..... **8**
**Ciliary Transport and Ciliary Compartments** ..... **8**
**Signalling through cilia** ..... **9**
Hedgehog pathway ..... 10
Wnt pathway ..... 11
Non-canonical Wnt - PCP pathway ..... 11
The Hippo pathway ..... 12
GPCR signalling ..... 12
**Ciliopathies** ..... **13**
Bardet-Biedl Syndrome ..... 15
Meckel-Gruber and Joubert Syndrome ..... 17
Alstrom Syndrome ..... 18
Carpenter Syndrome ..... 19
**Mouse ciliopathy models** ..... **20**
**The zebrafish model** ..... **22**
**Cilia in zebrafish organs** ..... **22**
Kupffer's Vesicle ..... 22
**Sensory Organs** ..... **24**
Photoreceptors ..... 24
Mechanosensory hair cells ..... 25
Olfactory sensory neurons ..... 27
Spinal Canal ..... 27

**Aims of This Study** ..... **30**

**ANALYSIS OF BBS MUTATIONS IN ZEBRAFISH** ..... **33**
**Introduction** ..... **33**
**Materials and Methods** ..... **35**
**Results** ..... **39**
**1.** *bbs* zebrafish mutants exhibit spinal cord deformities ..... 39
**2.** *bbs2* homozygous mutants exhibit pharyngeal jaw deformities ..... 40
**3.** Absence of early cartilage or bone defects in the *bbs2*$^{-/-}$ mutants at larval stages ..... 40
**4.** Absence of retinal degeneration in the *bbs2* mutants ..... 40
**5.** *bbs9*$^{-/-}$ mutants manifest severe opsin mislocalization while *bbs2*$^{-/-}$ mutants have increased proliferation in the outer nuclear layer of the retina ..... 41
**Discussion** ..... **42**
**Figures** ..... **45**

**ANALYSIS OF CEP290 FUNCTION IN ZEBRAFISH** ..... **53**
**Introduction** ..... **53**
**Materials and Methods** ..... **55**
**Results** ..... **57**
**1.** *cep290*$^{-/-}$ zebrafish mutants do not exhibit obvious external phenotypes ..... **57**
**2.** *cep290*$^{-/-}$ mutants do not display ciliogenesis defects ..... 57
**3**. *cep290*$^{-/-}$ mutants do not display retinal dystrophy ..... 58
**4.** *cep290*$^{-/-}$ mutants have abnormal number of otoliths at larval stages ..... 58
**5.** *cep290*$^{-/-}$ adult s are hyperactive and display inner ear polarity defects ..... 59
**Discussion** ..... **63**
**Figures** ..... **66**

**ANALYSIS OF ALMS1 IN THE ZEBRAFISH MODEL** ..... **75**
**Introduction** ..... **75**
**Materials and Methods** ..... **77**
**Results** ..... **78**

**1.** The *alms1* homozygous mutant zebrafish larvae display body plan defects .....78
**2.** The *alms1* homozygous mutants lack olfactory cilia .....79
**3.** *Alms1* homozygous mutants display retina defects .....79
**4.** Heart defects are observed in the *alms1* homozygous mutants .....80
**5.** Hippo pathway is misregulated in the heart of *alms1* mutants .....80
**Discussion** .....**81**
**Figures** .....**84**

**ANALYSIS OF THE RAB23 AND TUBBY FUNCTION DURING ZEBRAFISH DEVELOPMENT** .....**89**
**Introduction** .....**89**
**Materials and Methods** .....**91**
**Results** .....**92**
**1.** *rab23*$^{-/-}$ zebrafish mutants exhibit curly body axis and heart looping defects .....92
**2.** *rab23*$^{-/-}$ mutants lack olfactory cilia and are developmentally delayed .....93
**3.** The *tub* zebrafish mutant displays retinal defects .....94
**Discussion** .....**94**
**Figures** .....**96**

**Summary, Conclusions and Future Directions** .....**99**
**Summary** .....**99**
**Conclusions and discussion of novel findings** .....**99**
The *bbs2* and *bb9* zebrafish mutants .....99
The *cep290* zebrafish mutant .....100
The *alms1* and *rab23* zebrafish mutant .....100
**Future directions** .....**101**

**APPENDIX** .....**103**

**REFERENCES** .....**114**

# CHAPTER I

# INTRODUCTION

## Ciliary Transport and Ciliary Compartments

Cilia are microscopic microtubule-based projections on the surface of most vertebrate cells. The structure of the ciliary shaft, or the axoneme, is very well conserved among species. On cross sections, the vast majority of cilia in organisms ranging from unicellular algae to mammals, feature nine evenly spaced peripheral microtubule doublets. A central pair of microtubules is also found in most motile cilia. This is known as the "9 + 2" arrangement of microtubules. This central pair is missing in most immotile cilia, which feature the "9 + 0" arrangement of microtubules (Fisch & Dupuis-Williams, 2011; Fliegauf, Benzing, & Omran, 2007).

Steps required for the cilium to be assembled have been studied in detail. Initially, basal bodies form and migrate to the apical cell surface where they dock (W. F. Marshall, Vucica, & Rosenbaum, 2001). During this migration, basal bodies bind to cytoplasmic vesicles and fusion of these vesicles to the plasma membrane is the first step for the formation of the ciliary membrane compartment (Basten & Giles, 2013). The basal body nucleates the growth of axonemal microtubules, which give rise to the cilium axoneme. The distal region of the basal body is known as the transition zone. The transition zone functions as a specialised barrier that controls the import and export of proteins into and out of the ciliary compartment. In the transition zone, Y-shaped linkers connect microtubules to the ciliary membrane (Gilula & Satir, 1972). Biochemical and genetic analyses of transition zone proteins showed that they are organised into functionally distinct modules. Three main modules have been identified thus far: the MKS, NPHP and the CEP290 (Chih et al., 2012; Garcia-Gonzalo et al., 2011; Sang et al., 2011). Mutations in transition zone proteins result in ciliopathy phenotypes (Malicki & Avidor-Reiss, 2014).

Since protein synthesis does not occur in the cilium, cilium elongation requires selective transport of proteins by the Intraflagellar Transport (IFT) proteins. This transport is bidirectional and is mediated by two IFT complexes. It is additionally dependent on two groups of microtubule motors, known as kinesins and dyneins (Rosenbaum, 2002; Scholey, 2012).

In addition to IFT, BBS proteins are important regulators of ciliary trafficking. They form a complex known as the BBSome (Hsiao, Tuz, & Ferland, 2012; Su et al., 2014). Disruption of the BBSome in *C.elegans* affects cohesion between the two IFT complexes and results in retrograde transport defects. It has been additionally shown that BBSome assembles IFT complexes at the cilia base, binds to anterograde IFT trains and regulates IFT recycling (Sung & Leroux, 2013). The BBSome is also crucial for trafficking receptors into cilia including the somatostatin (SSTR3), melanin concentrated hormone (MCHR1) and serotonin receptors (HT6) (Berbari, Johnson, Lewis, Askwith, & Mykytyn, 2008).

Cilia are essential both for embryonic development and for proper physiological function of fully formed organs. They play a role in a multitude of signal transduction pathways that mediate processes as diverse as embryonic patterning, vision, olfaction, and metabolism (Goetz & Anderson, 2010; Louvi & Grove, 2011; Schou, Pedersen, & Christensen, 2015). While motile cilia propagate fluid flow and propel the movement of cells, such as sperm cells or unicellular algae, immotile cilia mediate the detection and/or transduction of extracellular signals in many biological processes ranging from photo transduction to Hedgehog signaling (Green & Mykytyn, 2010; Kennedy & Malicki, 2009; Kobayashi & Takeda, 2012).

In the embryo, cilia are involved in the determination of left-right symmetry, limb and neural tube morphogenesis, and the differentiation of sensory neurons, such as photoreceptors in the eye (Basu & Brueckner, 2008; Haycraft et al., 2005; Tissir & Goffinet, 2010; Tsujikawa & Malicki, 2004). In developmentally mature vertebrates, cilia mediate sperm cell motility, maintenance of kidney ducts, the clearing of debris from the respiratory tract, vision, olfaction, metabolism, and even perhaps some higher brain functions (Afzelius, 2004; Cardenas-Rodriguez & Badano, 2009; Guemez-Gamboa, Coufal, & Gleeson, 2014; Zimmerman & Yoder, 2015). As cilia widely contribute to biological processes that play a role in nearly all aspects of vertebrate biology, it is not surprising that they have attracted considerable attention.

## Signalling through cilia

Cilia are often characterised as the cell's antenna. This description reflects the fact that cilia mediate a wide variety of signalling events in the cell. Cilia are involved in signalling via multiple pathways, including Hedgehog, Wnt, PDGFR, mTOR, Notch, Hippo, TGFβ, as well as vision, olfaction and mechanosensation

related pathways (Singla & Reiter, 2006).

Hedgehog pathway

The best studied example of cilia function in signalling comes from the study of Hedgehog pathway. IFT proteins are required for processing GliAs (activators) and GliRs (repressors) (Goetz & Anderson, 2010; Huangfu & Anderson, 2005; H. L. May-Simera & M. W. Kelley, 2012). *IFT* mouse mutant embryos show loss of Hh signalling in the neural tube due to GliA defects while others are characterised by polydactyly at later stages due to loss of GliRs. Similarly, zebrafish lacking *ift88* display Hh related defects in the neural tube and the somites (Huang & Schier, 2009). Mutations in basal body-related proteins such as the oral-facial-digital-syndrome 1 (*OFD1*), *RPGRIP1L*, *MKS1* and *EVC* cause Hh related human ciliopathies (Delous et al., 2007; Ferrante et al., 2006; Vierkotten, Dildrop, Peters, Wang, & Ruther, 2007; Weatherbee, Niswander, & Anderson, 2009). Based on the genetic studies associating cilia with Hh it has been show that PTCH1 and SMO exhibit Hh dependent trafficking in cilia (Corbit et al., 2005; Rohatgi, Milenkovic, & Scott, 2007). In the presence of Hh, PTCH1 localises at the cilia base and in the absence of Hh, PTCH1 loses its cilia localisation while SMO enters cilia. Additionally, Gli transcription factors are enriched in cilia: both Gli2 and Gli3 localise at cilia tips (Haycraft et al., 2005). SUFU, a negative regulator of the Hh pathway also localises in cilia (Schematic 1) (Endoh-Yamagami et al., 2009; Haycraft et al., 2005). It becomes evident that that the cilium and Hh are tied together with the cilium functioning as a Hh dedicated organelle during early developmental stages.

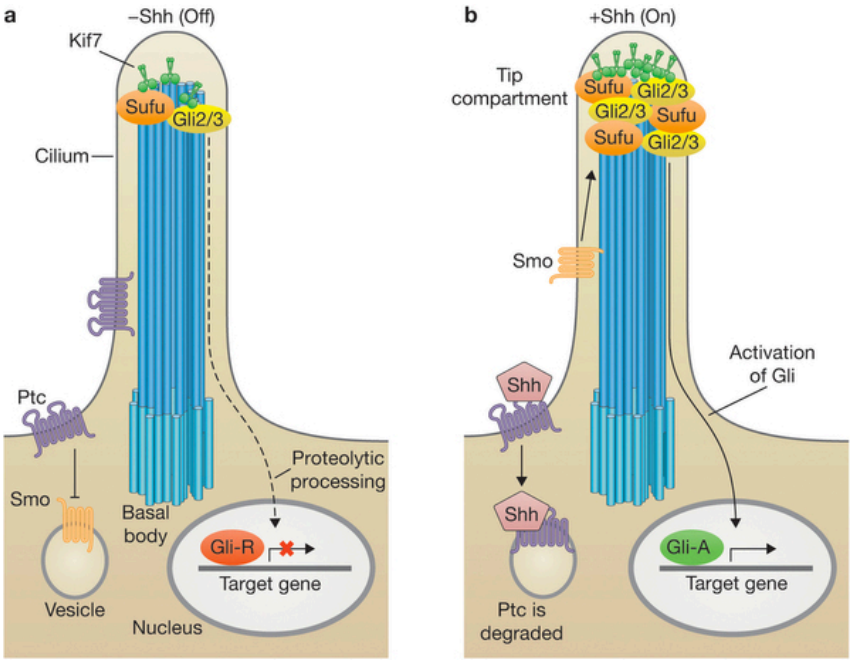

Schematic 1. Hedgehog signalling in cilia. **A**. In the absence of Shh, Ptc inhibits the Smo translocation into the cilium. In this case, Gli Repressors (GliRs) inhibit the transcriptional activation of Hedgehog targets. **B**. In the presence of the ligand, Smo is translocated into the cilium where it activates the Gli transcription factors (Gli2 and Gli3). Gli activators (GliAs) promote Hedgehog related transcriptional activation. The role of SuFu is unclear: it could act as a buffer mechanism for Gli or alternatively Hh signalling at cilia activates Gli proteins by relieving SuFu inhibition (after Pedersen & Akhmanova, 2014))

Wnt pathway

Another major pathway associated with cilia is the canonical Wnt pathway. Downregulation of *BBS1, BBS4, MKKS, KIF3A* as well as *Ift88* and *Ofd1* in mouse derived cells leads to nuclear accumulation of β-catenin and consequently increased transcriptional activity of the Wnt target genes (Corbit et al., 2008; Gerdes et al., 2007). Nuclear β-catenin is a common characteristic of renal cysts, a cilia-related phenotype. Cilia defects promote Wnt hyper-responsiveness in vertebrates (Corbit et al., 2008). In contrast to this finding, it has been shown that *Ift* mouse mutants have no detectable misregulation of the canonical Wnt pathway (Ocbina, Tuson, & Anderson, 2009). It is thus obvious that the exact role of cilia in Wnt signalling is not clearly established. Overall, the cilia/ β-catenin signalling defects are less severe compared to those caused by ciliary Hh defects (Wallingford & Mitchell, 2011).

Non-canonical Wnt - PCP pathway

PCP (Planar Cell Polarity) genes have been shown to influence cilia orientation (T. J. Park, Mitchell, Abitua, Kintner, & Wallingford, 2008). They were shown to affect the position of kinocilia in the cochlea, directional cilia beating of the brain ependymal cells and the kidney. It is known that several cilia genes interact with the PCP locus, Vangl2, mutations in which result in cochlear stereocilia misorientation and convergent extension defects (Wallingford & Mitchell, 2011).

The inner ear provides one the best examples of the relationship between cilia and PCP. Each hair cell in the ear sensory epithelium has on its apical surface a bundle of specialized protrusions. These bundles are composed of stereocilia and a single kinocilium, a specialised primary cilium that defines hair cell PCP within the tissue. There are many examples highlighting the connection between PCP and cilia. Mutations in *ift88*, which is critical for kinocilium but not stereocilia formation, results in a disorganisation of PCP orientation of the

stereocilia and inhibits formation of the kinocilia (Jones et al., 2008). Similarly, mouse mutants of ciliary genes, *BBS4* and *BBS6,* display hair bundle orientation defects, which were sometimes accompanied by misorientation of the kinocilium itself (Ross et al., 2005). Additionally, *ALMS1* mutations, which are associated with hearing loss, have also been associated with stereociliary bundle defects. The kinocilium is mislocalised in the *Alms1*$^{-/-}$ mutant cochlea (Jagger et al., 2011). Lastly, morpholino knockdown of PCP effectors *Inturned* and *Fuzzy* causes ciliogenesis defects, showing that PCP and cilia are closely related (Zilber et al., 2013). It is clear that there is a connection between cilia and PCP, however the exact interplay between the cilium and this pathway remains unclear.

The Hippo pathway

The Hippo pathway is not classically associated with ciliary function or ciliopathies, however, recent studies have hinted at a relationship between the Hippo signalling and ciliary components. Firstly, knockdown of the ciliary transition zone protein *NPHP4* phenocopies loss of TAZ function, a Hippo pathway component and NPHP4 interacts with Lats1, a kinase involved in the Hippo pathway (Habbig et al., 2011). Secondly, the transmembrane protein Crumbs3, involved in the regulation of the Hippo pathway, is localised to the cilium (Olsen et al., 2007; Robinson, Huang, Hong, & Moberg, 2010). Thirdly, mislocalisation of Hippo pathway components YAP and TAZ have been identified in ciliopathy, polycystic kidney disease patients (Happe et al., 2011). Despite these findings, the molecular basis of contribution of the Hippo pathway to ciliopathy phenotypes is still not clear.

GPCR signalling

In many cell types, signalling by primary cilia involves G Protein Coupled Receptors (GPCRs). GPCRs constitute a highly diverse family of seven transmembrane receptors that transmit signals from the extracellular environment to the cell through both G-protein dependent and independent pathways. GPCRs enable cells to respond to sensory stimuli including light, nucleotides, hormones, neurotransmitters, and odorants. The ciliary GPCRs identified thus far belong to 3 classes: A (rhodopsin like receptors), B (secretin receptors) and F (Frizzled/ Smoothened receptors) (Schou et al., 2015).

The BBSome as well as *Tubby* genes are crucial for trafficking GPCRs into cilia. It has been shown that Tubby as well as BBS protein defects lead to aberrant ciliary localisation of melanin concentrating hormone 1 (MCHR1) and somatostatin receptor (SSTR3) (Berbari, Lewis, Bishop, Askwith, & Mykytyn,

2008; X. Sun et al., 2012). Most of the neurons in the brain possess a primary cilium, however, only a subset displays MCHR1 in the ciliary membrane (Handel et al., 1999). MCHR1 is concentrated in neuronal cilia within the mouse hypothalamus and it has been suggested to regulate energy homeostasis (Antal-Zimanyi & Khawaja, 2009). In *BBS2*$^{-/-}$ and *BBS4*$^{-/-}$ mice, these neuronal cilia fail to accumulate SSTR3 or MCHR1. Similarly, mutations in the *Tubby* family of proteins also cause failure of SSTR3 and MCHR1 transport to cilia. There is thus a clear link between GPCR targeting to cilia and energy homeostasis since these receptors participate in the neuronal regulation of food consumption (Hervieu, 2003).

A variety of GPCRs have been associated with ciliary functions. Examples include dopamine as well as neuropeptide Y receptors, which were found to localise to primary cilia in different cell types (Loktev et al., 2008). Another GPCR class comprising of the SMO (Smoothened) and FZD (Frizzled) receptors also localises to cilia. FZD is a receptor for the WNT5A ligand but the functional coupling between this receptor and cilia is elusive, in contrast to the well-described ciliary function of SMO. Another well characterised GPCR is the light sensitive rhodopsin, which localises in the photoreceptor outer segments and absorbs photons to activate transducin, causing hyperpolarisation of cells (Schou et al., 2015). Furthermore, constitutively active rhodopsin is causing a variety of inherited disorders including the ciliopathy LCA (P. S. Park, 2014). Lastly, olfactory transduction, which is widely dependent on ciliated neurons is also regulated through class A GPCRs (Mombaerts, 1999). In conclusion, GPCRs traffic into the ciliary compartment and are associated with a spectrum of cilia mediated processes including metabolism, development and sensory functions.

## Ciliopathies

Mutations in ciliary genes cause rare genetic disorders known as ciliopathies. More than a dozen disorders are now included within the ciliopathy spectrum. The classic ciliopathies are: Bardet-Biedl Syndrome (BBS), Joubert Syndrome (JBTS), Meckel Gruber Syndrome (MKS), Alstrom Syndrome (Alms), Nephronopthisis (NPHP), Leber Congenital Amaurosis (LCA), and Polycystic Kidney Disease (PKD). These disorders manifest phenotypic defects in almost every major organ including the kidney, brain, retina, ear, and lungs, highlighting not only the diversity of symptoms but the also the importance of cilia in development and homeostasis.

Common phenotypes are shared between the ciliopathies (Schematic 2), suggesting pleiotropic phenotypic effects emerging from mutations in cilia genes. Although certain mutations in ciliary genes are associated with a single ciliopathy, many examples exist showing the involvement of mutations of a single ciliary gene in multiple disorders (Schematic 3). The most characteristic example includes mutations in *CEP290. Cep290* mutations are reported in MKS, JBTS, BBS, NPHP and LCA, causing a wide range of phenotypes and of variable severity ranging from retinal defects to embryonic lethality. Over 100 unique *CEP290* mutations have been identified including truncation, missense and splicing mutations. The association between the genotype and the phenotypic outcome has not been established; studies however suggest the contribution of modifier alleles (Leitch et al., 2008). In contrast to this hypothesis, it has been recently shown that the phenotypic outcome of *CEP290* mutations could be predicted based on an exon skipping model that predicts the amount of protein produced after certain mutations (Drivas, Wojno, Tucker, Stone, & Bennett, 2015). In a similar pattern to CEP290, 80 mutations have been identified for the transition zone protein TMEM67, mutations in which have been involved in MKS and some form of JBTS with liver fibrosis. Significant missense mutations are associated with the TMEM67 exons 8-15, a region with currently unknown function (Iannicelli et al., 2010).

On the other hand, mutations of cilia genes associated with the manifestation of only one syndrome do also exist. An example involves mutations in *ALMS1* which are only associated with the manifestation of ALMS. Most pathogenic variants are truncating mutations (J. D. Marshall et al., 2015). Furthermore, *ARL13B* mutations are restricted to patients with JBTS, although it is not clear if the gene is only associated with a restricted phenotypic range or not all mutations have been identified (Novarino, Akizu, & Gleeson, 2011).

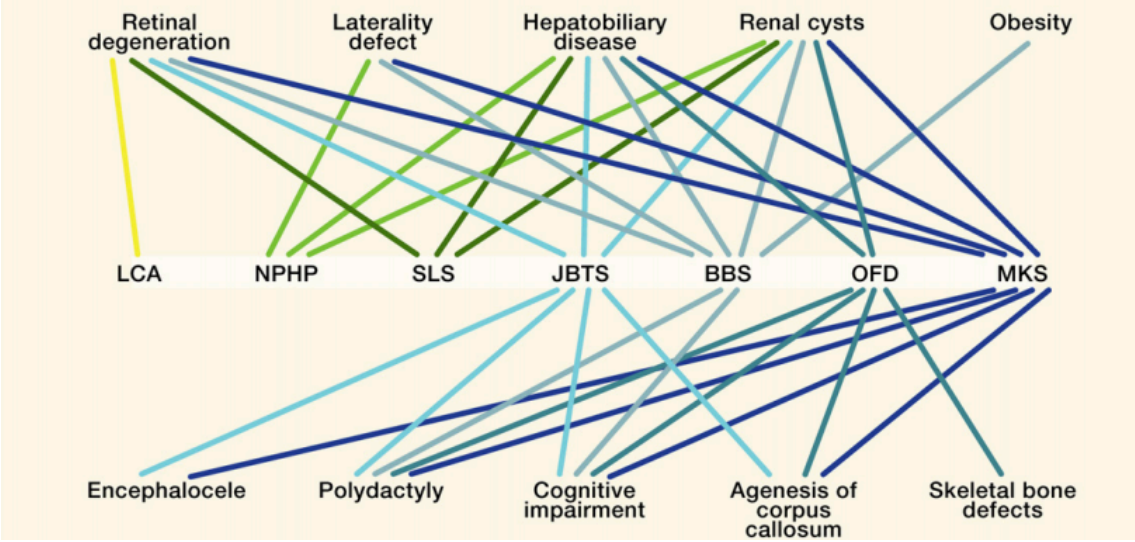

Schematic 2. Summary of ciliopathies and associated phenotypes. LCA: Leber Congenital Amaurosis, NPHP: Nephronopthisis, SLS: Senior Loken Syndrome, JBTS: Joubert Syndrome, BBS: Bardet-Biedl Syndrome, OFD: Orofacial Digital Syndrome, MKS: Meckel Gruber Syndrome (after Novarino et al., 2014)

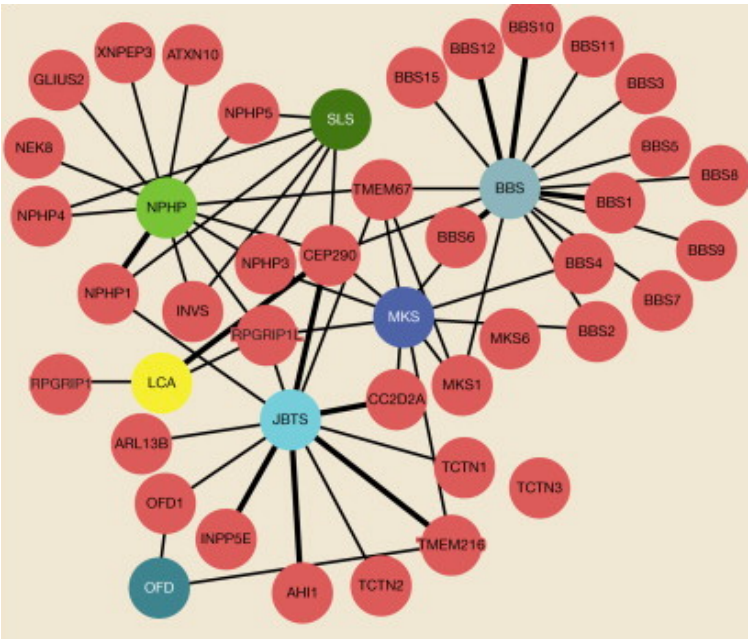


Schematic 3. Interactome diversity of ciliopathies. Major ciliopathies and genes mutated in each condition. Some Transition Zone proteins are found mutated in BBS patients (e.g. CEP290, NPHP4) but also BBS proteins are implicated in other ciliopathies (e.g. BBS6 is implicated in the manifestation of MKS). (After Novarino et al., 2014)

## Bardet-Biedl Syndrome

BBS is a rare autosomal recessive disease characterised by several phenotypes including rod-cone dystrophy, obesity, polydactyly, kidney cysts, and mental retardation. Genetic studies on human BBS patients have identified 21 causative genes. The frequency of mutations in different *BBS* genes is not equal among human patients (Schematic 3). These genes are named BBS1-21 and their functions remain largely unknown (Heon et al., 2016). The syndrome's prevalence is 1:140,000-1:160,000 for North American and European populations (M'Hamdi et al., 2014) while populations with a higher BBS frequency exist in Kuwait and Newfoundland with a prevalence of 1:17,000-1:18,000 (Farag & Teebi, 1989; Moore et al., 2005). In European and Caucasian populations the most commonly mutated genes are *BBS1* and

*BBS10* (Janssen et al., 2011). In the Tunisian population mutations have been frequently found in *BBS1*, *BBS2* and *BBS8* (M'Hamdi et al., 2014) while *BBS1*, *BBS3* and *BBS4* are frequently mutated in Saudi Arabia (Abu Safieh et al., 2010). The syndrome is diagnosed when at least four symptoms present (Table 1). Severe retinal degeneration defects occur before the second decade of life and either cones or rods could be initially affected, followed by defects in the second photoreceptor type. Obesity occurs with a frequency of 72-92% in the syndrome. It begins during early childhood and some of the patients develop type 2 diabetes. Interestingly, mouse models of the syndrome exhibit leptin resistance and it has been additionally shown that BBS protein silencing leads to impaired trafficking of the leptin receptor (Guo et al., 2016). Major cause of mortality among the BBS patients is renal failure (Mihai, Marshall, & Stoicescu, 2011). Most BBS patients have urinary concentrating defects with normal kidney function and no major cysts (Putoux, Attie-Bitach, Martinovic, & Gubler, 2012).

| Clinical feature | Frequency |
|---|---|
| **Major** | |
| Rod-cone dystrophy | 90-100 |
| Obesity | 72-92 |
| Polydactyly | 63-81 |
| Genital anomalies | 59-98 |
| Learning difficulties | 50-61 |
| Renal anomalies | 20-53 |
| | |
| **Minor** | |
| Speech delay | 54-81 |
| Developmental delay | 50-91 |
| Diabetes mellitus | 6-48 |
| Dental anomalies | 51 |
| Congenital Heart Disease | 7 |
| Brachydactyly/syndactyly | 46-100 |
| Ataxia | 40-86 |
| Cardiopathy | 10 |
| Deafness | 11-12 |
| Anosmia | 60 |

Table 1. Major and minor clinical features for the diagnosis of BBS in human patients (after Beales, Elcioglu, Woolf, Parker, & Flinter, 1999).

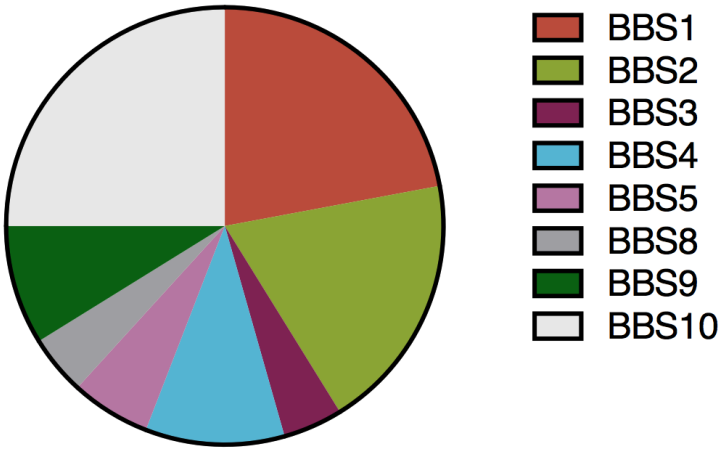


Schematic 3. Frequency of mutations encountered in BBS patients. Only the BBSome components are included (after Khan et al., 2016).

Meckel-Gruber and Joubert Syndrome

MKS is a lethal autosomal recessive disorder, which has been mapped to 13 different loci. The most common phenotypes is the occipital encephalocele, a sac-like protrusion of the brain; large polycystic kidneys; and postaxial polydactyly (Table 2). Lethality can occur *in utero* or within days after birth with pulmonary hypoplasia being the leading cause of death (Alam, Adhi, Bano, Zubair, & Mushtaq, 2013). Diagnosis of the syndrome can be achieved as early as 10 weeks of gestation. The incidence of MKS is 1:13,250-1:140,000. Finnish population has higher incidence of the syndrome with a prevalence of 1:9,000, Belgians and Bedouins in Kuwait have a prevalence of 1:3,500 while the highest incidence is among Gujarati Indians with a 1:300 frequency (Parelkar et al., 2013; Shetty, Alva, Patil, & Shetty, 2012). The genetic heterogeneity of MKS is not fully captured as a study showed that only half of the cases can be traced to a mutation in any of the known genes (Hopp et al., 2011).

| Clinical feature | Frequency |
|---|---|
| Cystic kidneys | 97.7 |
| Polydactyly | 87.3 |
| Encephalocels | 83.8 |
| Fibrotic liver | 65.5 |
| Orofacial clefts | 31.8 |

Table 2. Clinical features of MKS and the frequency of their appearance in human patients (after Barisic et al., 2015).

JBTS is an autosomal recessive and occasionally X-linked related syndrome with the obligatory characteristic of the molar tooth sign, a midbrain-hindbrain malformation. Diagnostic criteria include hypotonia, ataxia, developmental delay, intellectual disability, abnormal eye movements, retinal dystrophy, mephronopthisis, hepatic fibrosis and polydactyly (Table 3). Additionally, mild to severe scoliosis may present. The incidence prevalence ranges from 1:80,000-1:100,000 (Brancati et al., 2008). 24 genes have been identified to be associated with the syndrome. CEP290 mutations are responsible for 50% of the JBTS subgroup of ciliopathies (Szymanska, Hartill, & Johnson, 2014; Waters & Beales, 2011).

| **Clinical feature** |
|---|
| **Major** |
| Molar tooth sign |
| Hypotonia |
| Developmental delay |
| |
| **Minor** |
| Abnormal breathing pattern |
| Abnormal eye movements |

Table 3. Clinical features of JBTS in human patients (after Brancati, Dallapiccola, & Valente, 2010).

Alstrom Syndrome

ALMS is a rare monogenic recessive disorder characterized by pleiotropic clinical manifestations beginning at the first year of life. Retinal degeneration is noticed in infancy and hearing loss presents within the first decade of life (Bahmad Jr et al., 2014). ALMS patients also exhibit obesity, with type 2 diabetes and other metabolic defects developing during childhood. Dilated cardiomyopathy can occur in infancy. Additionally, children with ALMS have respiratory defects and renal failure can develop in late adolescence and childhood (Izzi et al., 2011). Most pathogenic variants of *ALMS1* are truncating frameshift or nonsense mutations resulting in early termination of the protein. There are now 239 identified disease-causing mutations in *ALMS1* (J. D.

Marshall et al., 2015). Phenotypic variation exists even within siblings or unrelated families with the same mutation. This suggests that besides the mutation variability, other factors can modify the phenotypic outcome, including genetic modifiers, environmental exposure and other stochastic events.

| Clinical feature |
|---|
| **Major** |
| vision (nystagmus, photophobia, rod-cone dystrophy) |
| **Minor** |
| obesity |
| dilated cardiomyopathy |
| hearing loss |
| hepatic dysfunction |
| renal failure |
| advanced bone age |
| short stature |
| hypogonadism |

Table 4. Clinical features of ALMS in human patients (after J. D. Marshall, Maffei, Collin, & Naggert, 2011)

Carpenter Syndrome

Carpenter Syndrome is an autosomal recessive disorder characterized by craniosynostosis, preaxial polydactyly of the feet, soft tissue syndactyly, short or absent phalanges of hands and feet, clinodactyly, short stature, obesity, congenital heart disease and mental retardation (Cohen, 2008). Mutations have been identified in *RAB23,* a member of the RAB guanosine triphosphatase and *MEGF,* a gene with unknown function.

| Clinical feature | Frequency |
|---|---|
| Craniosynostosis | 100 |
| Postaxial polydactyly | 53 |
| Cutaneous syndactyly | 94 |
| Syndactyly | 100 |
| Obesity | 90 |
| Learning disability | 46 |

Table 5. Clinical features and their frequency in Carpenter Syndrome patients (after D. Jenkins et al., 2007)).

## Mouse ciliopathy models

Given the limitations of studying human patients, mouse research has proved to be invaluable to understand the role of cilia in disease. Mouse model is a term often used to describe genetic variants generated in the mouse even if the model does not fully recapitulate human phenotypes. These models include mice with spontaneous or chemically generated mutations or alternatively carrying genetically engineered alleles. Conditional mutations are also a useful tool to study mutants in a spatiotemporal manner. An example of how modelling a mutation can give insight into functions of the genes derives from mutants lacking *Kif3a* or *Kif3b,* the kinesin 2 family motors. These mice lack nodal cilia and die by mid-gestation (Marszalek, Ruiz-Lozano, Roberts, Chien, & Goldstein, 1999; Nonaka et al., 1998). It soon became evident that lethality was caused from a requirement for IFT in Hh signalling (Huangfu et al., 2003).

In an effort to model JBTS in the mouse system, two mouse mutants for *Cep290* have been characterised. The first is a naturally occurring allele known as *rd16* (Chang et al., 2006) while the second is a null *Cep290* allele (Lancaster et al., 2011). Both of these mouse models exhibit early onset retinal degeneration, however only the null allele is characterised by anosmia and cerebellar hypoplasia. If all aspects of JBTS can be modelled in mouse is difficult to assess, as the molar tooth sign might be specific to human patients (Norris & Grimes, 2012).

Multiple mouse models for BBS do also exist. *Bbs1* mutant alleles have been analysed and for one of the alleles almost half of the homozygotes die *in utero*. From those surviving, 10% are obese and 30% exhibit retinal degeneration by 10 weeks of age. However, no polydactyly, renal, liver or laterality defects were observed (Kulaga et al., 2004). For the second allele in attempt to model a commonly encountered *BBS1* mutation, retinal degeneration, male infertility and obesity were reported (Davis et al., 2007). A *Bbs2* mutant allele was also generated with the homozygous adults being viable but exhibiting retinal degeneration and obesity. Cystic kidneys were also evident as well as male infertility. It was also reported that olfaction was defective (Nishimura et al., 2004). Additionally, *Bbs10*$^{-/-}$ mice display obesity, retinal degeneration, renal abnormalities and increased diuresis (Cognard et al., 2015). No mouse model for *Bbs9* mutations exists. In conclusion, BBS models in mice seem to recapitulate most of the clinical features of the human patients and can

definitely recapitulate the metabolic defects of the disorder. Absence of polydactyly has been observed in all generated mutant strains.

Three *Alms* mouse mutants have been also described. The *Foz* allele is a naturally occurring allele with impaired hearing, obesity, type 2 diabetes, dilated renal tubules and sterility (Arsov et al., 2006). The second described allele derives from ENU mutagenesis, is a weaker allele but causes renal cilia loss and obesity along with rhodopsin transport defects (G. Li et al., 2007). The third described allele is gene trap derived, exhibiting progressive photoreceptor degeneration, obesity, hypogonadism and enlarged kidneys (Collin et al., 2005). This specific allele was shown to have increased cardiomyocyte proliferation with increased heart to body ratio (Shenje et al., 2014). Overall, *Alms1* mutant mouse models seem to recapitulate the human phenotypes to a high degree.

For the Carpenter Syndrome one ENU induced mouse model exists with two alleles reported, known as the *opb* (open brain*)* model with mutations in *Rab23*. Homozygous mutants die during the second half of gestation with open neural tube in the head and spinal cord, abnormal somites and not fully developed eyes (Eggenschwiler, Espinoza, & Anderson, 2001; Gunther, Struwe, Aguzzi, & Schughart, 1994). In summary, the Carpenter Syndrome is a not extensively characterised ciliopathy and the mouse model fails to recapitulate the most prominent phenotype of the disease, the craniosynostosis. It is furthermore surprising that although human Carpenter syndrome patients are viable, the mouse homozygous mutants are lethal.

In conclusion, mouse mutants of cilia disorder related disease can recapitulate the human phenotypes to a certain extent. The BBS model can recapitulate the metabolic defects found in the BBS patients; the ALMS model can also recapitulate most of the disease phenotypes. A problem occurring with mouse knockouts is that they are lethal while the human ciliopathy patients exhibit a range of severity that cannot be modelled in a knockout mutant. A way to overcome this issue is the generation of hypomorphic alleles or conditional mutants in order to study gene specific functions during a specific developmental stage and at certain tissues.

The following sections regarding the zebrafish model and cilia in zebrafish organs is adapted from (Leventea, Hazime, Zhao, & Malicki, 2016).

## The zebrafish model

Zebrafish have several advantages compared to other vertebrate animal models including: 1) a short generation time, 2) small size 3) transparency that allows observation and manipulation from the earliest developmental stages 4) high fecundity, which allows one to generate large numbers of offspring, giving the opportunity to perform parallel experiments in sibling animals.

The zebrafish is thus an excellent vertebrate model for genetic analysis and imaging of cilia related processes. It is easy to examine the morphology and movement of cilia during development in zebrafish (Kishi, Slack, Uchiyama, & Zhdanova, 2009; Kramer-Zucker et al., 2005; Zhao & Malicki, 2007). Another important feature of the zebrafish model is that cilia mutants usually manifest a curly-body axis, a phenotype that is very easy to detect during genetic screens (Z. Sun et al., 2004; Tsujikawa & Malicki, 2004). Consequently, a rich collection of zebrafish ciliary mutants is available (Becker-Heck et al., 2011; Brand et al., 1996; Cao, Park, & Sun, 2010; Malicki et al., 1996).

Although historically forward genetic strategies have been the strength of the zebrafish model, recent advances in targeted mutagenesis, using TALEN and CRISPR/Cas9 nuclease systems make zebrafish reverse genetics equally attractive. Although in general less reliable, fast and inexpensive antisense knockdown approaches have been also used in zebrafish for a number of years (Eisen & Smith, 2008; Nasevicius & Ekker, 2000). These approaches are valuable as tools to study the genetic bases of cilia function in a living embryo. They also make it straightforward to generate zebrafish models of human disorders (Mitchison et al., 2012; Panizzi et al., 2012).

### Cilia in zebrafish organs

Below there is a description of the developmental timing of cilia differentiation, morphology and distribution in several zebrafish organs, including the Kupffer's vesicle (KV), the spinal canal, the eye, the ear and the olfactory pit (Schematic 4).

Kupffer's Vesicle

KV, a mouse node analogue, is a cyst-like structure with the average diameter of ca. 65 µm that appears in the tail bud of the zebrafish embryo around 12 hours post fertilization (hpf) (Matsui, Ishikawa, & Bessho, 2015; May-Simera et al., 2010). The inner surface of the KV is ciliated. The highest concentration

of cilia in the KV is found in the anterior region of its dorsal surface (Kreiling, Prabhat, Williams, & Creton, 2007; Oteiza et al., 2010). Both motile and immotile cilia are found in the KV. Motile cilia are responsible for the circular fluid movement inside the vesicle (Essner, Amack, Nyholm, Harris, & Yost, 2005; Yuan, Zhao, Brueckner, & Sun, 2015). Cilia motility in the KV mediates the initial symmetry-breaking process in the embryo and eventually determines organ laterality (Borovina, Superina, Voskas, & Ciruna, 2010; Kreiling et al., 2007). Calcium oscillations in motile cilia have been thought to be associated with this process. They are significantly more frequent on the left side of the KV and their onset coincides with the appearance of cilia motility providing evidence that fluid flow induces their appearance (Yuan et al., 2015). Recent evidence shows, however, that calcium waves do not occur in cilia (Delling et al., 2016). The KV is the earliest ciliated structure described in the zebrafish embryo so far. It can be easily imaged at 4 to 8 somite stage (11-13 hpf at 28.5$^0$C).

Defects in KV cilia lead to abnormal left-right asymmetry, which first manifests itself as cardiac abnormalities. At 24 hpf, as the heart tube begins to form, the future atrial end of the heart moves to the left side. This process is referred to as cardiac jogging (Chen et al., 2001; Khodiyar, Howe, Talmud, Breckenridge, & Lovering, 2013). Leftward position of the linear heart tube ("jogging") is the first known morphological feature of zebrafish embryogenesis that can be used to evaluate LR asymmetry. Later on, another heart phenotype, cardiac looping is a good laterality indicator. Looping refers to the bending of the heart ventricle to the right, which occurs by 36 hpf and persists until at least 72 hpf. In wild-type zebrafish, the leftward jogging precedes the rightward looping (Chen et al., 1997).

Cardiac asymmetry defects are common in mutants and morphants of zebrafish cilia genes (Jaffe et al., 2016). This manifests itself by the randomization of heart jogging and looping so that some embryos do not display any looping or loop their hearts in the wrong direction. The frequencies of these phenotypes vary. One also has to keep in mind that LR asymmetry defects occur with the frequency of low single digit percentages also in wild-type strains (Becker-Heck et al., 2011; Mitchison et al., 2012). In addition to the heart, other organs are affected by left-right asymmetry defects, including liver, the gut and the pancreas (Chen et al., 2001). Finally, central nervous system structures have been found to develop asymmetrically. An example is the diencephalic habenula in the larval zebrafish brain (Aizawa, Goto, Sato, &

Okamoto, 2007). These brain structures can also be used as asymmetry indicators (Doll, Burkart, Hope, Halpern, & Gamse, 2011).

## Sensory Organs

Vertebrate sensory neurons frequently display epithelial characteristics and their apical surface contains sensory apparatus that frequently includes cilia (Falk, Losl, Schroder, & Giessl, 2015). Vertebrate photoreceptors, olfactory sensory neurons, and mechanosensory hair cells all feature prominent apical cilia. The zebrafish is no exception.

Photoreceptors

Similar to the mammalian eye, the zebrafish retina consists of seven major cell classes arranged in distinct layers (Malicki, Pooranachandran, Nikolaev, Fang, & Avanesov, 2016). Zebrafish photoreceptors form the outermost layer of the retina and display similar morphological characteristics to these in mouse and human eyes (Kennedy & Malicki, 2009). Cilia of vertebrate photoreceptors are among the most structurally complex described by biologists thus far. They consist of the so-called "outer segment" and a narrow stalk, known as the "connecting cilium" that bridges the outer segment with the cell body. The connecting cilium is currently thought to largely correspond to the ciliary transition zone (Szymanska & Johnson, 2012). Outer segments differentiate hundreds of membrane folds that harbor the visual pigment and other proteins that mediate phototransduction. Light is detected by opsin molecules tightly packed in outer segment membranes (Fotiadis et al., 2003). It is estimated that one billion visual pigment molecules are found in the photoreceptor outer segment of some species.

On cross sections, the photoreceptor connecting cilium features the arrangement of microtubules typical of primary cilia (Kennedy & Malicki, 2009). Apical to the connecting cilium, microtubules continue to run parallel to each other but gradually lose their regular circular arrangement and distribute around the circumference of a semicircular area that closely apposes outer segment discs (Zhao, Omori, Brodowska, Kovach, & Malicki, 2012). Similar to other cilia, microtubule doublets transform into singlets towards the distal portion of the outer segment. In zebrafish, rudimentary outer segments become first visible on electron micrographs around 54 hpf in the ventral retina and gradually enlarge thereafter (Branchek, 1984).

The zebrafish retina features five types of photoreceptor cells. The sizes and positions of outer segments vary in different photoreceptor types. The outer segments of short single cones are closest to the synaptic layer of the outer retina while rod outer segments are farthest away. In vertebrate eyes, membrane arrangement in cone outer segments differs from that in rods: rod outer segments form closed discs; whereas cones contain membrane folds that are open to the extracellular environment (Szymanska et al., 2014). The zebrafish retina is cone-rich. In the larval eye approximately 80% of photoreceptors are cones. Mutants of intraflagellar transport invariably lead to photoreceptor outer segment loss and cell death (Doerre & Malicki, 2002).

Mechanosensory hair cells

In the auditory system, mechanosensory hair cells are found in several specialized patches of cells (Whitfield et al., 1996). These cells differentiate prominent apical cilia, known as kinocilia. The tether cells, which are thought to be hair cell precursors (Tanimoto, Ota, Inoue, & Oda, 2011), appear at about 18-18.5 hpf and are located in two groups, one in the anterior and the other in the posterior part of the otic vesicle (Stooke-Vaughan, Obholzer, Baxendale, Megason, & Whitfield, 2015). They are associated with otoliths, deposits of proteins and calcium salts that facilitate the detection of body movements (Haddon & Lewis, 1996). Later during development, new cells are gradually added next to tether cells, forming patches of sensory epithelia known as the anterior (utricular) and the posterior (saccular) macula (Haddon & Lewis, 1996). A third macula differentiates substantially later at around 21 to 25 dpf, in the lagena, the third sensory chamber of the ear (Bang, Sewell, & Malicki, 2001).

At about 3 dpf, three additional sensory patches of hair cells, the anterior, lateral and posterior cristae, appear in semicircular canals. In adult zebrafish, areas of semicircular canals that contain cristae widen to form bulb-shaped ampulae. The kinocilia of the lateral crista can be observed in living zebrafish larvae at 5 dpf using a good quality stereomicroscope (Nicolson et al., 1998). They are unusual in that they are very long and rigid, compared to most immotile cilia (Haddon & Lewis, 1996). Despite being immotile, they feature, however, the “9 + 2” arrangement of microtubules characteristic of motile cilia. Perhaps reflecting these unusual morphological and mechanical characteristics, kinocilia of cristae also rely on distinct ciliary transport

mechanisms, compared to kinocilia in other groups of hair cells (Pooranachandran & Malicki, 2016).

In addition to the kinocilium, the apical surface of hair cells features so-called stereocilia. These are also finger-like protrusions of smaller diameter compared to the kinocilium. The name “stereocilia” is misleading as it suggests that these structures are related to cilia. Their cytoskeleton does not contain microtubules; rather it is actin-rich, and so stereocilia are related to villi, not cilia (Tanimoto et al., 2011). Stereocilia form a bundle at the apical surface adjacent to the kinocilium. Their length gradually decreases with the distance from the kinocilium. They are easy to visualize using actin stains, such as phalloidin.

The hair cell detects mechanical stimuli, such as sound waves, through the physical displacement of the stereociliary bundle (Hudspeth, 2001). The function of the kinocilium in sound detection is not clear. In mammals, hair cell kinocilia are resorbed in the cochlea during development, indicating that they are dispensable for hearing in adult animals (Kimura, 1969). This is not the case in zebrafish, where hair cells maintain kinocilia throughout adulthood (Bang et al., 2001). Zebrafish kinocilia may contribute to mechanosensation during early stages of development. Links are observed between kinocilia and stereocilia in immature zebrafish hair cells at 3 dpf and loss of kinocilia affects mechanosensitivity of nascent hair cells. Mature zebrafish hair cells rely on stereocilia-mediated mechanotransduction (Kindt, Finch, & Nicolson, 2012).

Apart from the mechanosensory patches found in the inner ear, the zebrafish and other aquatic vertebrates differentiate hair cell patches in organs called neuromasts on their body surface. Their role is to detect hydrodynamic movements. Neuromasts are found on both the head and the trunk of the fish: the former belong to the anterior lateral line system and the latter to the posterior lateral line.

Hair cell ciliogenesis is closely associated with planar cell polarity. This is evident in the relative positions of the kinocilium and stereocilia, which in neighboring cells are aligned along the same axis both in the zebrafish and in mammals (Bang et al., 2001). In the mouse, mutations in the *ift88* gene lead to planar cell polarity defects in hair cells of the cochlea (Jones et al., 2008).Likewise, mutations in a number of other ciliary genes lead to planar polarity defects in ear epithelia (Leightner et al., 2013). Neuromasts of the

lateral line are also polarized in the plane of the skin surface (Lopez-Schier & Hudspeth, 2006). This is already visible by 3 dpf. The polarity of lateral line neuromasts makes them an attractive site for the genetic analysis of mechanisms that regulate planar cell polarity (Lopez-Schier & Hudspeth, 2006).

Olfactory sensory neurons

Cilia are present in the olfactory system of zebrafish and other vertebrate species already at early developmental stages. In zebrafish, olfactory placodes form by 17-18 hpf and the nasal pit appears by 32 hpf (Hansen & Zeiske, 1993). Zebrafish differentiate three types of sensory neurons in the nasal pit: ciliated, microvillous and crypt cells (Hansen & Zeiske, 1998). The apical surface of ciliated sensory cells differentiates a prominent olfactory knob, which contains 3-7 cilia. Microvillous sensory cells, on the other hand, feature less prominent olfactory knobs and contain 10-30 microvilli. Crypt cells bear microvilli and cilia that are submerged in the apical part of the cell body. Odorant specificities of these cells differ. Microvillous olfactory neurons respond to amino acids, but not to amines or bile acids, while ciliated olfactory neurons are stimulated by amines, nucleotides and bile acids, but not by amino acids (DeMaria et al., 2013). Odorant detection in ciliated and microvillous cells is achieved though olfactory and vomeronasal G-coupled protein receptors, respectively. The identity of crypt cell olfactory receptors is currently unknown (Kermen, Franco, Wyatt, & Yaksi, 2013).

The olfactory system of zebrafish contains motile and immotile cilia. Structurally, zebrafish olfactory cilia display “9 + 2” microtubule configuration, they are however immotile as they lack dynein arms (Hansen & Zeiske, 1998). Non-sensory motile multiciliated cells are also found in the olfactory epithelium (Hansen & Zeiske, 1998). These cells are thought to facilitate odorant clearance and to move the mucus in the nasal pit (P. M. Jenkins, McEwen, & Martens, 2009). Similar to photoreceptor outer segments, and some invertebrate cilia, the tips of zebrafish olfactory cilia feature microtubule singlets (Zhao & Malicki, 2011). Zebrafish larval olfactory cilia can be easily visualized in whole animals.

Spinal Canal

The zebrafish spinal canal starts to differentiate in the neural keel at about 18 hpf. In vertebrates, ependymal epithelial cells that line the spinal canal lumen differentiate cilia (Nakayama & Loomis, 1974). Cilia have been also

documented in the neural tube of zebrafish embryos and early larvae (Borovina et al., 2010). These cilia feature both the "9 + 0" and "9+2" arrangement of microtubules, they are motile and propagate cerebrospinal fluid flow in brain ventricles and the spinal canal (Kramer-Zucker et al., 2005). Disruption of spinal canal cilia in zebrafish leads to hydrocephalus, an abnormal expansion of the brain ventricle. Also in the spinal canal, neuroepithelial cells display planar cell polarity. This is evident in the asymmetric localization of cilia to the posterior apical surface of neuroepithelial cells (Borovina et al., 2010).

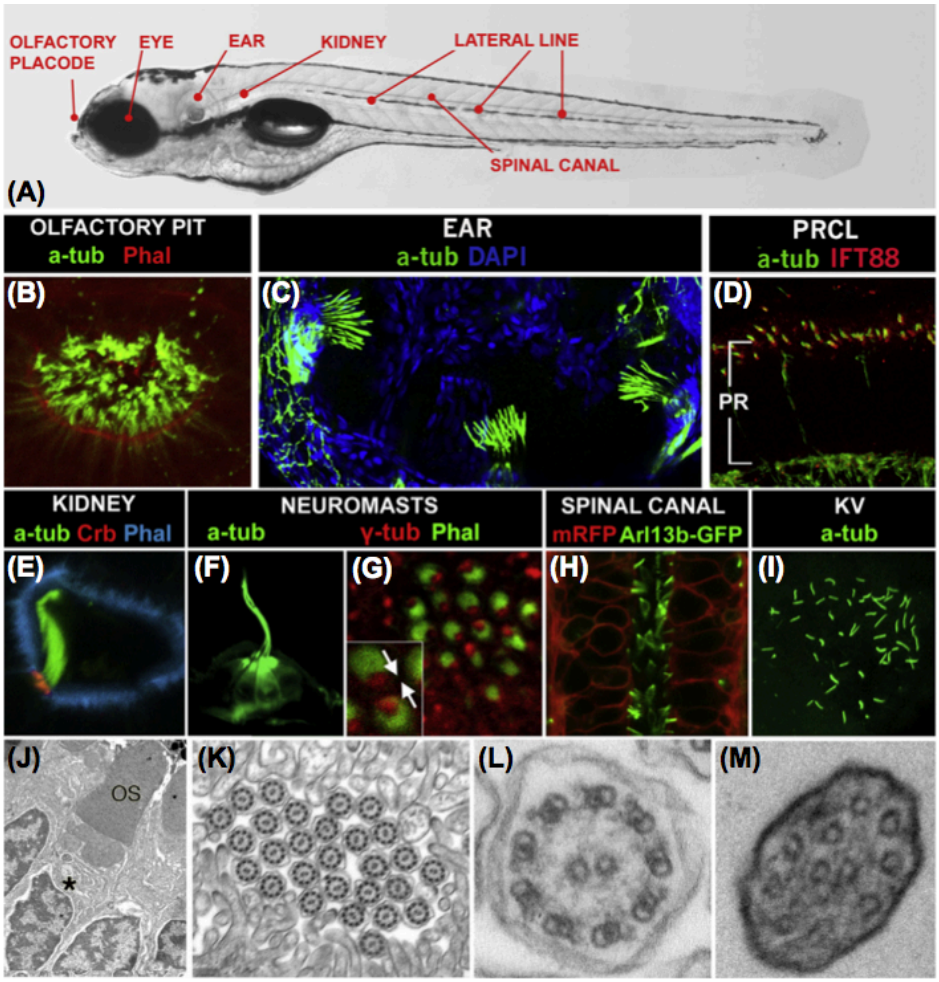


Schematic 4. Cilia in zebrafish. **(A)** The zebrafish larva at approximately 120 hpf. The locations of tissues that feature prominent cilia are indicated. **(B)** Confocal image of olfactory cilia stained with anti-acetylated tubulin antibody (green) at 3 dpf. F-actin is labelled with fluorophore-conjugated phalloidin (in red) to visualize the morphology of the olfactory pit. **(C)** Transverse cryosection through the retina at 3 dpf. Cilia are stained with anti-acetylated tubulin (green) and anti-Ift88 (red) antibodies, and imaged using confocal microscopy. The photoreceptor cell layer is indicated with a bracket. IFT88 signal is enriched at the base of cilia (green). **(D) (E) (F)** Transverse

cryosection through the trunk exposes the pronephric duct at 4 dpf. Its apical surface differentiates actin-rich microvilli and is easy to visualize with phalloidin (blue). A bundle of ciliary axoneme on the apical surface of a multi-ciliated cell is visualized with anti-acetylated-tubulin antibodies (green). The apical surface of this cell is visualized with anti-Crumbs antibodies (red). **(G)** Confocal image of a lateral line neuromast in whole embryo. Hair cells and their cilia are visualized with anti-acetylated tubulin staining. **(H)** Confocal en face image of a neuromast stained with phalloidin (green) and anti-γ-tubulin antibody (red). Arrows in the inset indicate planar orientation of neuromast hair cells. **(I)** Spinal canal cells visualized via the expression of a Sco-GFP transgene. To visualize cell membranes, embryos were injected with mRNA encoding membrane-bound RFP. **(J)** Kuppfer's vesicle cilia labelled using antibodies to acetylated alpha-tubulin in a whole embryo. **(K)** Transverse section through the central retina at 5 dpf. An electron micrograph showing retinal photoreceptors. Note differentiated outer segment (OS). Asterisk marks the photoreceptor cell soma. **(L)** An electron micrograph showing numerous cilia and villae in the lumen of the pronephric duct. A transverse section through the zebrafish trunk at 4 dpf. **(M) (N)** Ultrathin section perpendicular to the distal tip of olfactory cilium in *kif17* mutant with visible singlet microtubules.

# Aims of This Study

Ciliopathies are characterised by overlapping as well as distinct phenotypes despite the fact that they all derive from ciliary defects. Important is the evaluation of the role of ciliary genes during development as this analysis would be resourceful to model human disease using animal models. The mouse has been a really useful ciliopathy model as it closely resembles the human physiology, sharing conservation for 99% of the human genes (Nguyen & Xu, 2008). Mutations in many cilia genes have been developed in mouse with many of them being embryonic or postnatally lethal, including *Kif3a*, *Kif3b*, *Dyn2ch1*, most of the *Mks* and many *Jbts* alleles (Norris & Grimes, 2012). Lethality at early developmental stages does not convey much information regarding the gene function and thus critical is the generation of hypomorphic or spatiotemporal controlled mutant alleles result in milder phenotypes, allowing the study of gene function. Zebrafish has emerged as a powerful model because of its external development, transparency and short generation time, enabling large genetic screen analysis. Many phenotypes identified in genetic screens are reminiscent of human disease. Zebrafish has been proved as a strong forward genetic tool to study gene function (Driever et al., 1996). Chemical mutagenesis by ENU is the standard approach for both forward and reverse genetic screens in zebrafish. Morpholino knockdown technology has emerged as a reverse genetic tool to study gene function in zebrafish. It became however apparent that morpholinos lead to artefacts and many of the generated phenotypes caused by specific binding to the target RNA were difficult to distinguish from non-specific binding (Eisen & Smith, 2008). On the other hand, ENU non-specific mutations can be eliminated by outcrosses and analysis of later generations (Schulte-Merker & Stainier, 2014). Recent studies provided evidence that morpholinos potentially introduce very high rates of false positive phenotypes after using genome editing techniques to introduce mutations in the same genes. This study concludes that generation and characterization of mutants should be the standard approach to define gene function in zebrafish (Kok et al., 2015).

Based on this report we aimed to conduct a genetic screen for ciliopathy related genes in zebrafish mutant alleles derived from ENU mutagenesis. The phenotypes of mutations in 6 different loci including two core *bbs* genes (*bbs2* and *bbs9*), *cep290, alms1*, *rab23* and *tub* are described in this thesis. Morpholino knockdowns have been used until now to mimic cilia disease phenotypes in the zebrafish model. Observed phenotypes include body curvature, defective melanosome transport, eye morphology and neural tube

defects as well as disruption of the KV (Baye et al., 2011; Yen et al., 2006). No phenotypic description of the *alms1*, *rab23* or *tub* mutations was previously reported in literature.

The overall objective of this study is to evaluate the role of specific disease related cilia genes during zebrafish development and establish ciliopathy models using zebrafish mutants. An overview of the ciliary localization of the proteins studied in this project is given in Fig. 1. We hypothesized that mutant zebrafish could be an alternative to the extensively used mouse ciliopathy model. More specifically we aimed to:

1. Test if morpholino based phenotypes for certain ciliopathy genes can be reproduced in zebrafish mutants derived from ENU mutagenesis
2. Explore how closely the zebrafish mutant model can recapitulate human ciliopathy phenotypes
3. Unravel the role of genes that have not been previously analysed in zebrafish, including *alms1* and *rab23*, two genes associated with human ciliopathies

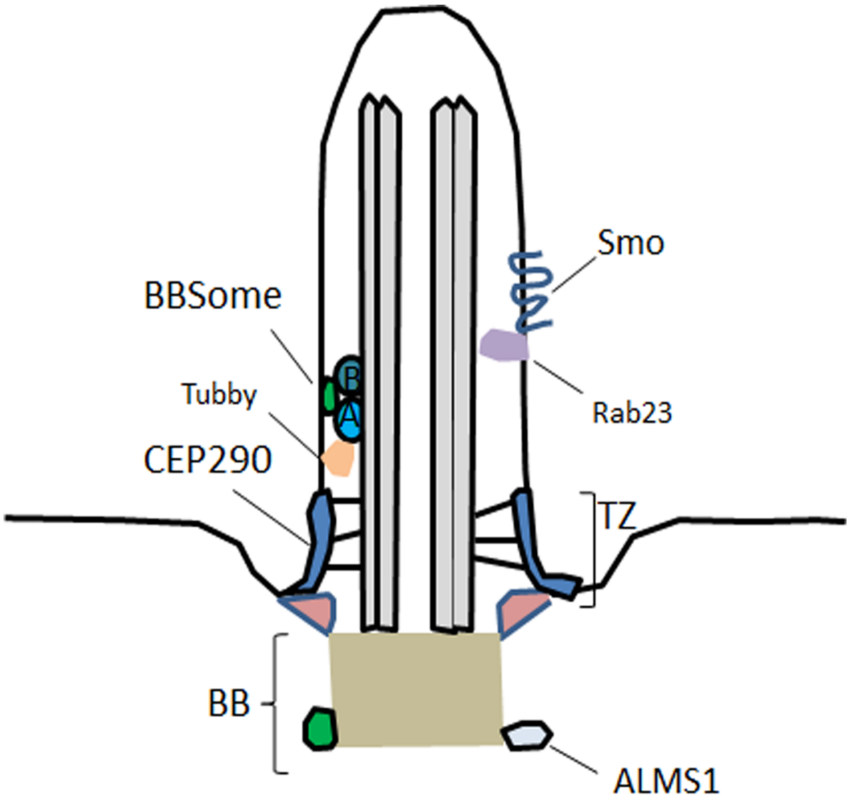


**Fig.1**: Overview of the ciliary localisation of proteins analysed in this project. The BBSome is a basal body protein and with the IFT complex forms a coat to traffic cargo into cilia. TUB interacts with IFT-A and is important for GPCR trafficking into cilia.

CEP290 is a transition zone protein, known as a gatekeeper for the cilium, while ALMS1 is another basal body protein involved in ALMS. RAB23 is a small GTPase found mutated in the Carpenter Syndrome and is thought to be responsible for Smoothened recycling in the cilium. BB: Basal Body, TZ: Transition Zone

# CHAPTER II

# ANALYSIS OF BBS MUTATIONS IN ZEBRAFISH

## Introduction

Mutations in genes, called *bbs* (Bardet-Biedl Syndrome) result in a rare autosomal recessive ciliopathy, known as the Bardet-Biedl Syndrome (BBS, OMIM 209900) (Forsythe & Beales, 2013; Mykytyn et al., 2002). BBS patients are characterized by rod-cone dystrophy, obesity, polydactyly, hypogonadism, mental retardation, renal anomalies, anosmia etc. (Zaghloul & Katsanis, 2009). There are currently 21 proteins associated with the syndrome and can be subdivided in two distinct groups. The first group is an octameric complex consisting of the proteins BBS1, BBS2, BBS4, BBS5, BBS7, BBS8, BBS9 and BBIP10, known as the BBSome (Loktev et al., 2008; Nachury et al., 2007). The BBSome was shown to bind Rabin8, a guanine nucleotide exchange factor for Rab8, and associates with the ciliary membrane (Nachury et al., 2007). The BBSome is also responsible for sorting membrane proteins into primary cilia (Jin et al., 2010). The second group consists of 13 proteins to date, which do not belong to the core complex and have diverse, unidentified domains and functions (Gascue et al., 2012). In this group a chaperonin complex exists which is important for the stability and formation of the core BBSome (Zhang, Yu, Seo, Stone, & Sheffield, 2012). BBSome proteins localize to the ciliary basal body and are responsible for trafficking of GPCRs (G Protein Coupled Receptors) including SSTR3, MCHR1, dopamine (DR), neuropeptide Y receptors and rhodopsin (Berbari, Johnson, et al., 2008; Loktev et al., 2008; Nachury, Seeley, & Jin, 2010).

Mouse and zebrafish models expanded our understanding regarding the function of BBS proteins. BBS mouse models recapitulate human phenotypes including obesity, retinal degeneration, anosmia, infertility and kidney cysts (Davis et al., 2007; Sheffield, 2010). Zebrafish models of BBS were established based on morpholino knockdown approaches. Zebrafish *bbs* morphants exhibit KV disruption leading to laterality defects; retrograde transport defects underlying the role of the BBS proteins in vesicle transport and normal retina morphology with unaffected outer segment (Yen et al., 2006). Other morpholino-based analyses report a smaller eye size and thinning of the photoreceptor cell layer (Bujakowska et al., 2015).

We evaluated the accuracy of the previously reported findings and attempted to establish a BBS model to study the role of the Bbs proteins in zebrafish development. Analysis of *bbs2* and *bbs9* mutants, which belong to the core BBSome complex, revealed differences between the previously reported morpholino based phenotypes. There is an obvious discrepancy between the reports of *bbs* morpholino generated phenotypes, as symptoms like retinal degeneration are encountered in some but not all of the studies. The observed retinal degeneration phenotype cannot however be reliable as morphant zebrafish pictures reveal that the dose of the morpholino used, induced toxicity to the embryo. This is evident from characteristics like heart edema and smaller eye size (Fig.2 Veleri et al., 2012). It is thus obvious that morpholino based analysis cannot be fully reliable as it induces the appearance of unrelated phenotypes deriving from toxicity. Additionally, morpholino experiments are not fully reproducible due to different volume of morpholino being injected in the embryos every time that the experiment is repeated.

In the ENU *bbs* mutants, we were unable to find evidence of retinal degeneration; we report however that *bbs2*$^{-/-}$ mutants are able to compensate for the photoreceptor loss by increased cell proliferation in the outer nuclear layer of the retina. We were also able to identify rhodopsin mislocalisation in the *bbs9*$^{-/-}$ mutant, in agreement with the role of the BBS proteins in GPCR trafficking. Unexpectedly, both *bbs2*$^{-/-}$ and *bbs9*$^{-/-}$ mutants were characterized by skeletal deformities appearing at early juvenile stages along with some structural defects at the base of the pharyngeal teeth. This specific skeletal phenotype is absent in both zebrafish morphants and mouse mutants it is however of major importance as a small percentage of BBS patients manifest scoliosis and other orthopedic symptoms (Ramirez, Marrero, Carlo, & Cornier, 2004). Our observations underline the importance of studying genetic mutants for cilia related phenotypes, as morpholinos often exhibit off target effects (Kok et al., 2015; Varshney et al., 2015). Our *bbs* mutant allele analysis deriving from ENU mutagenesis, reveals that zebrafish mutants can recapitulate human phenotypes to a certain extent, including phenotypes like opsin mislocalisation and skeletal defects. On the other hand, morphant phenotypes produce phenotypes that could be associated with the deregulation of the BBSome function, however these phenotypes are not connected to human manifestations of the syndrome. Additionally, morphant phenotypes can only be analysed until 3 to 4 days post injection, excluding the possibility of observing later onset phenotypes. In conclusion, although *bbs*$^{-/-}$ zebrafish mutants cannot fully recapitulate the human phenotypes they can be considered more accurate models oh human disease compared to morphants, which often produce

misleading results. In conclusion, these mutants can be resourceful models for studying the role of Bbs proteins in bone morphogenesis and GPCR trafficking.

## Materials and Methods

Zebrafish Strains and Mutants

*bbs2*$^{sa2952}$ and *bbs9*$^{sa14425}$ alleles were obtained from the Sanger Institute. Zebrafish were maintained in accordance with the UK Home Office and UK Animals Act 1986. An effort to eliminate background mutations deriving from ENU mutagenesis was made by outcrossing heterozygous mutant fish with wild type lines for at least three generations before the phenotypic analysis. The results displayed here refer to the progeny of an incross between the heterozygous mutant fish of the third generation.

Embryos and larvae were maintained in E3 medium containing 1mM NaCl, 0.17mM KCl, 0.33mM MgSO4 and $10^{-5}$% Methylene Blue in $dH_2O$. Larvae were maintained until 5 dpf in an incubator at $28^0$C in Petri dishes at density of 40 larvae/ dish. After 5 dpf, larvae were transferred into aquarium tanks and incorporated into the aquarium system to be raised to adulthood.

For cilia staining and cryosections, genotypes of the fish were confirmed by fin clipping followed by DNA isolation and PCR locus specific amplification at 3 dpf. Alternatively, the genotype of the adult fish was confirmed by fin clipping at 3 months of age. All fish were genotyped even after the identification of the bone curvature phenotype for the bbs2 homozygous mutants. The frequency of the phenotype was of Mendelian ratio.

A search for gene paralogues was made using the Ensembl online database, which confirmed that there are no paralogues for *bbs2* and *9.* Confirming that there are no paralogous genes is of major importance, as it is known that the zebrafish genome underwent a duplication event.

Adult zebrafish images

Adult fish were photographed after being anesthetized in 4.2%Tricaine in aquarium water. Tricaine (Sigma, E10521); Stock Solution: 4 mg/mL. The fish were placed into plastic boats (611-9179, VWR) filled with 20 mL of the Tricaine solution and were positioned with the lateral side up. Photographs were obtained using a 12 megapixel digital camera.

Bone and Cartilage Structural Analysis

Alizarin Red staining was performed at 4 dpf and 3 months of age. For staining of the adult fish, zebrafish were fixed in 4% paraformaldehyde (PFA) overnight at 4°C. The following day the skin and inner organs were manually removed along with the muscles using Dumont No.5 forceps. The specimens were incubated in 100% acetone for 2 days at room temperature to remove the fat, washed with tap water and incubated in trypsin-EDTA 0.05% (Gibco, Life Technologies, 25300-054) overnight in saturated borax solution. Staining was performed with a staining solution containing 0.04mg/mL Alizarin Red powder (TCS Biosciences HD1055-25) dissolved in 50% ethanol and 1% KOH for 4 hours. The fish were destained in a 3% $H_2O_2$ and 1% KOH solution for 20min and were cleared up in progressive glycerol series.

Alizarin Red staining at 4 dpf was performed as following: the larvae were fixed in 4% PFA overnight at 4°C, PFA was washed and incubated in 50% ethanol for 10 minutes. 500mg of Alizarin Red were dissolved in 50mL of water. 1mL staining solution was added to the samples, which were incubated overnight on a rocker at room temperature. The larvae were washed with water and bleached in 1.5% $H_2O_2$ and 1% KOH for 20 minutes. Samples were cleared up in glycerol series.

For the pharyngeal teeth analysis Alizarin Red staining was performed at 3 months of age as described above (adult protocol). Light-sheet microscopy was used to visualize different angles of the ceratobranchial 5 structure using a 20x lens of the Zeiss Z.1 microscope.

MicroCT analysis was performed at 4% PFA fixed specimens at 3 months of age to assess for skeletal deformities.

Cartilage staining for craniofacial defects analysis was performed at 6 dpf. Larvae were fixed with 4% PFA overnight at 4°C. They were then washed with $H_2O$ and dehydrated with 50% ethanol at room temperature for 10 minutes. The staining solution consisted of 0.02% Alcian blue (8GS, AppliChem 74240), 200mM MgCl2 and 70% ethanol. The samples were stained overnight on a rocker at room temperature. The specimens were bleached using 1.5% $H_2O_2$ and 1% KOH and washed with tap water. Tissues were cleared up in progressive glycerol series.

Retinal Analysis

Plastic Epon (Epoxy embedding medium) transverse sections were performed using the Leica EMUG6 Ultramicrotome. Sections were cut at 5um thickness.

Adult retinae were dissected using Dumont No.5 forceps and fixed overnight in 4% PFA at $4^0$C on an orbital shaker. PFA was washed with PBS and the samples were dehydrated in progressive ethanol series (15%, 20%, 35%, 40%, 50%, 70%, 85%, 90% and 100%) for 15 minutes in each ethanol concentration. The samples were incubated in Epoxy for one hour and later in a 1:2 resin: epoxy mixture for 2 hours on a shaker. The mixture was replaced by 2:1 resin: epoxy and the samples were incubated overnight at room temperature on an orbital shaker. The specimens were embedded in silicone molds (PELCO double end molds G3549, Agar) and left to solidify at $60^o$C for 48h. The solidified sample blocks were trimmed using scalpel blades and were positioned on the microtome for sectioning using glass knives. Sections were stained for 15 seconds with a Toluidine Blue solution prepared with 0.1 g Toluidine Blue O (T3260, Sigma Aldrich) in 100 mL $H_2O$. Slides were dehydrated in 96% ethanol for 1 minute and mounted using permount mounting media (SP15-100, Fisher Scientific), covering by a glass coverslip.

Immunohistochemistry and Microscopy

Immunohistochemistry was performed using standard lab protocols. Specimens were fixed overnight in 4% PFA at $4^o$C, followed by overnight incubation in cold 30% sucrose at $4^0$C, incubated for 30 minutes in tissue freezing media (OCT, 361603E, VWR) and then processed for cryosections using a Leica CM1850 cryostat. Section thickness was 15 um. For PCNA staining adult retinae were fixed and injected with 4% PFA followed by injection of 30 % sucrose and overnight incubation. Retinae were immersed in methanol and acetone overnight before sectioning. Embryos or adult retinae were briefly incubated in OCT and embedded with the posterior end up (for embryos) or with the lens facing the bottom of the slide (for retinae) in plastic cylindrical molds filled with OCT and immediately frozen on dry ice. The plastic molds were cut out and embedded on cryostat holders using OCT. The sections were cut with 15um thickness and transferred on Superfrost plus slides (LifeTechnologies, J180AMN2). The sections were then air dried at room temperature for 2 hours, rehydrated for 5 minutes in PBS and blocked using Blocking buffer: 5% goat serum, 0.1 % Tween-20 and 0.5% Triton X in PBS. The primary antibodies used for cryosections are: anti-zpr3 (rhodopsin staining) (Zebrafish International resource centre, 1:500 dilution), anti-PCNA (proliferation marker) (GeneTex, GTX124496, 1:200 dilution), anti-acetylated tubulin (cilia marker) (Sigma, 6-11B-1, 1:500 dilution) and secondary antibodies: goat anti-mouse Alexa Fluor 488 (ab150113, Abcam, 1:500) or goat anti-rabbit Alexa Fluor 633 (ab150115, Abcam 1:500 dilution). Sections were incubated overnight at $4^0$C for both the

primary and secondary antibody and washed with PBS 5 times for 15 minutes each. The sections were mounted with Vectashield mounting medium (Vector Laboratories, H-1200) covered by 22x60mm coverslips (Menzel Glaser, 630-2102), and imaged using a confocal Olympus FV1000 microscope with a 20x, 40x or 60x oil lens.

Wholemount zebrafish staining

Wholemount zebrafish cilia staining was performed at 5dpf. Larvae were fixed in 4%PFA overnight, followed by two washes with PBS 5 min each. The sample was incubated in a PBS, 10% Triton solution for 8 hours and was blocked for 2 hours using blocking buffer (as in cryosections protocol). The larvae were incubated with primary antibody (anti-acetylated tubulin, 1:500) overnight at $4^0$C on an orbital shaker. The antibody was washed with 4 times 10 minutes washes with PBS and secondary antibody was added (goat anti-mouse Alexa 488) for 3 hours at room temperature in the dark. The antibody was washed with 4 times 10 minutes washes with PBS and was incubated in DAPI (1µg/mL) for 15 minutes. Larvae were mounted on 35mm dishes filled with 0.5% agarose and imaged using a 40x or 60x water dipping lens. DAPI was used as counterstain.

Behavioral Analysis

Adult zebrafish at 3 months of age were habituated in the Viewpoint Zebrabox chamber for one hour before the initiation of the behavioral assay. The zebrafish swimming pattern was recorded using the tracking option of the Viewpoint software. First the swimming behavior was recorded with the lights on (presence of light) for 10 minutes and then the light was turned off for 5 seconds and then immediately back on. The light intensity was at 10% on a 100% scale. The swimming behavior of the fish was recorded for 5 min after the lights off period. The tracking system generates swimming track images representative of the zebrafish movement. Red colored lines correspond to fast swimming (>6cm/s) while green lines correspond to slow swimming speed (<3cm/s). The tracking data were exported to Excel Files.

Statistical Analysis

All statistical analysis was performed using GraphPad Prism 7.

# Results

**1.** *bbs* zebrafish mutants exhibit spinal cord deformities

In order to investigate the role of Bbs in zebrafish development, we obtained the *bbs2* ENU generated mutant allele sa2952 from the Sanger mutant collection. Truncation of the Bbs2 protein is caused by a nonsense point mutation (Fig.1 A), which results in the generation of a premature stop codon at the position of 353 of the total 715 aa (Fig.1 A'). *bbs2*$^{-/-}$ zebrafish mutants do not exhibit any obvious external phenotype at larval stages (until 5 dpf) but appear with an obvious body curvature at early juvenile stages (3 weeks) (Fig.2 A-A'). Nevertheless the severe body axis deformity of the *bbs* mutants, adult homozygotes are viable (Fig.2 A-A'). The malformation observed in the homozygous *bbs2* mutants was further analyzed at 3 months of age with Alizarin Red bone staining and microCT scan analysis to confirm that the observed body curvature derives from bone defects (Fig.2 B-C'). This analysis, confirmed that the bone malformation was limited to the skeleton, as the fins were not structurally or numerically affected. No specific region of deformation was observed among the individuals examined.

To investigate further the role of the Bbs protein complex in bone formation and exclude the possibility that the skeletal deformity is a Bbs2 specific phenotype, we obtained a second ENU mutagenized allele for the core Bbsome complex protein, Bbs9, where a point mutation (Fig.1 B) results in an early truncated Bbs9 protein at the position of 121 of the total 978 aa (Fig.1 B'). Similar to the *bbs2*$^{-/-}$ zebrafish mutant, *bbs9*$^{-/-}$ larvae did not exhibit any obvious external phenotypes; but still the characteristic body curvature appeared at 3 weeks, resembling the appearance of the bbs2 $^{-/-}$ fish (Fig.3 A, A'). Alizarin Red staining of adult *bbs9*$^{-/-}$ mutants revealed bone deformity of the skeleton (Fig.3 B, B').

Additionally, *bbs2* and *bbs9* adult homozygotes are not able to give progeny, a fact that can be attributed either to infertility in males or to the severe spinal cord curvature. We were unable to limit the options in one possibility as homozygous mutants failed to produce offsprings even when they were outcrossed with wt fish.

Taken together, these data reveal the involvement of the core Bbs proteins in skeletal bone morphogenesis, a previously unreported phenotype in zebrafish knockdowns or mouse models of BBS. This observation is in agreement with rare orthopedic manifestations of BBS patients with scoliosis (Ramirez et al., 2004).In conclusion, the zebrafish is a useful model to study less usual phenotypes of BBS related to orthopedic defects.

**2.** *bbs2* homozygous mutants exhibit pharyngeal jaw deformities

Further to the observation that *bbs* mutants exhibit skeletal deformities, Alizarin Red staining revealed the presence of abnormally shaped cavities at the base of the fifth branchial arch (the jaw) of the *bbs2*$^{-/-}$ adults (Fig. 4B- C'). This branchial arch is the bone of attachment for the pharyngeal teeth, which numerically and structurally do not differ between the *bbs2*$^{-/-}$ adults and their non-mutant siblings (Fig. 4A-A'). A more detailed analysis of the jaw revealed the structural differences of this bone in the *bbs2*$^{-/-}$ homozygotes, which seems to be less extended compared to the wt (Fig. 4 B, B') harboring more compact, denser cavities which however do not differ in number (Fig. 4C-C').

Overall, these observations lead to the conclusion that the role of the Bbs in bone morphogenesis is more general and not limited to the skeletal bone. In agreement with dental abnormalities in BBS patients (Forsythe & Beales, 2013), *bbs2*$^{-/-}$ zebrafish mutants have pharyngeal jaw structural abnormalities at the base of the pharyngeal teeth, which confirms that the zebrafish model could be useful to analyze bone related defects associated with BBS manifestations.

**3.** Absence of early cartilage or bone defects in the *bbs2*$^{-/-}$ mutants at larval stages

In order to identify the developmental stage when the bone defects arise, staining for the cartilage and the bone was performed during larval stages. Alcian Blue staining for cartilage was performed at 6 dpf and landmark based morphometric analysis of the centroid size between *bbs2*$^{-/-}$ larvae and their siblings did not reveal obvious differences (Fig. 5 A, A', C). This observation is contradictory to previous results produced from morphant *bbs* knockdowns, which often display craniofacial defects (Tobin et al., 2008).

In addition to cartilage analysis at larval stages, bone analysis was performed at 4 dpf. No significant difference was observed in the bone calcification and development at this stage (Fig.5 B, B'), suggesting that the onset of the skeletal malformation observed at juvenile stages occurs at a later than 4 dpf developmental stage (between 4-21 dpf).

In summary, no cartilage malformations were observed at larval stages until 6 dpf. Furthermore, no bone calcification defects were observed at 4 dpf, revealing a later onset bone morphogenesis defect, which results in the skeletal malformation observed at 3 weeks of age.

**4.** Absence of retinal degeneration in the *bbs2*$^{-/-}$ mutants

Although *bbs* mutants manifest severe skeletal malformations, they are viable and survive to adulthood (Fig.2 A, A' and Fig.3 A, A'). One of the symptoms of ciliopathy patients is rod cone dystrophy, which is successfully recapitulated in the mouse BBS model (Nishimura et al., 2004). Surprisingly, analysis of the zebrafish adult retina did not reveal photoreceptor degeneration in the *bbs2*$^{-/-}$ retina at both 3 and 6 months of age (Fig.6 A-C').

In order to assess the photoreceptor function in the *bbs2*$^{-/-}$ fish, an assay was designed based on the well-established ON-OFF optokinetic reflex response. During the "lights ON" period, adult zebrafish showed an increase in the swimming speed for a small period of time, characteristic of the startle response while later their activity returned to baseline (Fig.6 E, F). During the "lights OFF" period, adult zebrafish "freeze" for a short period of time, followed by increased swimming speed and a swimming pattern which covers the radius of the whole experimental tank (Fig.6 E', F').

Comparison of both the swimming pattern and the distance travelled during the duration of the assay of *bbs2*$^{-/-}$ adults and their wt siblings did not reveal any statistical differences (Fig.6 .G, G').

In conclusion, *bbs2*$^{-/-}$ mutants do not manifest retinal degeneration and their optokinetic reflex response is not affected. These data reveal that the zebrafish model cannot recapitulate the photoreceptor loss manifested in the BBS2 mouse model.

**5.** *bbs9*$^{-/-}$ mutants manifest severe opsin mislocalization while *bbs2*$^{-/-}$ mutants have increased proliferation in the outer nuclear layer of the retina

Opsin mislocalisation was assessed in both the *bbs2*$^{-/-}$ and *bbs9*$^{-/-}$ mutant retina at 5 dpf. *bbs2*$^{-/-}$ mutants do not manifest opsin mislocalisation in contrast to the bbs9$^{-/-}$ mutants, which manifest severe opsin mislocalization at the same age. Opsin was mislocalised in the surroundings of the outer nuclear layer while it should only localize to the outer segment of the retina (Doerre & Malicki, 2002) (Fig.7 A-B').

The unaffected opsin localisation in the *bbs2*$^{-/-}$ retina and the absence of retinal degeneration led to the hypothesis that the mutant photoreceptors can compensate for the degeneration (photoreceptor loss) by increased proliferation in the outer nuclear layer. During adulthood, proliferation in the retina is limited (Fig. 7C) as was confirmed with PCNA staining in the retina of 6 month old wt fish. Unexpectedly, proliferation in the *bbs2*$^{-/-}$ mutant retina was increased and proliferating cells were present throughout the outer nuclear layer (Fig.7 C').

In summary, a striking difference in the proliferation levels was observed between the cells of the ONL in the wt and the *bbs2*$^{-/-}$ mutant retina (Fig.7 D), confirming the hypothesis that there is a compensation for the photoreceptor loss caused by the *bbs2* mutation. In contrast, *bbs9*$^{-/-}$ zebrafish appear with the expected opsin mislocalisation (Fig.7 B'), highlighting a differential role of the Bbs proteins in zebrafish. This observation leads to the hypothesis that mutations in different Bbsome proteins can result in variable phenotypes related to BBS. Alternatively, the possibility that the specific *bbs2* allele analyzed is hypomorphic cannot be excluded.

**6.** The *bbs2* mutation does not affect olfactory cilia in zebrafish

It has been previously reported that 47% of the BBS patients are anosmic, although not all *bbs* mutations result in anosmia. Null *Bbs1* and *Bbs4* mice have short olfactory cilia compared to wt littermates and exhibit reduced response to odorants (Katsanis et al., 2001). Aiming to identify olfactory cilia defects in the *bbs2*$^{-/-}$ zebrafish mutants, the length of cilia in the nasal pit of wt and homozygous mutant siblings at 5 dpf was compared. Comparative analysis revealed no significant difference in the cilia length of these animals (Fig.8 A-C).

Cilia in the olfactory pit were only structurally assessed; however there could still be a possibility that the olfactory function is compromised albeit structure remains unaffected. For this reason, olfactory neuron activity should be assessed in order to reach a definite conclusion.

## Discussion

BBS proteins have been associated with the manifestation of BBS in humans; however the function of most of these proteins is largely unknown. Seven of these proteins form a stable complex, known as the BBSome which function and structure are being unraveled (Jin et al., 2010; Nachury et al., 2007; Wei et al., 2012), the role of individual proteins of this complex remains enigmatic. In human patients, mutations in any of the 21 known BBS proteins result in the manifestation of BBS (Heon et al., 2016). Mouse models of this syndrome successfully recapitulate the human symptoms (Mykytyn et al., 2004; Nishimura et al., 2004). The role of Bbs in zebrafish development has not been clarified, since only morpholino knockdowns were used to model the disease thus far (Tayeh et al., 2008; Veleri et al., 2012; Zaghloul et al., 2010). Using two ENU generated alleles for two of the three core protein of the BBSome (Bbs2 and Bbs9); we found body curvature defects at juvenile stages for both mutant alleles. We also report another bone related defect at the base of the adult *bbs2*$^{-/-}$ mutant pharyngeal teeth. Both of these observations are novel, as

mouse BBS models do not display teeth related or skeletal defects, they do however exhibit impaired ciliogenesis in chondrocyte cilia and reduced cartilage thickness, suggesting that BBS function is important for extracellular matrix production in the articular cartilage (Kaushik, Martin, Zhang, Sheffield, & Morcuende, 2009). The specific mutations studied are not directly correlated to known human mutations and we cannot conclude that the alleles studied are nulls. Specifically, the *bbs2* allele harbors a point mutation in the middle of the protein, however there is any known domain within the protein that would lead to the conclusion that this mutation results in functional abolishment. The *bbs9* allele derives from an early mutation within the N-terminal PTHB1 domain of the protein. This early stop codon could be however skipped, resulting in a functional protein. The generation of *bbs2;bbs9* mutants could possibly give insight into the nature of the specific alleles. If both alleles are nulls then the whole BBSome complex would not be functional as these two proteins are required for the BBSome assembly. No zebrafish antibodies exist for the Bbs2 and 9 proteins that would enable us to confirm that the studied alleles are nulls. Alternatively, we could perform assays for nonsense-mediated decay that would indicate protein loss of function.

Interestingly, a fraction of BBS patients manifest orthopedic symptoms other than polydactyly, with scoliosis being one of them (Ramirez et al., 2004). Another interesting recent finding shows the involvement of motile cilia in the development of idiopathic scoliosis in zebrafish (Grimes et al., 2016). Based on this, we cannot exclude the possibility that mutations in *bbs* affect cilia motility, which is substantial at early stages for proper skeletal morphogenesis. The spinal curvature of the two *bbs* mutants described here could be a result of vertebral deformities during development but this phenotype could alternatively derive from early segmentation or muscle arrangement defects. We could test this hypothesis by analyzing the regular morphology and spacing of somites using muscle differentiation markers like *myoD* and *Xirp2a*. Visualization of other somite related markers like *pax9* could reveal sclerotome defects. Muscle defects could be also detected by analysis of the muscle actin filament arrangement around the spine using phalloidin staining. Simple morphological analysis after transverse sectioning of juvenile fish could additionally reveal muscle structural defects.

One of the most characteristic symptoms for the diagnosis of BBS in human patients is retinal dystrophy. Mouse BBS models are able to recapitulate the rod cone dystrophy (Zhang et al., 2013), but our study highlights that the zebrafish *bbs2* mutant is not able to manifest the retinal degeneration phenotype due to

its regenerative capabilities. We were thus unable to find retinal degeneration in the *bbs2*$^{-/-}$ adult mutants. *bbs2*$^{-/-}$ mutants do however exhibit increased proliferation levels in the outer nuclear layer of the retina as shown by the increased expression of proliferation markers. This result indicates the involvement of regeneration in the adult *bbs2*$^{-/-}$ retina, which is able to compensate for the photoreceptor loss caused by the mutation. As previously reported, mechanical injury is not required to trigger the regeneration process (Brockerhoff & Fadool, 2011; Tappeiner et al., 2013). Unlike the *bbs2*$^{-/-}$ mutant, *bbs9*$^{-/-}$ mutants are characterized by opsin mislocalisation as early as 5dpf, indicating the defective mechanism of rhodopsin trafficking in the retina caused by the mutation.

The different retina related phenotypes observed in the two core *bbs* mutants imply that although these two proteins belong in the same complex, they do have different functions. Their function is unknown based on the current bibliography. It seems that Bbs9 is substantial for vision and sustainability of the photoreceptors. In contrast, *bbs2*$^{-/-}$ mutants can compensate for the photoreceptor loss, probably through a mechanism, which triggers regeneration. An alternative possibility is that the *bbs2* mutation analysed is milder than the *bbs9* one. It was previously reported that individuals with BBS2 mutations were unaffected and a third mutation in another *bbs* gene was required for the manifestation of the syndrome (Katsanis et al., 2001). This is known as triallelic inheritance in BBS and we hypothesize that another mutation in the *bbs2* mutant background would cause a more severe phenotype in zebrafish.

Additionally, mutations in the *bbs2* gene did not result in olfaction related phenotypes. The possibility that the function of the ciliated olfactory neurons is however compromised cannot be excluded.

Overall, although only the *bbs9* zebrafish mutant can recapitulate the retinal degeneration defect, both *bbs2* and *bbs9* mutants would be a useful tool to study more rare symptoms related to orthopedic defects like scoliosis and dental defects, encountered in the human BBS patients.

# Figures

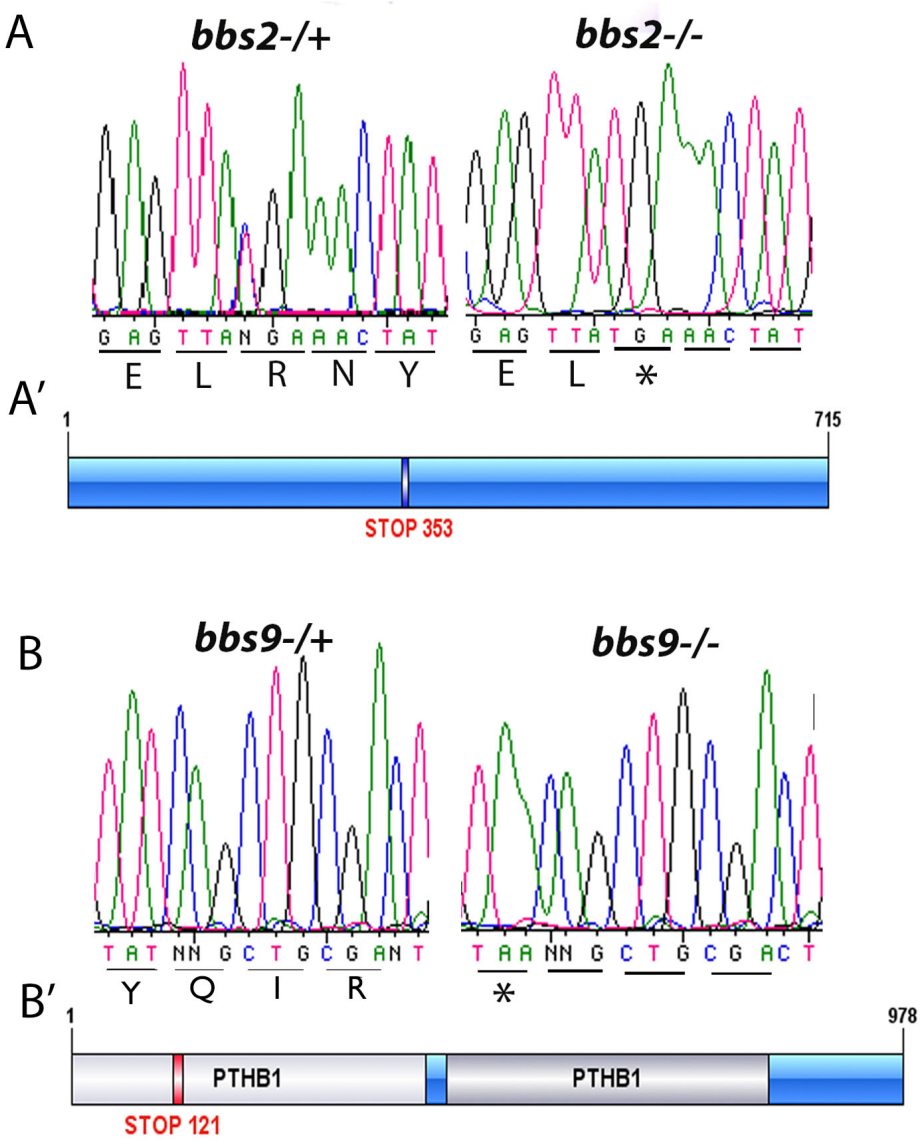


**Figure 1. The location of mutations of the analysed *bbs* alleles**. **A**. Representative sequences from *bbs2* heterozygous and *bbs2* homozygous mutant zebrafish. The amino acids of the protein sequence are indicated. **A'**. Schematic representation of the position of mutation that causes a premature stop codon at the position of 353 out of the 715 total amino acids in the Bbs2 protein sequence. **B**. Representative sequences from *bbs9* heterozygous and *bbs9* homozygous mutant zebrafish. **B'**. Schematic representation of the mutation position that causes the appearance of a premature stop codon within the PTHB1 N-terminal domain and specifically at the amino acid 121 out of the total 978 amino acids of the Bbs9 protein. Asterisks indicate the appearance of the stop codon in the homozygous mutant sequence.

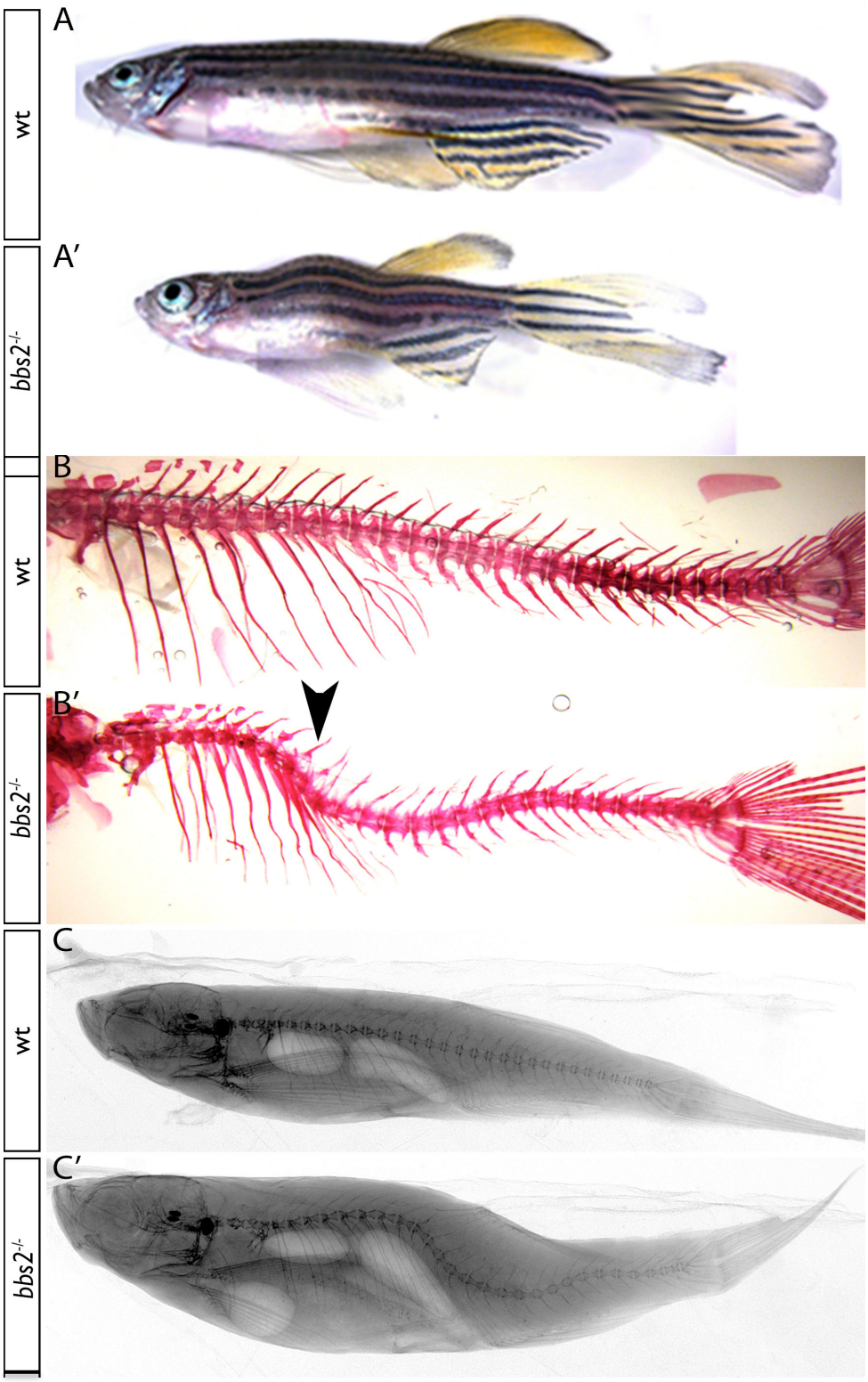


**Fig.2 External phenotype of *bbs2*$^{-/-}$ adult mutant fish. A, A'.** Images from wt (**A**) and *bbs2*$^{-/-}$ adult mutants (**A'**) at 3 months of age. **B, B'.** Alizarin Red staining of wt (**B**) and *bbs2*$^{-/-}$ (**B'**) adult zebrafish at 3 months of age. The skeleton of the *bbs2* homozygous mutants appears deformed as pointed by an arrowhead. The fins are removed in order to reveal a clear image of the skeletal deformity phenotype. **C, C'**. MicroCT scan images of 3 months old wt (**C**) and *bbs2* homozygous mutants(**C'**).

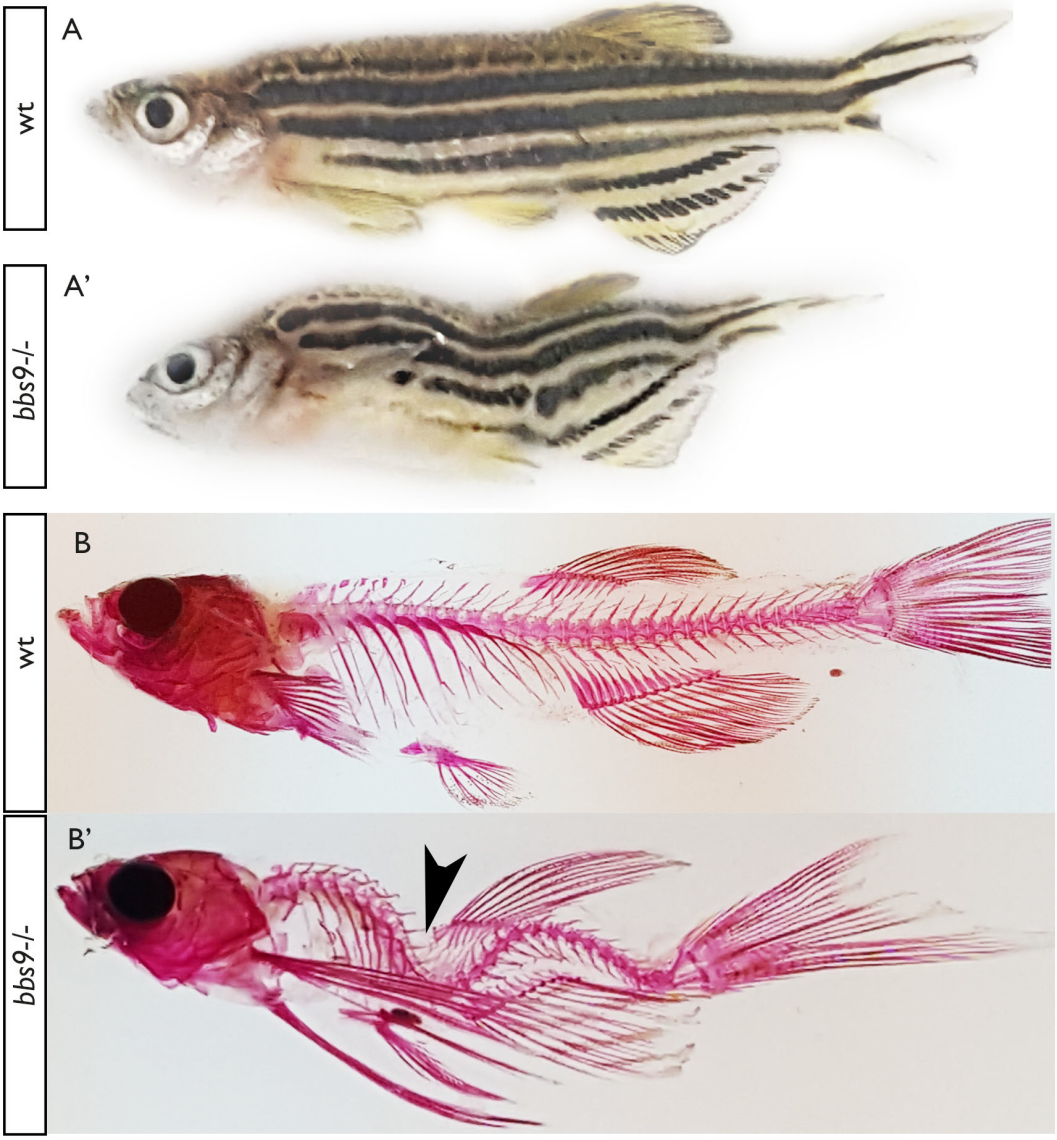


**Fig.3 External phenotype of *bbs9*$^{-/-}$ adult zebrafish.A, A'.** Images from wt (**A**) and bbs9$^{-/-}$ adults (**A'**) at 3 months of age. B, B'. Alizarin Red staining of wt (**B**) and *bbs9*$^{-/-}$ (**B'**) adult zebrafish. The skeleton of the *bbs9* homozygous mutants appears deformed as pointed by an arrowhead.

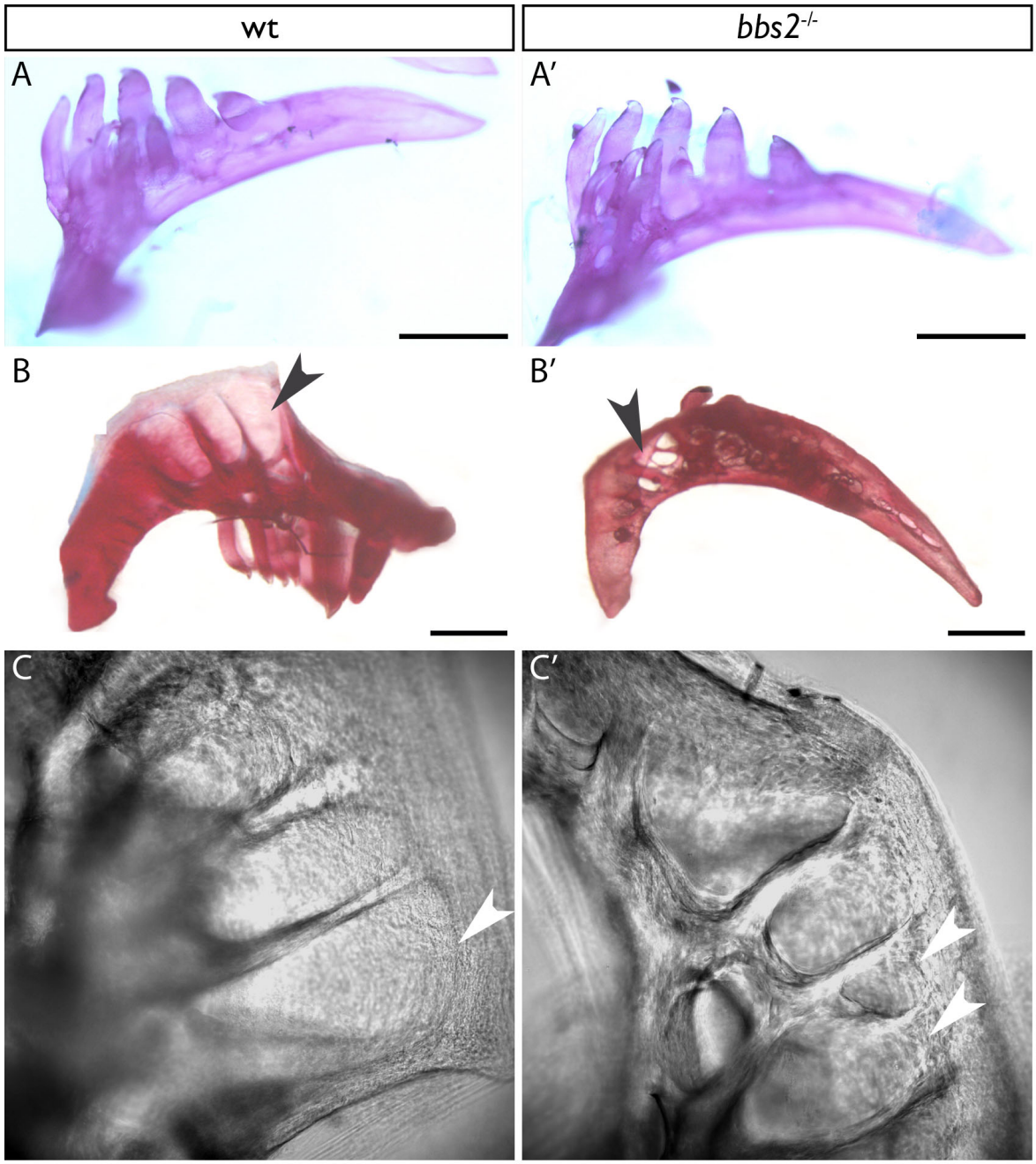


**Fig.4 The pharyngeal teeth phenotype of the *bbs2*$^{-/-}$ mutants. A, A'.** Representative images of the left pharyngeal jaw with pharyngeal teeth of wt (**A**) and *bbs2* homozygous mutants (**A'**) stained with Alizarin Red at 3 months of age. No difference is observed in the number of teeth. **B, B'**. Images of the pharyngeal jaw stained with Alizarin Red and photographed with the pharyngeal teeth pointing down. The two samples are positioned differently in order to allow the observation of structural differences. wt (**B**) and *bbs2* $^{-/-}$ (**B'**) jaw morphology differs at the base of the pharyngeal teeth, as indicated by arrowheads. **C, C'**. Light sheet microscopy images of the base of pharyngeal teeth, 20 x magnification. Note the differences in the shape and size of the cavities as pointed by arrowheads. Scalebars are 500µm.

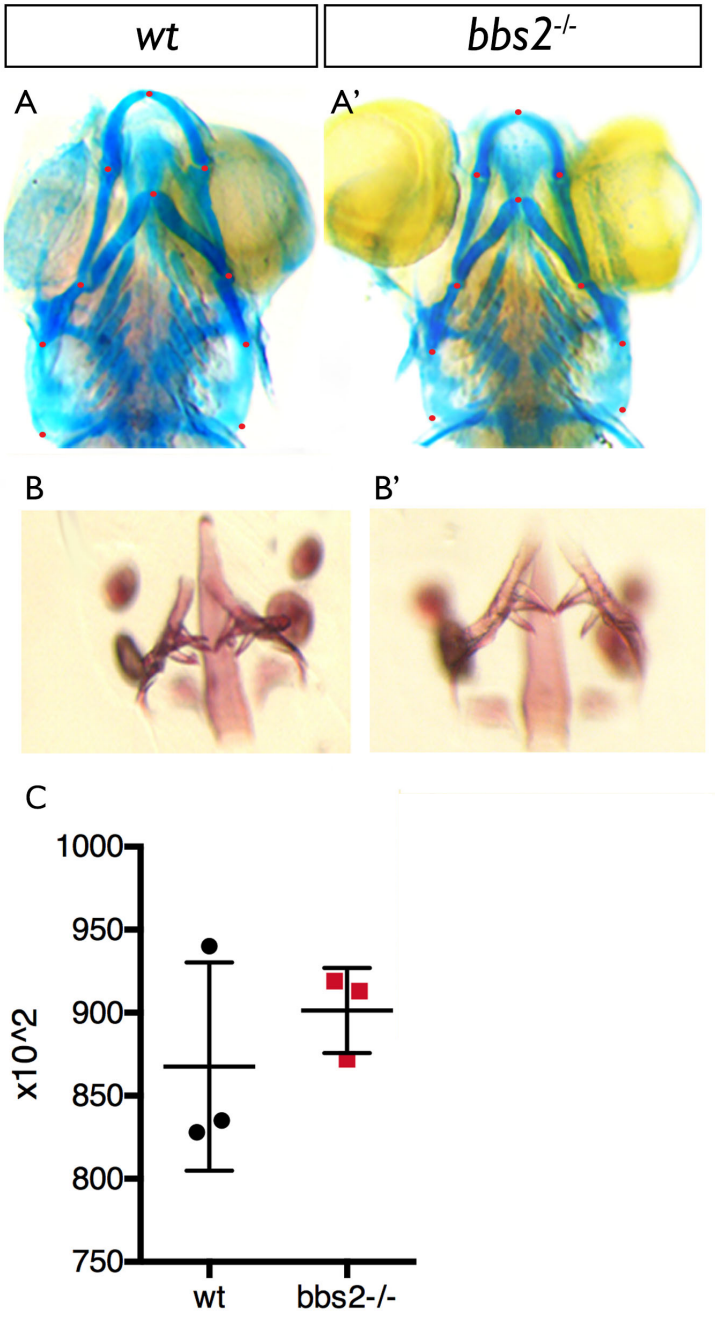


**Fig.5 Analysis of larval bone and cartilage morphology. A, A'**. Images of Alcian Blue stained *bbs2*$^{-/-}$ and wt siblings at 6 dpf. Only the craniofacial characteristics are depicted in the images shown. Red circles represent the landmarks that were used for the morphometric analysis of centroid size between homozygous mutants and wt siblings **C.** (non-significant, t-test, p=0.4058). **B, B'**. Alizarin Red staining at 4 dpf showing the bone ossification of wt and *bbs2*$^{-/-}$ larvae.

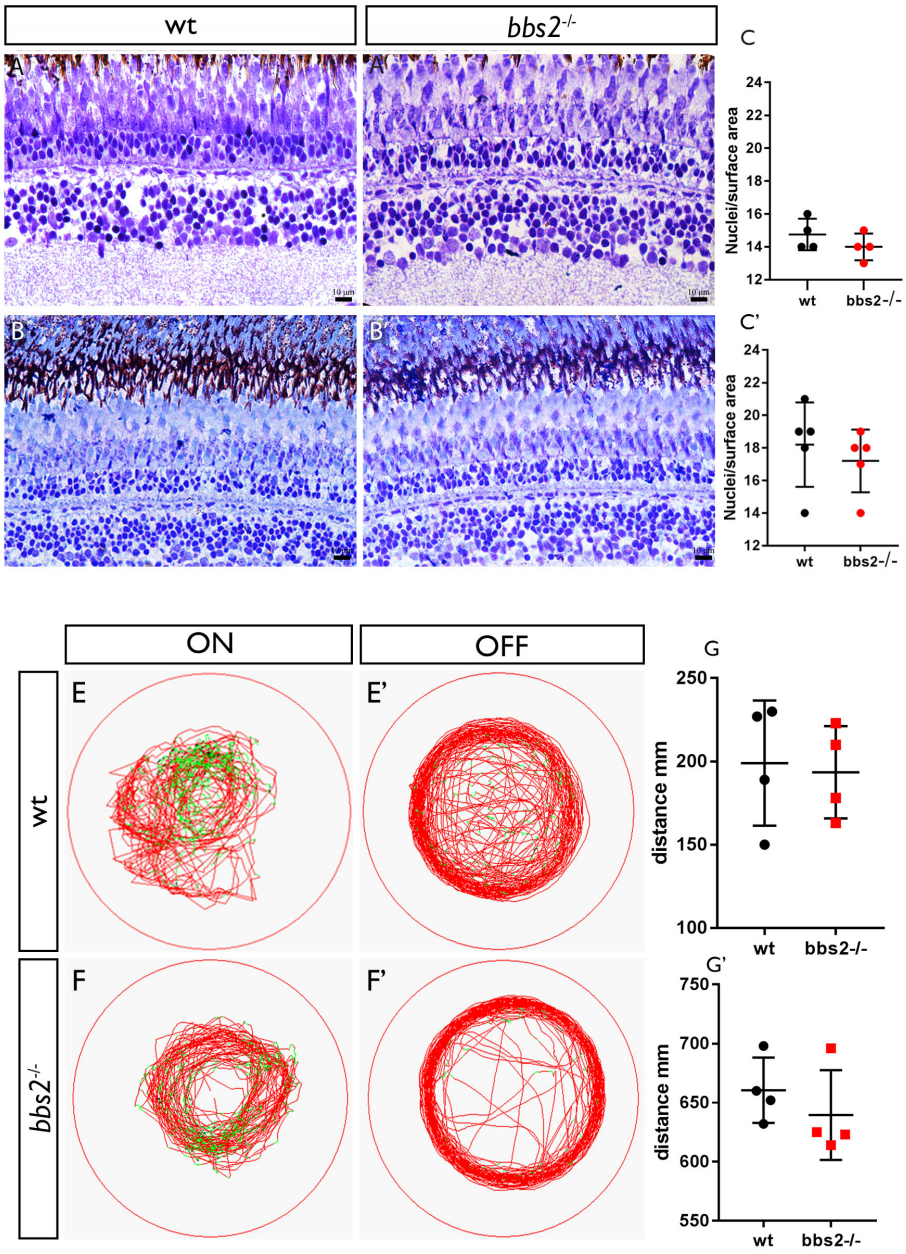


**Fig.6 Retina morphological and functional analysis. A-B'.** Epon plastic sections stained with Toluidine blue of wt and *bbs2*$^{-/-}$ derived retina at 3 (**A, A'**) and 6 (**B, B'**) months of age. **C.** Quantification of nuclei per 10x6 mm square surface area at 3 months (n=4 retinae, counts for 1 section/retina, non-significant difference, t-test, p=0.2782) and **C'**. at 6 months (n=5 retinae, counts for 1 section/ retina, non-significant difference, p=0.5077). **E-F'**. Lights OFF (darkness) response of wt and *bbs2* $^{-/-}$ zebrafish at 3 months of age. Note that both wt and homozygous mutants swim in the centre of the tank in the presence of light (ON), while they have stressed swimming response, moving throughout the whole tank diameter in the absence of light (OFF). **G.** Quantification of the distance travelled during 10 minutes of the assay in the presence of light (ON) (n=4 individuals, non-significant, t-test, p=0.8218). **G'**. Quantification of the distance travelled during 10 minutes of the assay in the absence of light (OFF) (n=4 individuals, non-significant, p=0.4056). Scalebars are 10µm.

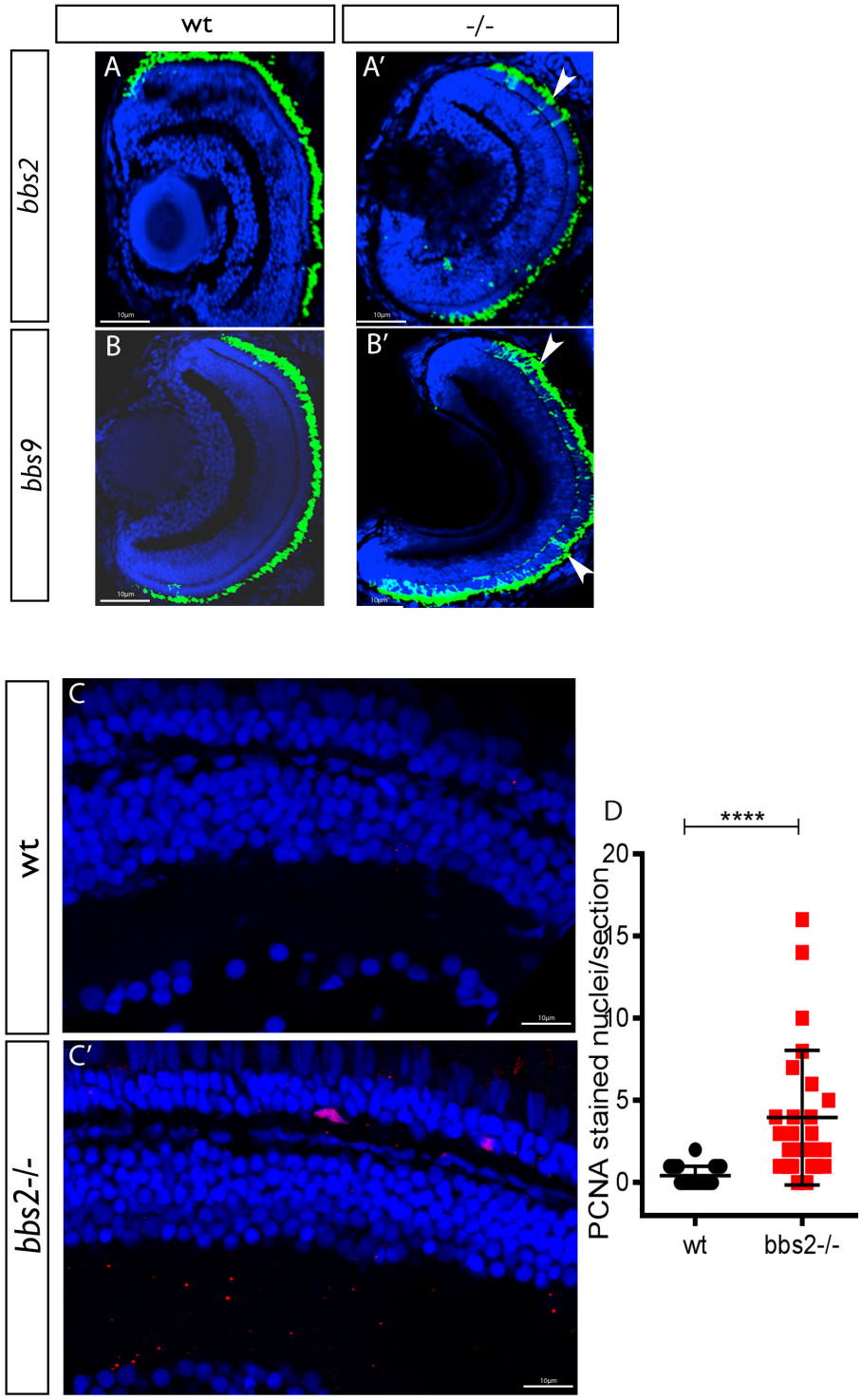


**Fig. 7 Analysis of rhodopsin localization and proliferation rates in the adult retina**. **A-B'**. *bbs2*$^{-/-}$ larvae at 5 dpf appear with a very mild mislocalisation phenotype of rhodopsin as indicated by an arrowhead (**A'**), while *bbs9* $^{-/-}$(**B'**) are clearly characterised by rhodopsin mislocalization in the outer nuclear layer. Arrowheads show regions of mislocalization **C, C'**. Proliferation of the cells in the outer nuclear layer of *bbs2*$^{-/-}$ adult mutants is increased compared to wt siblings at 3 months of age. **D**. Quantification of the proliferating cells per section, marked by PCNA expression (magenta) in the outer nuclear layer. Retinae of 9 individuals were examined and 3 sections were analysed for each individual retina. (n=27 sections, t-test, $p<0.0001$) Blue: DAPI, green: anti-zpr3 (rhodopsin), magenta: anti-PCNA. Scalebars are 10µm.

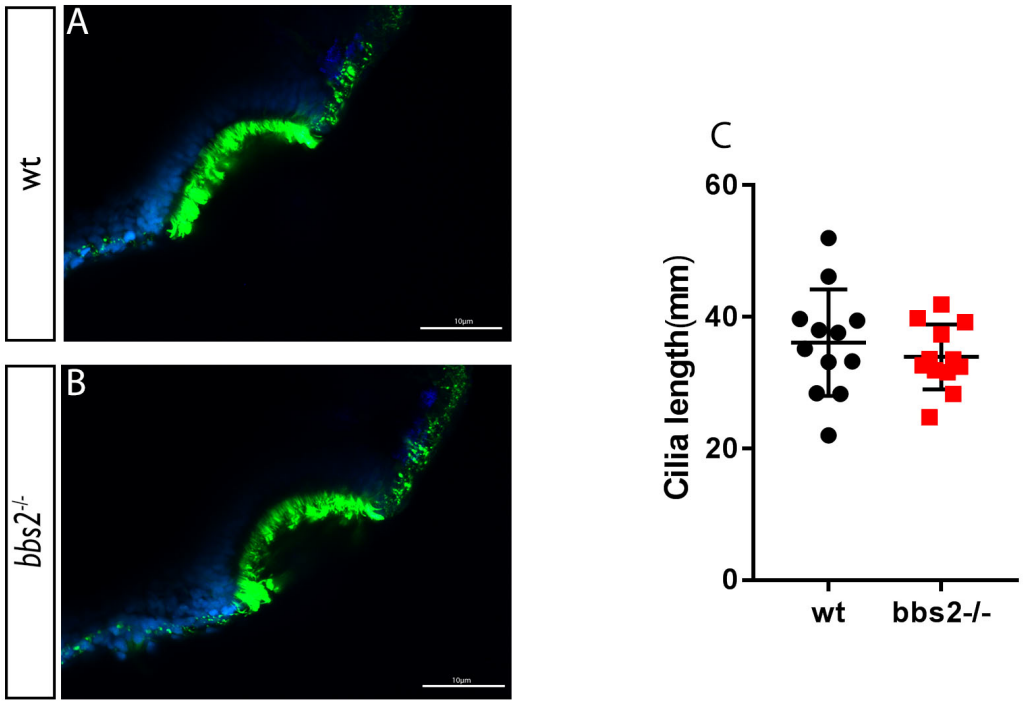


**Fig.8 Olfactory cilia analysis A-B**. Olfactory cilia were visualised at 5 dpf in wt and *bbs2*$^{-/-}$ mutant larvae. **C**. Comparison of cilia length in the olfactory pit of wt and *bbs2*$^{-/-}$ larvae reveals no significant difference (n=12 individual larvae, t-test, p=0.4366). Blue: DAPI, green: anti-acetylated tubulin. Scalebars are 10µm.

# CHAPTER III

# ANALYSIS OF CEP290 FUNCTION IN ZEBRAFISH

## Introduction

Mutations in centrosomal protein of 290kDa (CEP290) cause a wide range of phenotypes with variable severity, from blindness to perinatal lethality (Coppieters, Lefever, Leroy, & De Baere, 2010). *CEP290* mutations are associated with Leber Congenital Amaurosis (LCA, OMIM 611755), the mildest of the syndromes caused by mutations in *CEP290*, Joubert Syndrome (JBTS, OMIM 610188), Bardet-Biedl Syndrome (BBS, OMIM 209900), Nephronophthisis (NPHP, OMIM 256100), and the lethal Meckel- Gruber Syndrome (MKS, OMIM 611134). Syndrome-related mutations include nonsense and missense single base-pair substitutions, splicing defects and frameshift-causing insertions/deletions throughout the 54 exons of the gene (Coppieters et al., 2010). The association of CEP290 with this wide range of syndromes and phenotypes has led to the hypothesis of the presence of second site modifier loci that can cause the variable syndrome severity (Bujakowska et al., 2015; Coppieters et al., 2010). Although the genetic and phenotypic pleiotropy associated with CEP290 mutations has been enigmatic, recent pleiotropic disease models suggest that the phenotypic variation can be explained by exon skipping. In this model, different mutations in *CEP290* result in different amount of protein production caused by alternative splicing. Exons 6, 9, 40 and 41 are the ones that are most likely to be involved in alternative splicing, causing unpredicted severity of the disease (Drivas et al., 2015).

CEP290 localises at the transition zone, close to the microtubule-membrane links and is required for their formation (Craige et al., 2010). It has additionally been proved in *Caenorhabditis elegans* that CEP290 acts as a central assembly factor for MKS proteins, which form one of the transition zone modules (C. Li et al., 2016). CEP290 specifically localises at the base of the transition zone, where it is essential for the assembly of other transition zone proteins (C. Li et al., 2016; Yang et al., 2015). CEP290 additionally interacts with PCM-1, a centriolar satellite protein and localizes to centriolar satellites (Kim, Krishnaswami, & Gleeson, 2008).

*In vitro* studies have shown that CEP290 is required for ciliogenesis and is involved in ciliary targeting of Rab8, which in association with the BBSome,

promotes ciliogenesis (Kim et al., 2008). The association of Cep290 with the BBSome has been further documented by depletion of *Cep290,* which results in defective recruitment of BBSome components in cilia (Stowe, Wilkinson, Iqbal, & Stearns, 2012). Finally, the physical and genetic interaction between CEP290 and the BBSome has been shown to occur within the N-terminal part of the protein (Bujakowska et al., 2015).

There are two naturally occurring animal models harbouring *Cep290* mutations: an Abyssinian cat pedigree and the *rd16* mouse. Both models display retinal degeneration but they do not have signs of cerebellar or renal abnormalities (Chang et al., 2006; Menotti-Raymond et al., 2007). Additionally, 80 % of mouse knockout mutants for *Cep290* die between birth and weaning, however those that survive do not develop hydrocephaly and display normal lifespan (Rachel et al., 2015). These individuals exhibit retinal degeneration with thinner outer nuclear layer, no outer segment and shortened inner segments. They also manifest distortion of the cerebellum and have age progressive renal defects (Rachel et al., 2015). The *rd16* mutant mice also show elevated hearing threshold (Rachel et al., 2012). Notably, in the same study, knockdown of *cep290* in zebrafish did not cause any obvious defect (Rachel et al., 2012). In another zebrafish study, however, morpholino knockdown of *cep290* aiming to mimic the intronic mutation c.2991+1655A>G, the most commonly encountered mutation in human LCA, resulted in a morpholino dosage dependent body axis defect, ranging from straight to bent or curly. Additionally, there was reduced KV size, delayed melanosome transport and reduced visual responsiveness (Baye et al., 2011).

Phenotypic variability encountered both in human patients and animal models carrying *Cep290/ CEP290* mutations reveals the need to study the genetics of *cep290* further. In this chapter, I show that in agreement with a previous brief report of the *cep290*$^{sa1383}$ mutant allele, no obvious external phenotype becomes apparent (Kok et al., 2015) and homozygous mutants survive to adulthood, with normal fertility and lifespan. We were unable to find any body axis related defects and ciliogenesis was not affected in the tissues examined. Furthermore, surprisingly no retinal degeneration was observed in both homozygous mutant larvae and adults, as was assessed by the morphology of the retina and the localisation of rhodopsin in retinal sections. Although no expected phenotypes are present in homozygous mutants, we observed a high frequency of ectopic otoliths at 1.5 dpf. The third otolith, does not persist till 2 dpf. *cep290*$^{-/-}$ mutant larvae appear with an increased responsiveness in the presence of stressors and specifically NaCl at 5 dpf. Interestingly, behavioural

swimming tests during adulthood revealed hyperactive behaviour for the *cep290*$^{-/-}$ individuals. The appearance of hyperactivity and stress related behavioural differences in *cep290*$^{sa1383}$ larvae and adult homozygotes led to the hypothesis that these defects are related to vestibular system dysfunction. Dissection of the inner ear revealed both polarity related defects in the macular epithelium as well as otolith structure abnormalities. Proteomic analysis of the utricular otoliths revealed reduced amounts of the ear specific protein Cochlin (Coch) in the *cep290*$^{sa1383}$ otoliths. In conclusion, although *cep290*$^{sa1383}$ zebrafish mutants do not reproduce phenotypes associated with *CEP290* mutations in human patients, our analysis revealed a novel function of Cep290 in otolith morphogenesis and maintenance.

## Materials and Methods

Microscopy

Larvae at 1.5 dpf were dechorionated, anaesthetized in 2% Tricaine in E3 media, positioned in 3% methylcellulose with the lateral side up and photographed in a Zeiss Axiozoom inverted microscope camera using a 20x lens.

Scanning electron microscopy-SEM: adult otoliths were dissected and washed in PBS for 10 minutes. The otoliths were fixed in 4% PFA overnight at 4$^{o}$C and dehydrated using 100% ethanol for 20 minutes till ethanol was completely evaporated. Otoliths were embedded on carbon adhesive discs mounted on SEM sample stubs, coated with a thin layer of gold and imaged on a Phillips XL-20 microscope.

Behavioral analysis

For the larva swimming behavior assay, 5 dpf larvae were placed in 24-well dish wells filled with 1 mL E3 medium and left to acclimatize for 30 minutes in the Zebrabox chamber. After the acclimatization period the swimming behavior of the larvae was tracked for 10 minutes with the lights off (dark chamber), as larvae at this stage “freeze” in the presence of light. The stress response of 5 dpf larvae was tested as follows: the larvae were placed into the 24-dish wells filled with E3 medium, a final concentration of 250mM NaCl was added in each well. The larvae were left in this solution for 10 minutes. After 10 minutes the NaCl solution was removed and replaced with fresh E3 medium for the remaining duration of the assay. The larvae swimming behavior was tracked for

10 minutes right after the solution replacement. Slow swimming speed <3mm/s, fast > 10mm/s.

Adult zebrafish (at 3 months of age) behavior was also recorded using the Zebrabox tracking system. Adult zebrafish were acclimatized for one hour in the Zebrabox chamber and their swimming activity was tracked with the lights on for 10 minutes. Red lines in the tracked behavior image is indicative of quick swimming speed >6cm/s while green lines are indicative of slow swimming speed <3cm/s.

Immunohistochemistry

Cilia staining was performed at 5 dpf using mouse anti-acetylated tubulin (1:500 dilution), as described in Chapter II. For the assessment of polarity in the inner ear, the utricles of adult fish were dissected using Dumont No.5 forceps, fixed in 4% PFA for 2 hours at room temperature, washed with PBS for 5 minutes and blocked in 1% goat serum, 0.5% Triton X and 0.1% Tween-20 in PBS for 1 hour at room temperature. The dissected tissues were incubated with mouse anti-acetylated tubulin (1:500 dilution) overnight at 4$^{o}$C without shaking, followed by 3 washes of 15 min each with PBS and incubation in secondary antibody anti-mouse Alexa 488 (1:500 dilution) for 3 hours at room temperature. The antibody was washed with PBS for a total of 30 minutes and the tissue was incubated in Phalloidin-Alexa Fluor 633 (A22284, ThermoFisher Scientific) for 1 hour at room temperature in the dark. Phalloidin was washed with PBS for 5 minutes and the utricle was flattened with a small incision in the middle of the epithelium using an insulin needle (BS-N1H2913, Myjector U-100 insulin needle) and mounted on simple glass microscopy slides. The tissues were mounted using Vectashield mounting medium (Vector Laboratories, H-1200) and covered by 22x60mm coverslips (Menzel Glaser, 630-2102). The images were obtained using a 60x oil lens in Olympus FV1000 confocal microscope.

Proteomic Analysis

Dissected utricular otoliths were decalcified overnight at 4$^{o}$C in 0.2M Tris-EDTA, pH 8.0. For this experiment specifically 4 otoliths were used (2 fish were sacrificed). After the overnight incubation a transparent structure remained at the bottom of the tube, representing the decalcified protein matrix of the otoliths, which was homogenized using a hand held homogenizer (47747-370, VWR). The samples were centrifuged on a benchtop centrifuge at 4$^{o}$C for 30 minutes at 13000rpm. After centrifugation a pellet becomes apparent at the bottom of the tube. The supernatant is transferred in a new tube and equal volume to the supernatant volume of 2x Laemmli buffer is added in the tube (soluble fraction).

The pellet is washed with cold acetone and centrifuged at 4$^{o}$C for 20 minutes at 13000rpm. Acetone is removed and the pellet is let to air dry for 15 minutes. 20ul 2x Laemmli are added in the tube and the pellet is homogenized with a pestle (insoluble fraction). The sample is heated at 95$^{o}$C for 10 minutes and loaded on a 10% SDS-PAGE gel with a Spectra Multicolor prestained protein ladder (26623, ThermoFisher Scientific). The gel ran at a 100V constant for 2 hours using the Mini-Protean Tetra system. The gel was then washed with $dH_2O$ for 20 minutes on an orbital shaker at room temperature and fixed overnight in a 40% methanol, 10% acetic acid, 50% $dH_20$ fixation solution on an orbital shaker at room temperature. The fixation solution was replaced with Coomasie Brilliant Blue R staining solution (161-0436, BioRad) and was incubated on an orbital shaker for 4 hours at room temperature. The gel was destained with $dH_2O$ after microwaving it for 6 times 1 minute each and incubating for 30 minutes in a 37$^{0}$C incubator. The gel was photographed using a white light illuminator box. Individual bands were cut with a scalpel blade and sent for mass spectrometry analysis.

## Results

**1.** *cep290*$^{-/-}$ zebrafish mutants do not exhibit obvious external phenotypes

Aiming to investigate the role of *Cep290* in zebrafish development, we obtained the *cep290* ENU generated allele sa1383 from the Sanger mutant collection. A nonsense point mutation in this specific allele results in the presence of a premature stop codon at the position 1844 of the coding sequence. This mutation occurs at the C-terminus of the Cep290 protein, a region connected with microtubule binding (Drivas et al., 2015) (Fig. 9 A-B). Zebrafish *cep290*$^{-/-}$ mutants do not display obvious external phenotypes related to body axis at both larval and adult stages and they survive to adulthood (Fig.9 C-C'). Adult *cep290*$^{-/-}$ mutants are able to normally reproduce. A paralogue search was made in the Ensembl database, which did not identify any gene paralogues.

This observation is contradictory to the *cep290* morphant phenotype, which exhibits a curly body axis when a high morpholino dose is applied (Baye et al., 2011); however it is in agreement with a report suggesting the absence of phenotype in the *cep290*$^{sa1383}$ mutant allele (Kok et al., 2015). In conclusion, the *cep290*$^{sa1383}$ zebrafish mutant phenotype differs from the morphant phenotype as will be extensively described later.

**2.** *cep290*$^{-/-}$ mutants do not display ciliogenesis defects

To test how the *cep290* mutation affects ciliogenesis, we investigated cilia morphology in 5 dpf old *cep290*$^{sa1383}$ homozygous mutants. Cilia in all the tissues examined, including the nasal pit, the ear (both maculae and cristae) and the lateral line were not affected (Fig.10 A-C'). This observation is in disagreement with cell culture ablation of *cep290,* which reduces ciliogenesis (Kim et al., 2008).

In conclusion, cilia in sensory organs seem to be unaffected in the *cep290* homozygous mutant, which explains the fact that mutants are able to survive to adulthood without developmental defects.

**3**. *cep290*$^{-/-}$ mutants do not display retinal dystrophy

The most common symptom in patients with mutations in *CEP290* is retinal dystrophy leading to blindness, known as LCA (Burnight et al., 2014). The mouse *Cep290* knockout is characterised by absence of connecting cilia in photoreceptor outer segments, indicating that CEP290 is essential for cilia formation in the photoreceptors. In order to investigate the role of Cep290 in the zebrafish retina, Epon sections were prepared at 3 months of age, surprisingly revealing the absence of retinal degeneration (Fig.11 A-B). In addition to the morphological analysis of the retina, rhodopsin localisation was assessed at 5 dpf. Consistent with histological analysis, rhodopsin was normally localised in photoreceptor outer segments (Fig.11 C, C'). The absence of retinal phenotype in both adult and larval stages, led to the hypothesis that the photoreceptors could regenerate, as previously observed in the *bbs2*$^{-/-}$ adult retina (Chapter I). Proliferation in the adult retina was examined at 3 months of age using the PCNA proliferation marker. This did not reveal any obvious difference in the proliferation rates between the homozygote mutants and their siblings in the outer nuclear layer of the retina (Fig.11 D-E).

We conclude that these data reveal the absence of retina dystrophy phenotype in the *cep290*$^{-/-}$ mutant zebrafish, which is contradictory to the human patient symptoms harbouring mutations in *CEP290*, where blindness and retinal dystrophy are the most characteristic phenotypes.

**4.** *cep290*$^{-/-}$ mutants have abnormal number of otoliths at larval stages

The otic vesicle is a structure that can be easily discerned in the developing zebrafish embryo by 18 hpf (Bever & Fekete, 2002). Cep290 has not been previously associated with otolith morphogenesis but we unexpectedly found

that *cep290*$^{-/-}$ mutants frequently display more than two otoliths in their otic vesicle at 1.5 dpf (Fig.12 A-B). More specifically, at this developmental stage only two otoliths should appear (Malicki et al., 1996). The anterior otolith is tethered in the utricular macula while the posterior otolith is tethered in the saccular macula. The lagena develops at later developmental stages. In contrast to the wt larvae, in the otic vesicle of the *cep290* homozygous mutants, three otoliths are present in the majority of the embryos (Fig.12 A'). The third otolith is most often observed at the posterior part of the vesicle, near to the saccular macula and persists until 2 dpf. At this stage, all the third otoliths in the *cep290*$^{-/-}$ mutant embryos are eliminated indicating that they are most probably fused to the posterior otolith, as there is not known mechanism of elimination of untethered otoliths in the otic vesicle. Only a small fraction of wt siblings have more than two otoliths at 1.5 dpf (Fig.12 B).

Abnormal otolith number has been associated with vestibular and balance defects in the zebrafish embryo (Whitfield et al., 1996). The presence of more than two otoliths led us to the hypothesis that *cep290*$^{-/-}$ larvae have vestibular or balance defects. At 5 dpf no characteristic balance defect was observed, as the larvae were able to maintain their upright position during swimming. A characteristic balance defect in zebrafish is accompanied by tilted position of the body during swimming (Baxendale & Whitfield, 2016; Chatterjee et al., 2015). The larvae swimming pattern was also observed in the Viewpoint tracking system and was compared to their non-mutant siblings. No difference in the speed or the distance swam during the 10 minutes of the assay was observed (Fig.12 C).

To test the behavioural response of 5 dpf larvae in the presence of a stress stimulant, we used sodium chloride in the embryo medium for a small time period before tracking their swimming behaviour (Fig.12 D, D'). This assay is using a hyperosmotic shock to trigger cortisol production, a hormone indicative of stress (Clark, Boczek, & Ekker, 2011). The presence of 250mM of NaCl caused a significant increase in the swimming activity of the *cep290* homozygous mutants compared to their wt siblings, indicating that the homozygous larvae are hyperactive and their cortisol levels are presumably increased in the presence of increased salinity (Fig.12 E).

In conclusion, these results indicate an early role for Cep290 in otolith biogenesis, which could be correlated with an early hyperactivity phenotype observed at 5 dpf homozygous mutant larvae.

**5.** *cep290*$^{-/-}$ adult s are hyperactive and display inner ear polarity defects

In order to investigate whether the hyperactivity defect persists till adulthood, adult *cep290* homozygous mutants and their siblings of 3 months of age were imposed in a swimming behavioural test (Fig.13 A, A'). During this test, the lights of the Viewpoint system were constantly on and only the swimming behaviour of the fish was tracked under normal conditions (no addition of chemical compounds or light changes). Comparison between the homozygotes and their siblings revealed a striking difference in the distance travelled during 10 minutes of tracking, enabling us to characterise the *cep290*$^{-/-}$ mutants as hyperactive (Fig.13 A-B). For most of the assay duration the *cep290*$^{-/-}$ mutants were found swimming with high speed (red lines) in contrast to their wt siblings (Fig.13 B).

This prominent hyperactivity phenotype led us to the examination of polarity defects in the inner ear epithelium as the inner ear is one of the most characteristic examples of planar cell polarity. Hair cells develop actin rich stereociliary bundles, which are uniformly oriented (H. May-Simera & M. W. Kelley, 2012) and each bundle has a primary cilium known as kinocilium. It has been shown that ablation of *Ift* genes results in misrotated sensory hair cells in the inner ear (Jones et al., 2008). Not surprisingly, mislocalisation of the kinocilia in some of the hair bundles of the inner ear was observed (Fig.13 C-D) in agreement with polarity defects in the ear of mouse knockouts of transition zone proteins (Abdelhamed et al., 2015).

In summary, these data show the progressive hyperactivity phenotype from larval stages to adulthood in *cep290* adult homozygotes, which could be possibly attributed to defective polarity in the inner ear epithelium.

**6.** Absence of Cep290 leads to otolith structural defects

Dissection of the inner ear of *cep290*$^{-/-}$ adults enabled the observation of the otoliths (Fig.14); biomineralised structures consisting of carbonate crystals and a small fraction of proteins. Otoliths are enclosed in three distinct chambers in the zebrafish ear, known as utricle, sacculus and lagena and lie above ciliated sensory epithelia (Lundberg, Xu, Thiessen, & Kramer, 2015; Malicki et al., 1996). Closer inspection of the three *cep290* homozygous mutant zebrafish otoliths, revealed the abnormal structure of the one of the three otolithic types, known as sagitta, the utricular otolith (Fig.14 A-C'). The *cep290* homozygous derived sagittae displayed jagged edges with unorganised crystal structure in the centre and edges of the otolith (Fig.14 B', C'). In contrast, the wt derived sagittae displayed smooth appearance with round edges (Fig.14 A, A'). SEM

analysis revealed the unorganised crystal arrangement in the centre and the edges of the sagittal otoliths of *cep290*$^{-/-}$ adults. This phenotype resembles the phenotype produced by *starmaker* knockdown, which leads to the formation of large calcite crystals in the otoliths. The affected otoliths with a star shape are still made of the polymorph aragonite, while the cubic crystal appearance otoliths have transitioned to the calcitic polymorph, suggesting that *starmaker* absence is disrupting the carbonate polymorph of the otoliths (Sollner et al., 2003). In contrast with the sagittal otoliths, the other two otoliths, known as lapillus and asteriscus did not seem to be structurally affected (Fig.14 D-E'), which could be attributed to the fact that the crystal polymorph type differs between the otoliths (Ichikawa, Shimomura, Yamada, & Ohkubo, 2003).

To test the possibility that the otolith phenotype is progressive, we examined older individuals at 3 years old. Sagittal otoliths of the older zebrafish were even more severely affected (Fig.15 B, B'). They exhibited more unorganised crystal arrangement on their surface, which was extended further than the otolithic centre and edges and occupied the whole otolith surface.

Overall, mutations in *cep290* cause a progressive otolith phenotype, which affects the arrangement of sagittal otolith crystals. In conclusion, it is shown for the first time that the ciliary transition zone protein Cep290 is involved in crystal bio mineralisation of the sagittal otoliths after the examination of otoliths deriving from two individual zebrafish generations.

The implication of otolith defects in human ciliopathies is not well established, there are however clinical data supporting that both Bardet-Biedl and Joubert Syndrome patients manifest balance and coordination related symptoms. More than 50% of the BBS patients are unable to walk on a straight line and this symptom cannot be attributed to cerebellar defects, raising the possibility that vestibular defects might be the source of this problem. Not many details exist regarding JBTS patients as they manifest severe phenotypes including cerebellar hypoplasia making the diagnosis difficult. Our results, regarding the role of transition zone proteins in otolith morphogenesis could give novel insight into the role of cilia in the ciliopathy patient encountered vestibular defects.

**7.** Proteomic analysis of the *cep290* mutant sagittal otoliths

As otoliths consist of calcium carbonate crystal polymorphs and a small fraction of proteins we sought to identify potential differences in the proteomic profile of the *cep290* homozygous mutant sagittal otoliths compared to wt derived otoliths.

The otolithic proteins derived from adult sagittal otoliths were extracted and ran on an SDS PAGE gel (Fig.16 A). Proteins from the mutant zebrafish exhibited quite different proteomic profile compared to the wt ones (Fig.16 A second lane). We observed differences in the following molecular weights: 240, 120, 55-60 and 45kDa. Although differences in these molecular weights were observed, the most prominent and consistent difference was the one at 45kDa. The *cep290* $^{-/-}$ otoliths have reduced levels of this specific otolithic protein compared to their non-mutant siblings. The identified protein is known as Coch (Fig.16 B). Noteworthy, the molecular weight of Coch is 60kDa we however observed the difference at 45kDa. Inspection of the mass spectrometry derived peptide analysis revealed peptide coverage only after the cleavage site of the protein, accounting for 81% of the protein length after the cleavage site (Fig.16 C). This observation indicates that the difference is specific for the cleaved form of Coch at 45kDa. The protein band observed at the same molecular weight in the supernatant does not correspond to Coch (Fig.16 A second panel), clarifying the fact that the protein only exists in the insoluble fraction of the otolith protein preparation, where the levels of the protein are reduced. This observation could suggest that Coch is unable to be incorporated in the otolith matrix and remains in the endolymphatic fluid of the ear or alternatively the *cep290* mutation leads to defective secretion of the protein.

In summary, these data reveal the differences in the proteomic profile of wt and *cep290* mutant derived sagittal otoliths. We show that the cleaved form of Coch, an ear specific and deafness related protein is reduced in the *cep290*$^{-/-}$ sagittal otoliths. The reduced Coch levels are possibly contributing in the defective sagittal otolith biomineralisation of the *cep290* $^{-/-}$ mutants. Interestingly, no Coch otolith localisation has been previously reported, possibly due to different protocols applied for the otolith protein extraction. How Coch is associated with otolith structure is currently unknown.

**8.** The *cep290* mutation leads to reduced Coch levels

Analysis of the *cep290* mutation in zebrafish led us to the construction of a model aiming to explain the role Cep290 in the adult zebrafish ear.

The data suggest that Coch is essential for the maintenance of the otolithic structure during adulthood, although no previous report associating Coch with otoliths or the otolithic membrane exists. Coch is a secreted protein and it is expected that in wt individuals is being released into the endolymphatic fluid of the ear. It is possible than Coch is being incorporated into the otolithic protein

matrix forming a complex with the otolithic proteins, which are responsible for the otolith growth and structure (Fig.17 A). When Coch normally presents in the endolymphatic fluid the crystal polymorph in the sagittal otoliths is aragonite. In contrast, the presence of the *cep290* mutation affects the Coch levels in the insoluble fraction of the otolithic proteins. This suggests that reduced amounts of Coch are being secreted in the ear lumen, leading to the hypothesis that Cep290 affects Coch secretion (Fig.17 B). Reduced levels of Coch in the *cep290*$^{-/-}$ mutant ear are causing the appearance of unorganized crystal structures of the sagittal otoliths, suggesting an impaired balance between the calcite and aragonite crystal polymorphs in the sagittae.

## Discussion

CEP290 defects have been associated with a wide spectrum of ciliopathies and phenotypes ranging from blindness to perinatal lethality (Coppieters et al., 2010). Animal models of *CEP290* mutations do not exhibit consistent phenotype, which makes it difficult to draw conclusions regarding the association between the genotype and phenotypic severity. Zebrafish knockdowns seem to produce a morpholino dosage dependent phenotype ranging from unaffected body plan to curly body axis (Baye et al., 2011). We analyzed the ENU generated *cep290*$^{sa1383}$ mutant allele resulting in a premature stop codon in exon 38 out of the 52 exons of the protein. No body plan defects were observed both during larval and adult stages. Additionally and in contrast to the tissue culture studies showing that depletion of *CEP290* results in defective ciliogenesis (Kim et al., 2008), cilia in the zebrafish mutants were not affected in all tissues examined. Although olfactory cilia seemed to be normal, the possibility that the ciliary neuron function is compromised cannot be excluded, as it was shown that hypomorphic *Cep290* mutations result in anosmia without defective olfactory cilia (McEwen et al., 2007). It is also shown that although *CEP290*/ *Cep290* mutations result in retinal dystrophy in human patients and animal models, *cep290* mutant zebrafish do not exhibit retinal degeneration. *cep290* morphants have normal retina histology and they do not exhibit defective visual responsiveness (Baye et al., 2011). The possibility that the specific zebrafish allele that we analyzed is hypomorphic cannot be excluded especially because the exon in which the mutation is occurring is prone to alternative splicing (Drivas et al., 2015). In agreement with absence of external phenotype in our *cep290* mutants, other labs have generated multiple *cep290* alleles, and they were unable to detect any obvious phenotype (unpublished data). Importantly the nonsense mutation of this specific allele occurs within the myosin tail region

of Cep290, which seems to be important in a vision specific role as it is partially deleted in the *rd16* mouse, which manifests retinal dystrophy. Another inconsistency regarding the Cep290 domain function is that the N-terminal region of the protein is sufficient to rescue the vision phenotype observed in the *cep290* zebrafish knockdown, suggesting that the N-terminal domains are important for visual function. The importance of the different Cep290 domains for visual function is unresolved, making the interpretation of the absence of the retina phenotype in the *cep290*$^{-/-}$ difficult.

Although no expected phenotypes were present in the *cep290* mutants, unique phenotypes were described. The appearance of ectopic otoliths in *cep290* homozygous larvae at 1.5 dpf resembles the phenotype found in PCM-1, *camk2g1* morphants (Kim et al., 2008; Rothschild et al., 2013), *iguana* and maternal zygotic *oval* mutants (Stooke-Vaughan, Huang, Hammond, Schier, & Whitfield, 2012; X. Yu, Lau, Ng, & Roy, 2011). The fact that otoliths form ectopically due to cilia motility defects cannot be excluded. Additionally, *cep290* homozygous mutant zebrafish display hyperactivity, which becomes apparent at 5 dpf and persists to adulthood. These defects possibly result from a combination of defective planar cell polarity in the macular ear epithelium, manifested by the misorientation of kinocilia and abnormal utricular otolith structure. Importantly, the structural defect is only observed in the utricular otoliths, possibly due to the different crystal polymorph composition of the otoliths. Proteomic analysis revealed that Coch levels are reduced in the insoluble fraction of the proteins present in *cep290*$^{-/-}$ mutant utricular otoliths, suggesting that the absence of Cep290 is leading to defective Coch secretion in the endolymphatic fluid. Consequently, the protein is not incorporated in the otolithic protein matrix. These results also suggest that Coch is important for the carbonate crystal arrangement in the utricular otoliths. Coch is potentially being secreted through kinocilia in the ear and is being assembled in the otolith organic matrix. Evidence of secretion through cilia has been reported. For example, enzyme-containing vesicles are secreted through *Chlamydomonas* flagella and are named ectosomes (Wood, Huang, Diener, & Rosenbaum, 2013). If secretion through cilia is the mechanism behind the defective otolith biomineralisation in the *cep290* homozygous mutants, then ectosomes would accumulate in the mutant cilia of the ear lacking the ability to be properly secreted. It is also notable that Coch levels in Meniere's disease patients are perturbed (Calzada, Lopez, Beltran Parrazal, Ishiyama, & Ishiyama, 2012). Meniere's disease patients suffer from vertigo and tinnitus (Havia, Kentala, & Pyykko, 2002), resembling the behavioral defects observed in the *cep290* homozygous mutants.

In summary, the study of a *cep290* zebrafish mutant reveals that the zebrafish model does not recapitulate the most commonly encountered human phenotypes; however, interestingly, it sheds light on a new function of Cep290 in otolith morphogenesis and maintenance. Our observations reveal that, unexpectedly, Cep290, a gatekeeper of the cilium known to localize to the transition zone at the cilia base is a determinant of otolith structure in the zebrafish ear.

# Figures

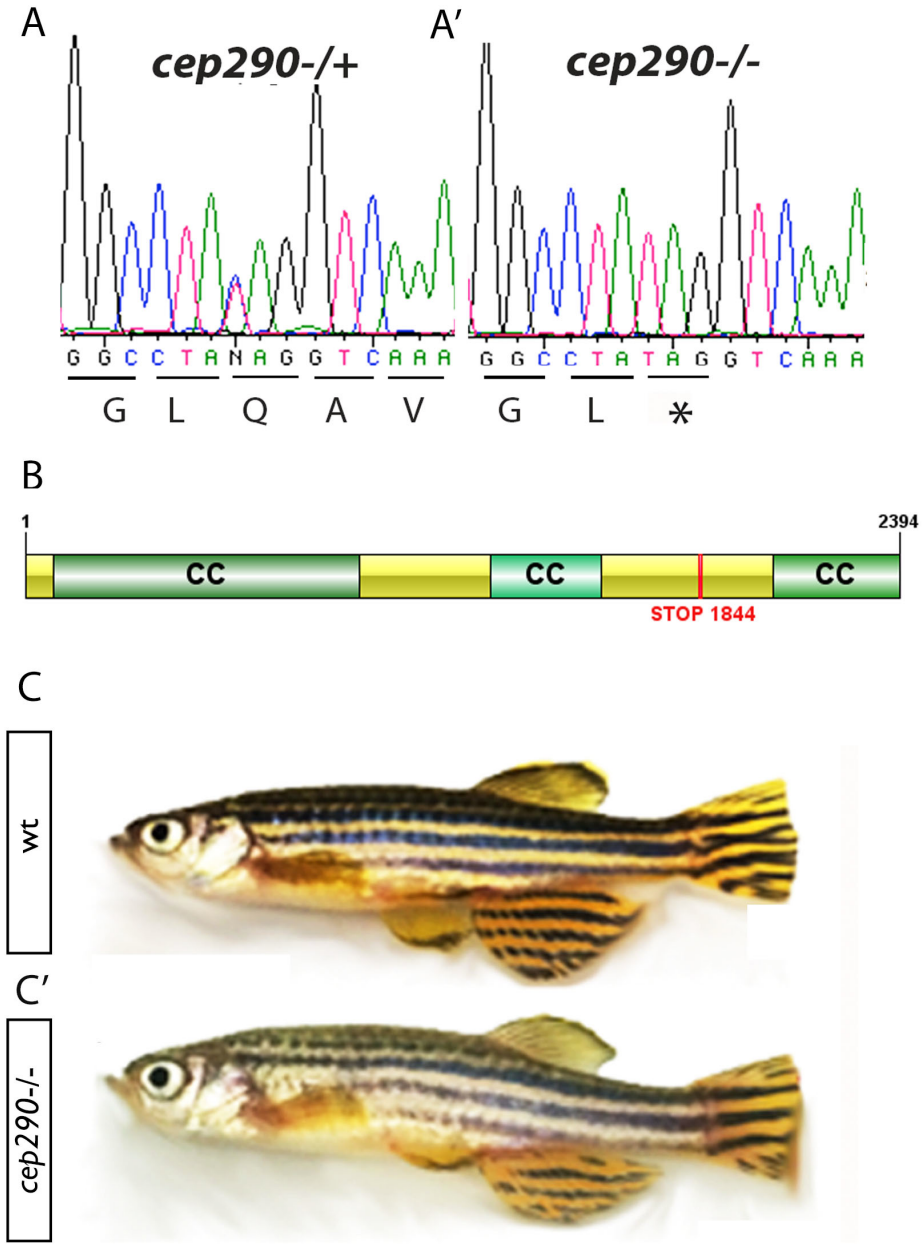


**Fig.1 Location of the *cep290* mutation and external phenotype of adult zebrafish**. Representative sequences of heterozygous (**A**) and *cep290* homozygous (**A'**) mutant sequences. The asterisk indicates the presence of a stop codon. **B**. Schematic representation of the location of the *cep290* mutation at the amino acid 1844 out of the otal 2394 amino acids. **C. C'**. Images of adult wt (**A**) and *cep290*$^{-/-}$ mutants (**A'**) at 3 months of age. No obvious external phenotype is observed**.**

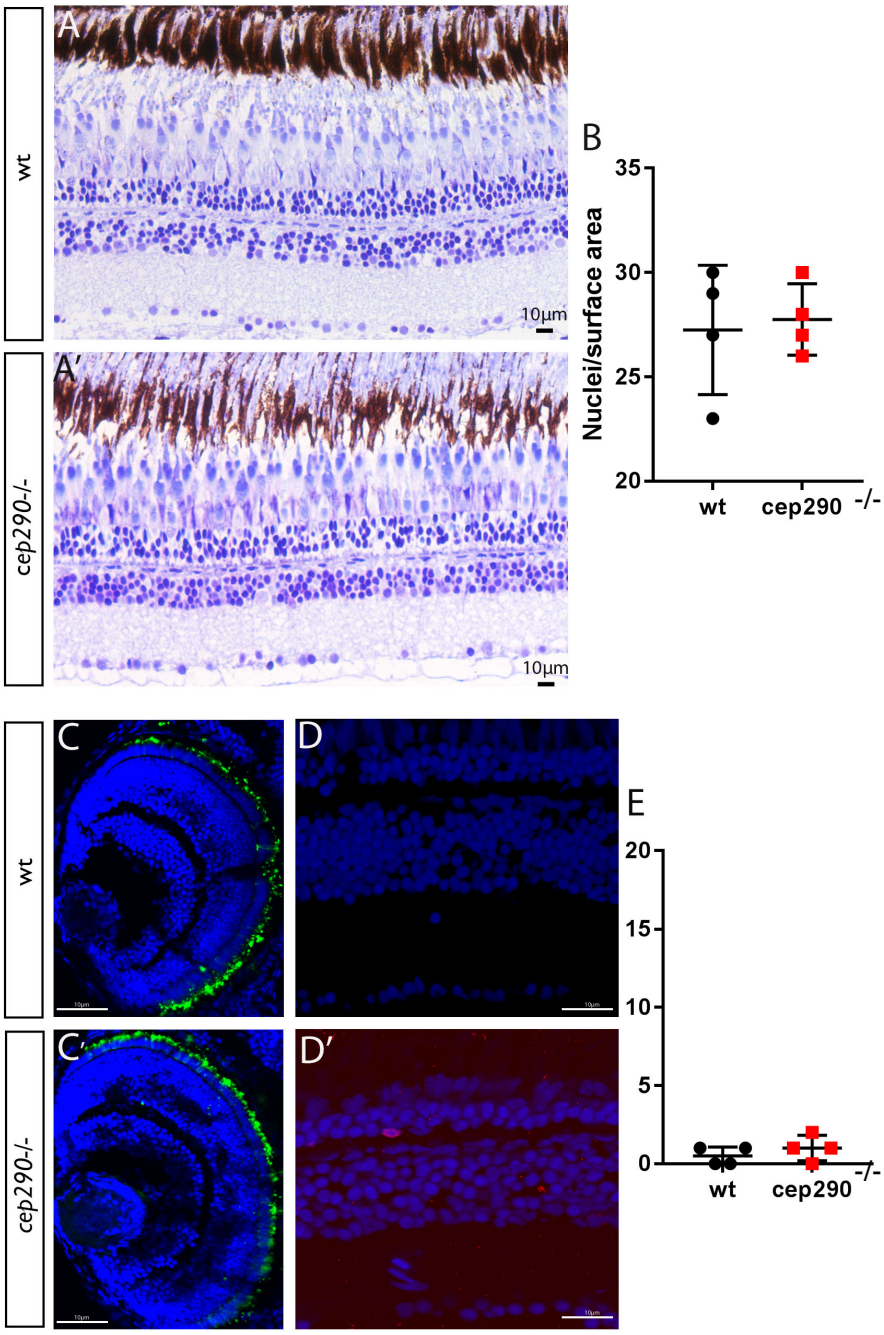


**Fig.2 Retinal analysis of the *cep290* mutant**. **A, A'**. Epon transverse plastic sections through the retina of wt (**A**) and *cep290*$^{-/-}$ fish (**A'**) stained with Toluidine blue at 3 months of age. **B**. Quantification of the nuclei number per 10x6mm square surface area of the outer nuclear layer (n=4 retinae, measurement of 1 section/retina, non-significant, t-test, p=0.7868). **C, C'**. Rhodopsin localization in the outer segments of wt (**C**) and *cep290*$^{-/-}$ (**C'**) 5 dpf larvae. **D, D'**. PCNA staining of proliferating cells in the outer nuclear layer of wt (**D**) and *cep290*$^{-/-}$ adults at 3 months and quantification of cells proliferating per section **E**. The analysis is based on two individual fish and 2 sections were analysed per fish (n=4, non-significant, t-test, p=0.3559). Blue: DAPI, green: anti-zpr3 (rhodopsin), magenta (PCNA). Scalebars are 10µm.

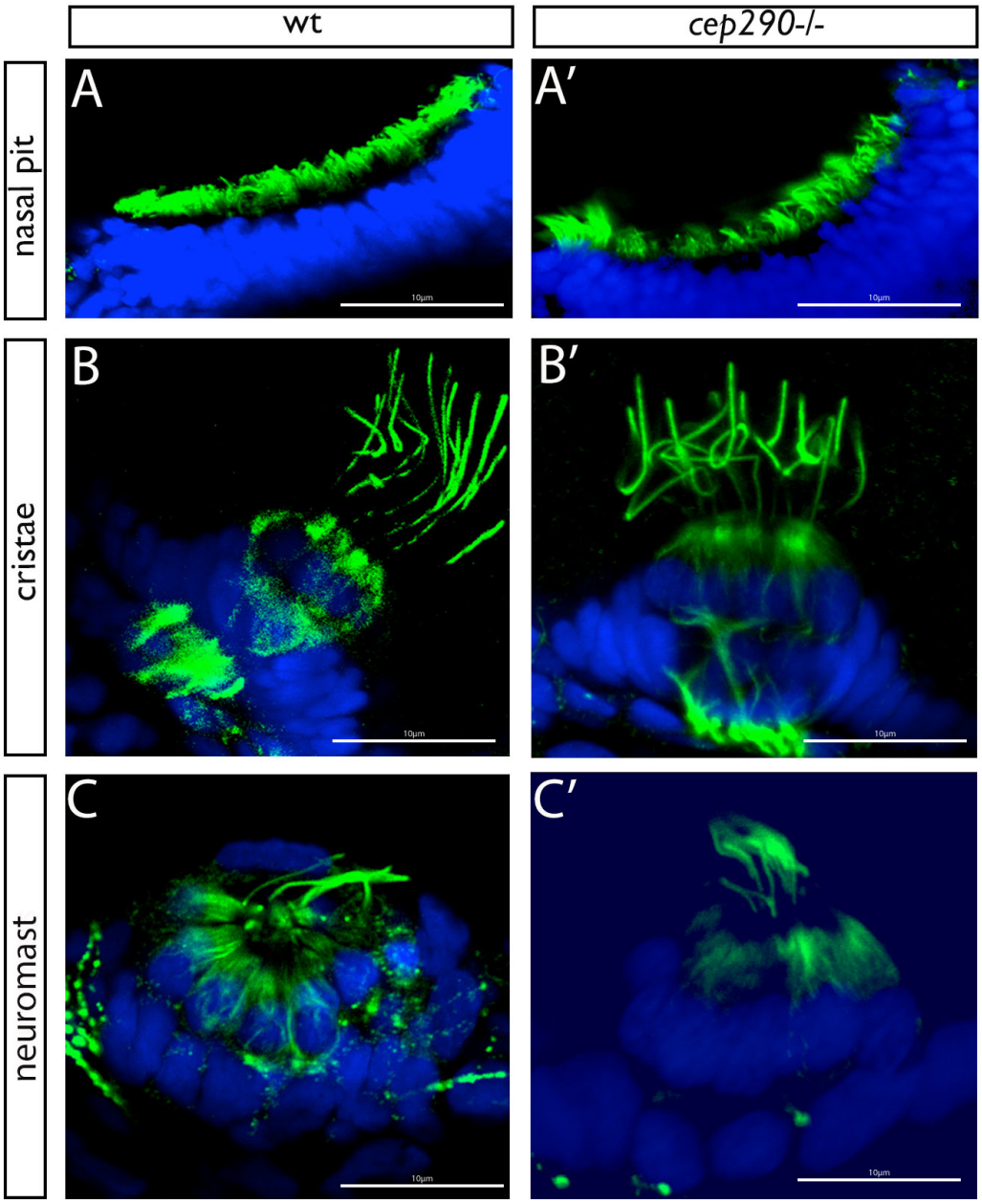


**Fig.3 Analysis of ciliogenesis in the *cep290*$^{-/-}$ mutants**. **A, A'**. Olfactory cilia staining, **B, B'**. Ear cristae cilia staining and **C, C'**. Lateral line neuromast cilia staining. Blue: DAPI, green: anti-acetylated tubulin. Scalebars are 10µm.

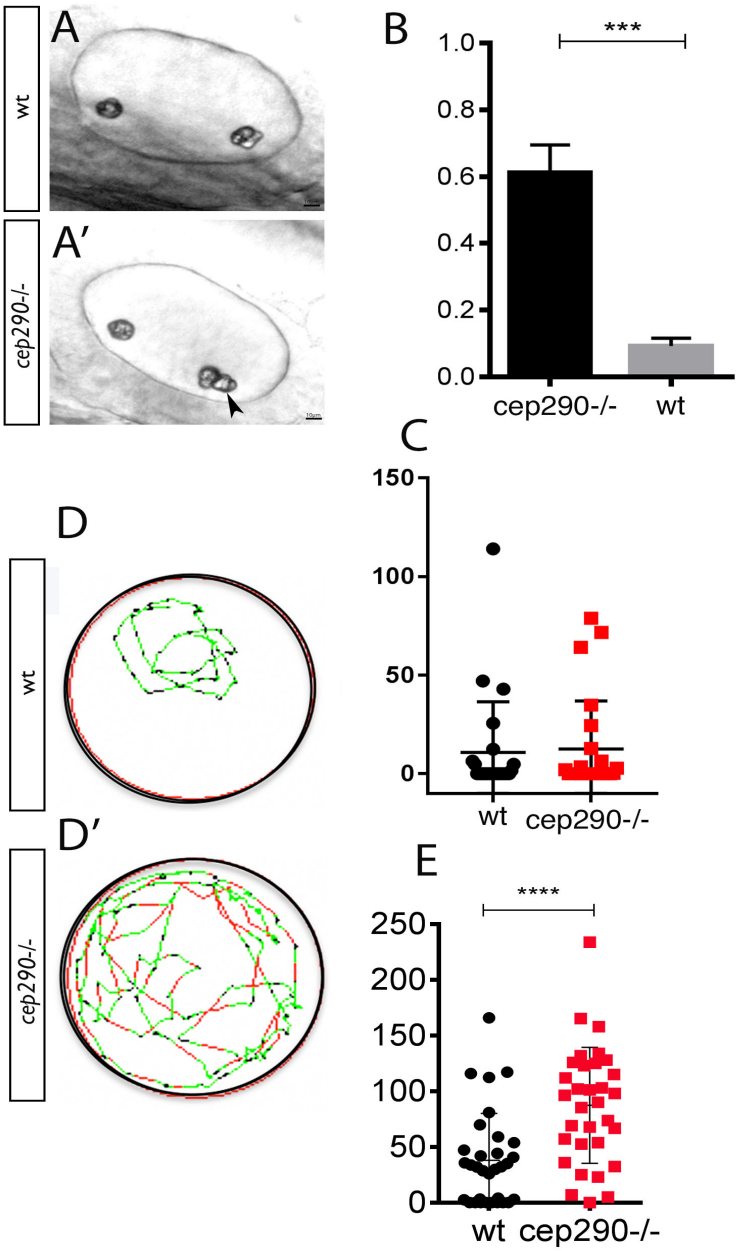


**Fig.4 Otolith defects and behavioural analysis at larval stages**. **A, A'**. Images of the otoliths in the otic vesicle of wt and *cep290*$^{-/-}$ embryos at 1.5 dpf. Note the appearance of a third otolith in the *cep290*$^{-/-}$ otic vesicle as indicated by an arrowhead. Scalebars are 10µm. **B.** Quantification of the appearance frequency of 3 otoliths in *cep290*$^{-/-}$ and wt siblings at 1.5 dpf (measurements from 3 individual crosses, n=200 larvae, t-test, p= 0.0005). **D, D'**. Representative swimming tracks of the swimming behaviour of 5 dpf larval zebrafish after the addition of a stressor (250mM NaCl). **E**. Quantification of the swimming distance travelled during the 10 minutes of the test for wt and *cep290*$^{-/-}$ larvae at 5 dpf after incubation in the hyperosmotic medium (n=32 larvae, 2 individual crosses, t-test, p<0.0001) and **C**. swimming distance travelled without the addition of the stressor in the medium (n= 24, 2 individual crosses, non-significant, t-test, p=0.5413).

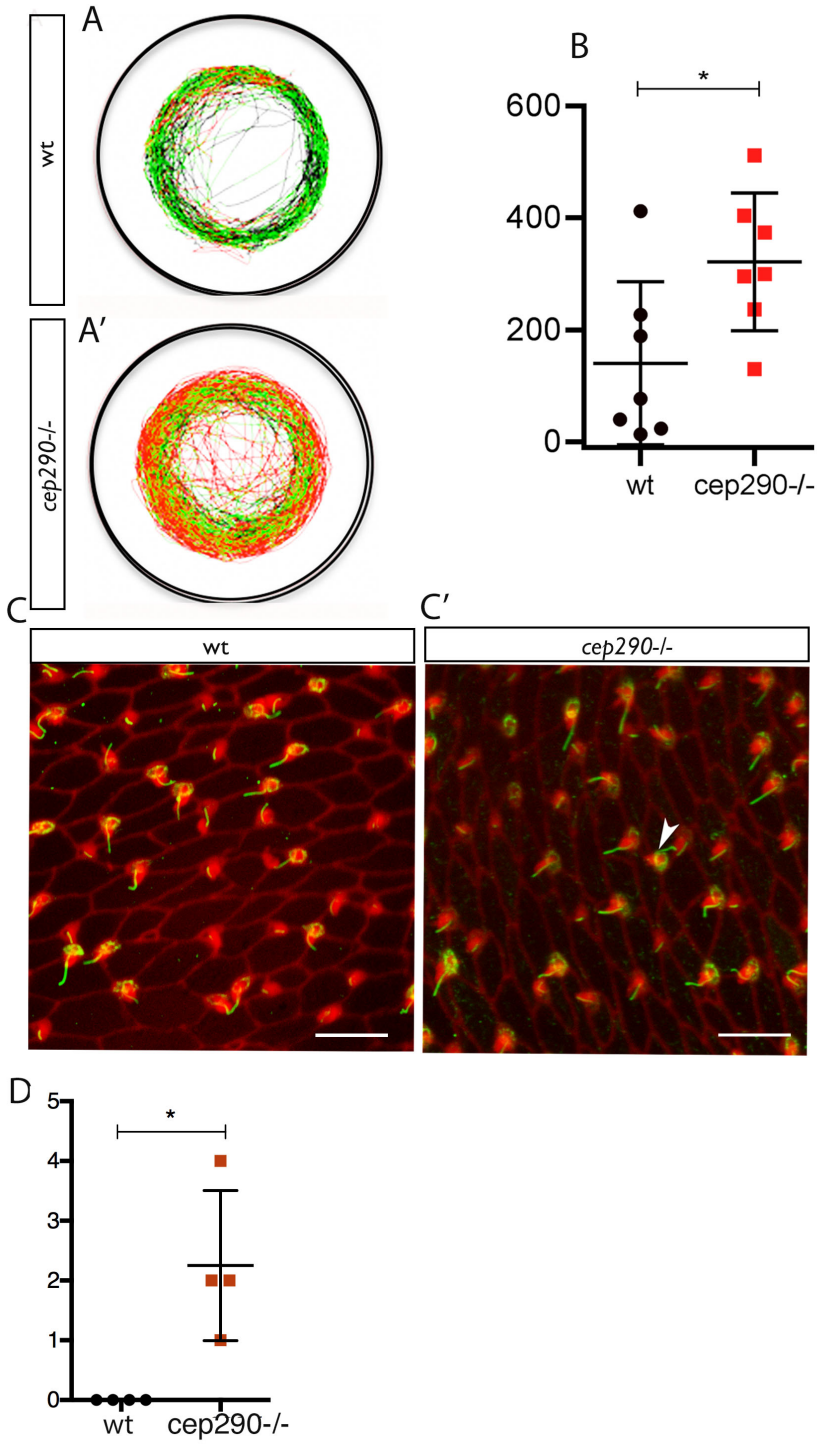


**Fig.5 Polarity defects in the ear epithelium of *cep290* homozygous mutants and adult hyperactivity behaviour**. **A., A'**. Swimming tracks of wt and *cep290*$^{-/-}$ adults at 3 months of age. The *cep290*$^{-/-}$ fish display hyperactive swimming behaviour quantified in **B**. as distance travelled during the 10 minutes of recording (n=7, t-test, p=0.027). **C, C'**. Utricle macular epithelium stained for kinocilia (acetylated tubulin: green) and stereocilia (phalloidin: red). Note the appearance of a misoriented kinocilium in the mutant epithelium pointed by an arrowhead. According to the polarity in this tissue, the kinocilium (green stained cilium) should extend from the posterior end of the hair bundle (ellipsoid green stained structure) but in contrast it extends from the anterior part of the bundle. In the wt epithelium all kinocilia extend from the posterior part of the

hair bundle. Scalebars are 5um. **D**. Quantification of the misoriented kinocilia in wt and *cep290*$^{-/-}$ maculae. (n=40 hair bundles, t-test, p=0.05)

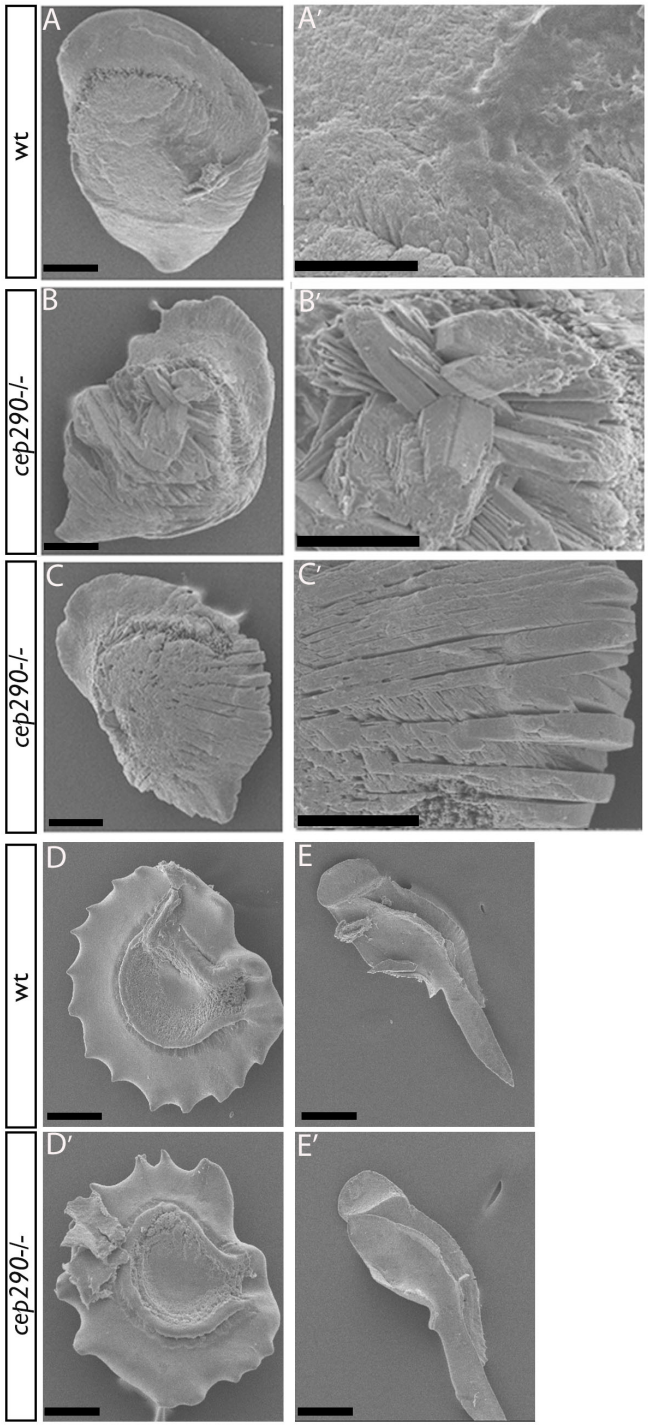


**Fig. 6 Adult otolith defects. A-C'**. SEM images of otoliths derived from wt and *cep290*$^{-/-}$ zebrafish at 2 years of age. Note the rough edges of the crystals derived from the centre of the otolith (**B'**) or the edges (**C'**) of the *cep290*$^{-/-}$ sagittae (**B'**, **C'**) compared to the smooth appearance of wt otoliths (**A'**). **D-E'**. SEM images of asterisci (note that debris exist on the surface of the *cep290*$^{-/-}$ asteriscus)(**D**, **D'**) and lapilli (**E**,**E'**) derived from wt and *cep290*$^{-/-}$ adults show no morphological differences. Scalebars are 200µm for A-C and 50µm for A'-C'.

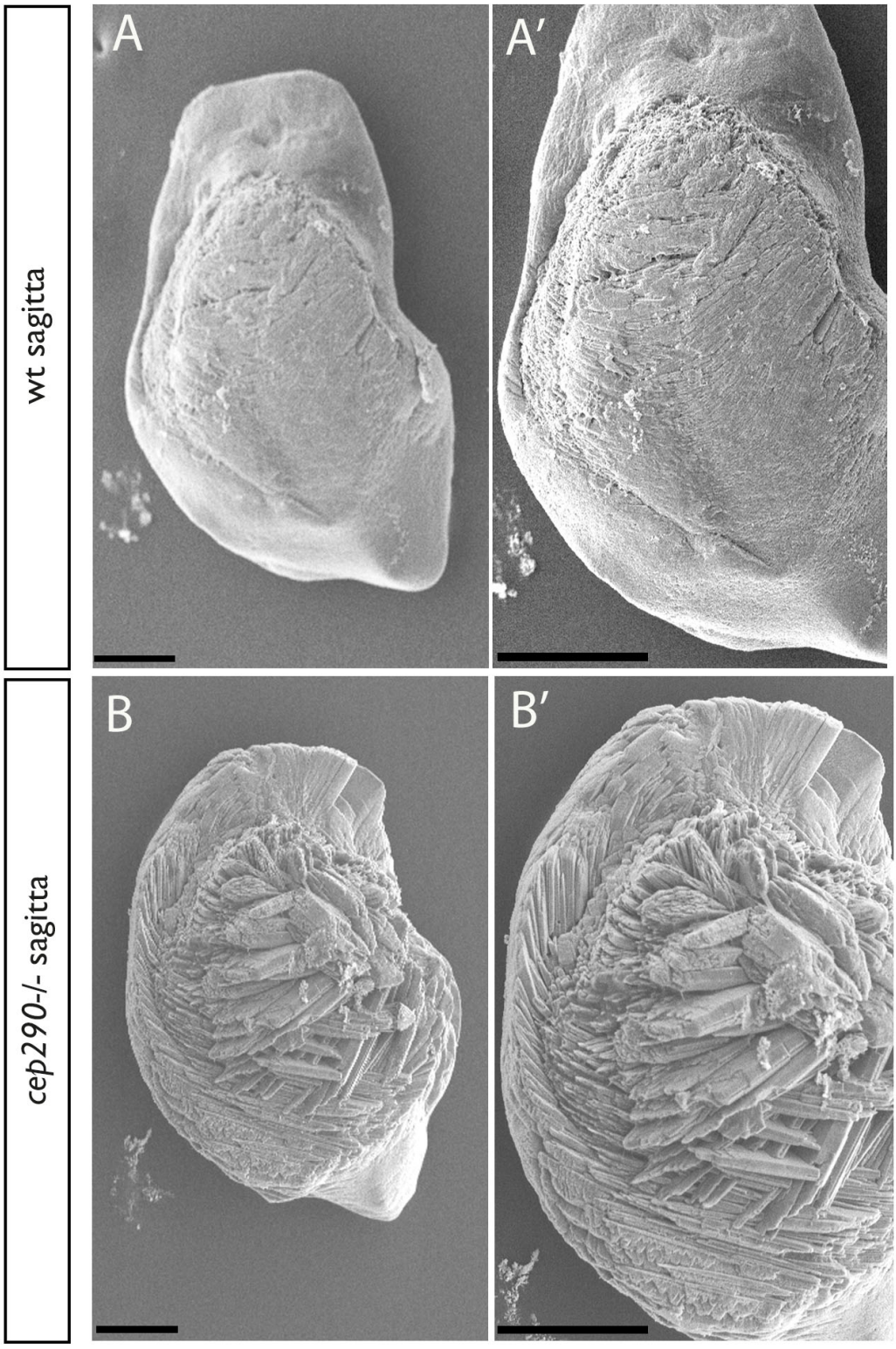


**Fig.7 Otoliths defects are deteriorated in sagittae derived from 3 year old zebrafish**. **A, A'**. SEM of wt derived sagittae and **B, B'**. Sagittae derived from *cep290*$^{-/-}$ 3 year old zebrafish. Scalebar is 200µm

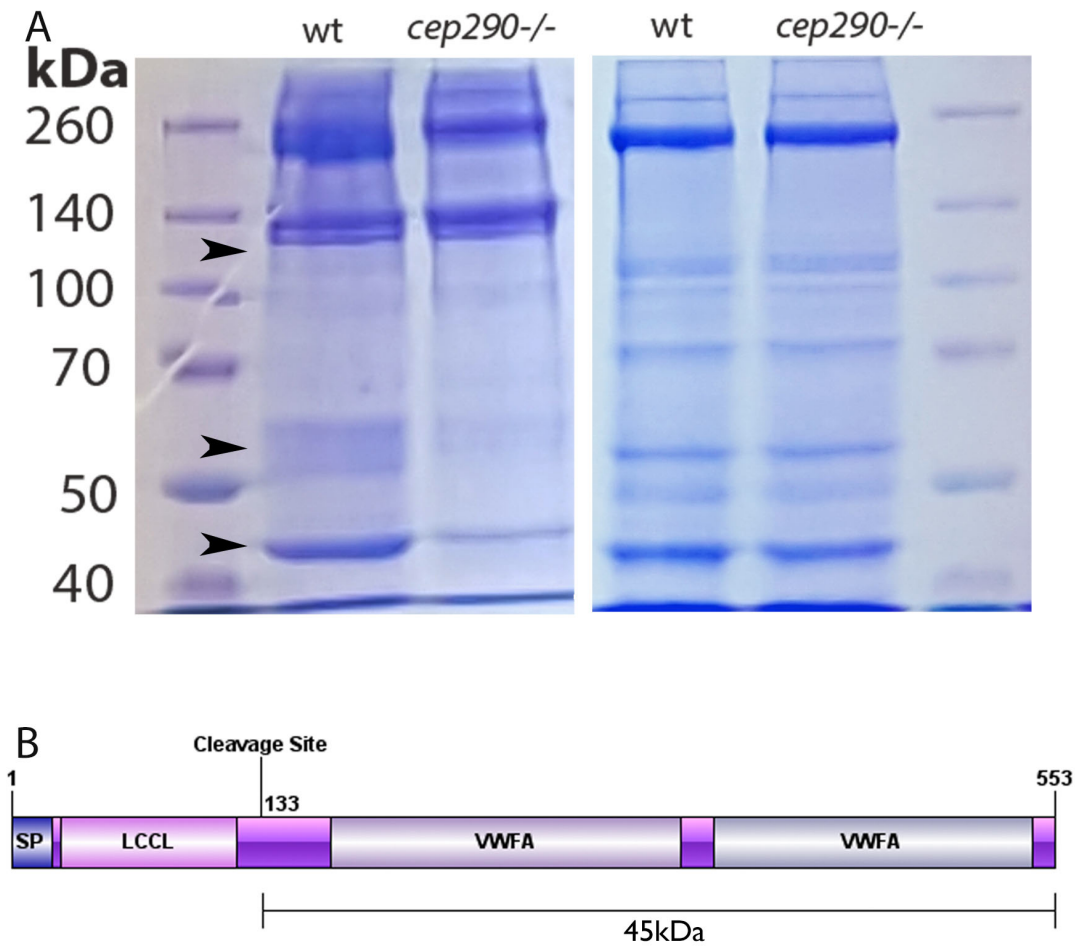


**Fig. 8 Proteomic analysis of adult sagittae**. **A**. 10% SDS-PAGE gel of sagittal otolith proteins stained by Coomasie Blue. The first panel (left) represents the non-soluble fraction of the protein sample while the second panel corresponds to the soluble fraction of it. Note the difference between the wt and *cep290*$^{-/-}$derived proteins at the 45kDa molecular weight. Other observed differences are pointed by arrowheads **B**. Schematic representation of the protein domains of the corresponding to the 45kDa difference protein, Coch. Coch length is 45kDa after it is cleaved at the 133 amino acid cleavage site (experiment was repeated 3 times) **C.** Peptide coverage of Coch. The cleavage site is indicated.

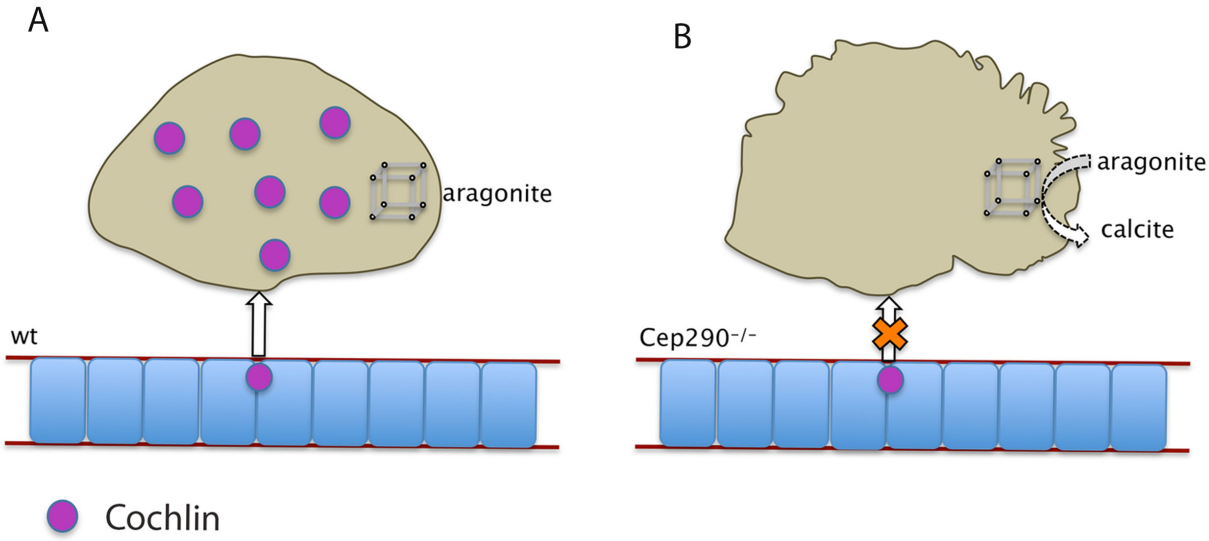


**Fig.9 Coch secretion model in the absence of Cep290 in the ear. A**. In the presence of Cep290, Coch is able to be secreted in the endolympatic fluid of the utricle lumen and can be incorporated in the otolithic protein matrix. The predominant crystal polymorph in the wt sagittae is aragonite. **B**. In the absence of Cep290, Coch secretion is presumably inhibited and Coch vesicles are accumulated in the apical membrane of the cells with the inability to be secreted in the endolympathic fluid. This secretion defect is possibly involved in the abnormal crystal arrangement in the *cep290*$^{-/-}$ derived utricles and it is furthermore possible that the ratio of aragonite/ calcite crystal polymorphs is disrupted.

# CHAPTER IV

# ANALYSIS OF ALMS1 IN THE ZEBRAFISH MODEL

## Introduction

Alstrom Syndrome (OMIM 203800) is the manifestation of mutations in a single gene, *ALMS1*. Notably, the phenotype of ALMS partially overlaps with the BBS phenotypes, although both display unique characteristics and are characterised by differences in gene expression (Hostelley, Lodh, & Zaghloul, 2016). The major features of ALMS include rod cone dystrophy, cardiomyopathy, hearing loss, obesity and diabetes 2 mellitus. Mutations found in ALMS patients include frameshift, nonsense variations and a chromosomal translocation. Most commonly, the mutations occur in exons 8, 10 and 16 of the *ALMS1* gene (J. D. Marshall, Beck, Maffei, & Naggert, 2007).

ALMS1 is essential for maintenance of sensory functions, as Alstrom patients exhibit retinal dystrophy one week after birth and are characterised by low vision at one year of age. Patients are additionally characterised by a degree of hearing loss by age seven, which can progress to deafness (J. D. Marshall et al., 2007). Mutations in *ALMS1* also lead to compromised cardiac function, as two thirds of the patients manifest cardiomyopathy that can occur during infancy due to defective cardiomyocyte differentiation (Louw et al., 2014; Shenje et al., 2014). Furthemore, dilated cardiomyopathy is known to cause cardiac enlargement in human patients, leading to abnormal blood volume pumping in the heart, as the heart contractions are defective (Ferrans, 1989; S. M. Park et al., 2009).

The role of the ALMS1 protein is unknown and distinct domains span the length of the protein. The human protein domains include a polyglutamic acid, polyalanine, tandem repeat, leucine zipper, serine rich and an ALMS motif domain at the C-terminus of the protein. The ALMS motif exhibits similarity to the human uncharacterised protein C10orf90, while another centrosomal protein, KIAA1731 also contains this specific motif (Knorz et al., 2010). These observations suggest that the ALMS motif contributes to the centrosomal localisation of these proteins, as all three of them localise to the centrosomes. The second very characteristic domain of the human ALMS1 protein is a very large tandem repeat domain accounting for almost half of the protein length, which consists of 34 repetitions of 47 amino acids (Hearn et al., 2002).

ALMS1 localizes at the centrosomes and the cilia base both in cultured human cells and mouse neuronal cell culture (Hearn et al., 2005; Heydet et al., 2013). It has been additionally shown that ALMS1 isoforms are related to the recycling endosome pathway (Collin et al., 2012); while it was recently shown ALMS1 interacts with Hippo pathway components (Couzens et al., 2013).

ALMS mouse models were generated using gene trap based genetics. The specific mutation characterised occurred in intron 13 and homozygotes exhibited obesity, with bodyweight significantly differing from wt littermates between 8 and 12 weeks of age. Additionally, *Alms1* homozygous mutants manifested cochlear and retinal degeneration, with rhodopsin mislocalization in the outer nuclear layer of the retina (Collin et al., 2005). A spontaneous *Alms1* mutation variant occurring in mice is found in the *fat aussie (foz)* strain. The specific mutation is an 11 base pair deletion in exon 8 and results in obesity and bodyweight related changes, which first become observable at 12 weeks of age. Additionally, homozygote males are infertile (Arsov et al., 2006). It has been also reported that *foz/foz* homozygotes display reduced number of cilia in their hypothalamic and hippocampal neurons after 3 weeks of age (Heydet et al., 2013). Another ALMS model is the *Alms1* $^{L2131X/L2131X}$ mutant that was generated by ENU mutagenesis and results in a truncated protein at exon 10. Homozygotes increase their body weight faster compared to their wt littermates between weeks 7 and 10. They are additionally characterised by rhodopsin mislocalization and dilated kidney tubules (G. Li et al., 2007). In conclusion, it becomes apparent that all three ALMS mouse models recapitulate to a certain degree the human phenotypes (Shenje et al., 2014).

No detailed description of ALMS model in zebrafish is currently reported, there is however a report comparing the pancreatic cell defects in *alms1* and *bbs* zebrafish knockdowns. This study reveals that β-cells specifically are those affected in the *alms1* knockdown pancreas in contrast to the *bbs* knockdowns which show a general defect in the pancreatic progenitor pool (Lodh, Hostelley, Leitch, O'Hare, & Zaghloul, 2016).

The absence of a zebrafish model for the *alms1* mutation as well as its largely unknown function triggered the study of an *alms1* zebrafish mutant. We characterised an *alms1* zebrafish mutant, harbouring a nonsense mutation in exon 4 and observed that homozygous *alms1* mutant larvae exhibit body axis curvature, a phenotype characteristic of cilia mutants (Leventea et al., 2016). We also observed the absence of olfactory cilia in the nasal pit of the *alms1* homozygotes, and by 6 dpf mutant larvae are characterised by enlarged heart ventricles and reduced heartbeat rate compared to their siblings. We

furthermore, analysed the Hippo pathway activity in the larval hearts and observed reduced activity of the Hippo pathway transcription product, BIRC2, suggesting that the Hippo pathway might be involved in the increased heart size of the *alms1*$^{-/-}$ mutants.

## Materials and Methods

Microscopy

Pictures of live larvae were obtained at 5dpf. Wt and homozygous *alms*1 larvae were anaesthetized in 2% Tricaine in E3 media (as previously described in Chapters II and III), positioned in 3% methylcellulose on a microscope slide and pictures were taken using a Zeiss Axiozoom V.16 microscope at 26x magnification.

Immunohistochemistry

Cilia staining was performed using mouse anti- acetylated-tubulin (1:500 dilution) as previously described. Similarly, rhodopsin staining was performed using anti-zpr3 antibody (1:500 dilution) for cryosections of the retina at 5dpf as previously described.

Heart measurements

Heart volume measurements were performed at 6 dpf larval stage. Homozygous and non-mutant *alms1* siblings were anesthetized using 2% Tricaine in E3 media in pairs for one minute, positioned with the lateral side up on glass microscopy slides and mounted using a drop of 0.7% melted agarose. The slides were placed under an Olympus inverted compound microscope and visualised using 20x objective and bright field optics. The heart was positioned in the middle of the optic field. Images were recorded with a Basler camera at 300 frames/ second (fps) using VideoSavant software. Measurements of the blood volume were performed using the ImageJ measurement tool.

Heartbeat measurements were obtained under a Zeiss Axiozoom V.16 microscope. 5dpf larvae were anaesthetised for 1 minute before the measurements and their heartbeat was recorded for 1 minute. The measurements were performed for one individual larva per time.

Western Blot

Hearts of 5dpf larvae were dissected using Dumont No.5 forceps under a dissecting microscope. The dissected hearts were washed using washing buffer (110mM NaCl, 3.5mM KCl, 2.7mM CaCl2 2H20 and 10mM Tris-HCl) and

centrifuged on a benchtop centrifuge for 2 minutes at 13000rpm. The wash buffer was removed and 20ul of (-)Lysis buffer (400mM PIPES, 1M MgCl2, 0.5M EDTA and 1M NaCl) were added to the pellet . The sample was homogenised using a handheld homogeniser. 20ul of (+) Lysis (same composition of (-) Lysis buffer with the addition of 100ul NP40) buffer were added to the sample. The sample was incubated on ice for 30 minutes. After 30 minutes the sample was centrifuged for 20 minutes at $4^{o}$C at maximum speed. The supernatant was transferred into a new clean Eppendorf and the pellet was discarded. Bradford assay (Bradford reagent 5x 39222.02, Serva) was performed on the lysates to determine the protein concentration. 2x Laemmli buffer with volume equal to the sample's volume was added to the tube and the sample was heated at $95^{o}$C for 10 minutes on a heating block. Samples were loaded on a 12% acrylamide gel and run initially at 90V and later at 130 V. The proteins were transferred on nitrocellulose membranes and blocked using 5% non-fat dry milk (B13448, Oxoid) in TBST (Tris buffered Saline with Tween 20) overnight at $4^{0}$C.

The primary antibody used was Birc2, (10022-1-AP 1:100, Proteintech). The membrane was incubated overnight in the antibody solution and then washed with TBST 3 times for 10 minutes. The membrane was incubated overnight with goat anti-rabbit HRP antibody (ab6721, Abcam at 1:10000 dilution) and washed 3 times for 10 minutes. It was then incubated for 1 minute in enhanced chemiluminescence (ECL) substrate (32109, Thermo Scientific) covered with Saran wrap and exposed using an X-Ray cassette for 1 minute on X-Ray blotting film (34090, ThermoFisher Scientific).

## Results

**1.** The *alms1* homozygous mutant zebrafish larvae display body plan defects

To analyse the role of Alms1 in zebrafish development for the first time we obtained the *alms1* ENU generated allele sa10311 from the Sanger mutant collection. Paralogue search in the Ensembl database did not identify any gene paralogues. A nonsense point mutation (Fig.18 B, B') in this allele results in the appearance of a premature stop codon at the position of 448 amino acids out of the 2105 total amino acids and specifically in exon 4 out of 18 (Fig.18 C). Sanger sequencing confirmed the mutation. This mutation occurs between two domains of the protein, a Leucine rich motif (LR) and a Leucine zipper (LZ) and removes the ALMS motif at the C-terminus of the protein. Zebrafish *alms1*$^{-/-}$ mutants display a curly body appearance, which becomes apparent at 3 dpf (Fig.18 A, A'). The homozygous mutants survive until 8 dpf with severe body axis curvature. *Alms*1$^{-/-}$ mutants are unable to survive longer as their curly body

does not allow them to swim properly in order to feed. No phenotype is observed in their heterozygous siblings.

This specific curly body phenotype is reminiscent of the classical curly body appearing in the zebrafish cilia mutants, which is easily distinguishable by 3 dpf. No morphant or mutant phenotype of *alms1* mutations was previously reported in the zebrafish model. Description of an *alms1* mutation in zebrafish reveals that the homozygous mutants display the curly body encountered in cilia mutants and is often accompanied by the appearance of kidney cysts.

**2.** The *alms1* homozygous mutants lack olfactory cilia

Ciliogenesis defects were investigated in the *alms1* homozygous mutants at 5 dpf. The tissues examined except the nasal pit, were characterised by normal appearance of cilia (Fig.19 B-C'). More specifically, cilia in the ear patches, including the cristae and the maculae at 5 dpf are characterised by unaffected ciliogenesis (Fig.19 B'), while the same applies for cilia of the neuromasts (Fig.19 C'). Surprisingly, cilia in the olfactory pit were absent at 5 dpf (Fig.19 A'), highlighting the importance of Alms1 in olfactory cilia. Absence of olfactory cilia in the nasal pit leads to the conclusion that *alms1* homozygotes are anosmic, similarly to *bbs* mutant mice and human patients with BBS (Katsanis et al., 2001). No evidence of the Alms1 role in olfaction was previously reported, however its neuronal sensory related role is known. In conclusion, lack of olfactory cilia at 5 dpf *alms1* homozygous mutants highlights the role of Alms1 in the development and/ or maintenance of olfactory cilia.

**3.** *Alms1* homozygous mutants display retina defects

ALMS patients are characterised by progressive blindness. Retinal analysis was performed in *alms1* homozygous mutants and their siblings to analyse the GPCR rhodopsin localisation in the photoreceptors. Rhodopsin localisation was examined at 5ndpf in the larva retina (Fig.20 A, A'), since rhodopsin mislocalisation could indicate retinal defects. *alms1*$^{-/-}$ mutants were characterised by rhodopsin mislocalisation (Fig.20 A'), as expression of the specific outer segment marker was not restricted in the outer segments. Rhodopsin in the mutant retina was not exclusively located in the photoreceptor outer segments but it also surrounded the outer nuclear layer nuclei.

We conclude that in agreement with the human phenotype, *alms1*$^{-/-}$ zebrafish mutants display retinal defects at larval stages. Analysis of later onset phenotypes related to photoreceptor loss is not possible, as the *alms1*$^{-/-}$ mutants survive only until 8 dpf.

**4.** Heart defects are observed in the *alms1* homozygous mutants

One of the major ALMS related phenotypes is cardiomyopathy that progresses as one of the main lethality causes in ALMS patients. Analysis of the cardiac blood volume at 6 dpf using high speed recording of the pumping heart, revealed increased blood accumulation in the *alms1*$^{-/-}$ mutant ventricle during cardiac diastole (Fig.21 A-B', D, E). The blood accumulation was also increased during the ventricular systole however a significant difference was only observed during the diastolic phase (Fig.21 D, E). This observation reveals that the ventricle of the heart of the homozygous mutants occupies larger area compared to their non-mutant siblings. Heartbeat analysis was also performed at 5 dpf, revealing that *alms1* homozygous mutants have decreased heartbeat compared to their siblings (Fig.21 C).

In conclusion, cardiac anomalies were observed in the *alms1*$^{-/-}$ mutants during larval stages, related to increased ventricle volume and heartbeat defects. These phenotypes could be correlated with early symptoms of cardiomyopathy in the *alms1*$^{-/-}$ zebrafish mutants, indicating that the zebrafish model could be resourceful to study heart defects encountered in human ciliopathies.

**5.** Hippo pathway is misregulated in the heart of *alms1* mutants

Recent proteomic studies have revealed the connection between ALMS1 and Hippo pathway components (Couzens et al., 2013), although no evidence of deregulation of the pathway in ALMS was previously reported. In addition, it has been shown that the Hippo pathway restrains cardiomyocyte proliferation and heart size (Heallen et al., 2011). These two evidence, suggest that the heart size defect observed in the *alms1* homozygous mutants might derive from defective Hippo pathway activity. To investigate this possibility, the hearts of *alms1*$^{-/-}$ mutants and their siblings were dissected and cardiac protein lysates were analysed for the expression of the Hippo pathway transcription product, BIRC2. BIRC2, also known as cIAP1, was found to be downregulated in the hearts of *alms1* homozygous mutants, indicating that Hippo activity is upregulated during this developmental stage (5 dpf) (Fig.22 A).

In conclusion, this observation highlights the role of Hippo signalling during the development of the *alms1*$^{-/-}$ mutant heart phenotype, revealing that the pathway is upregulated, as the expression of its transcription products is diminished, and possibly the observed activity is crucial for the determination of heart size (Miesfeld & Link, 2014; Zhou, Li, Zhao, & Guan, 2015).

## Discussion

*Alms1* is the only causative gene, responsible for the manifestation of ALMS, a ciliopathy with phenotypes related to sensory loss (retinal degeneration, hearing loss), dilated cardiomyopathy and metabolic defects including obesity and hyperinsulinemia. Significantly, alignment of the ALMS1 protein from human, mouse and zebrafish revealed striking differences. More specifically, differences are observed in the protein length of the three species: the human protein consists of 4169 aa, the mouse protein 3251 aa while the zebrafish protein length is 2105 aa. This analysis revealed the absence of the human 1219 N-terminal aa from the zebrafish protein. The tandem repeat domain, a large part of the human protein is completely absent in zebrafish, while a Leucine rich motif still exists. Comparison between the mouse and human protein revealed that the N-terminal is not very well conserved in the two species and similarly, the tandem repeat domain is almost absent in the mouse. In contrast to the N-terminal, the C-terminal of the protein is conserved and the ALMS motif is present in all three species, suggesting that the C-terminal of the protein is important for the protein localisation and presumably function. It is however worth mentioning that ciliogenesis defects were rescued using the 1282 N-terminal amino acids of the mouse cDNA (G. Li et al., 2007).

Analysis of the *alms1* mutant in zebrafish with a mutation in the N-terminal part of the protein revealed that homozygous mutants exhibit the often-encountered curly body shape, which can be first observed at 3 dpf. Homozygous mutant larvae survive until 8 dpf possibly due to the fact that their body structure does not allow them to feed properly. Interestingly, scoliosis or kyphosis are common among ALMS patients (Maffei, Munno, Marshall, Scandellari, & Sicolo, 2002), indicating that the curly body of the mutants might derive from skeletal morphogenesis defects, as the first calcified bone structures appear already at 3 dpf (Aceto et al., 2015). Cilia staining at 5 dpf did further reveal that ciliogenesis was unaffected in the ear sensory patches, including the crista and the macula, and the lateral line neuromasts. In contrast, olfactory cilia in the nasal pit were shorter and sometimes absent (20% of the stained larvae

exhibited complete absence of cilia). The olfactory pit ciliogenesis defect underlines the role of Alms1 in the development of the cilia of the olfactory neurons and indicates that homozygous mutant larvae are anosmic. It is noteworthy, that the nasal pit structure is not affected indicating that the observed phenotype does not derive from nose morphogenesis structural defects.

The role of Alms1 in olfactory cilia was not previously reported but it is in contrast with the fact that cilia of the olfactory epithelium are unaffected, having normal microtubule configuration in the *Alms1* mutant mice (Collin et al., 2005). Although ultrastructural analysis of motile cilia is shown, it is known that olfactory cilia in zebrafish display ‘’9+2’’ microtubule configuration they are however immotile as they lack dynein arms (P. M. Jenkins et al., 2009; Leventea et al., 2016). Nonsensory motile multiciliated cells are also found in the olfactory epithelium to facilitate odorant and mucus clearance (Hansen & Zeiske, 1998).In conclusion, the cross section of motile cilia shown most possibly derives from nonsensory cells and cannot provide evidence for the function of the sensory olfactory cilia of the homozygous mutants. It is unlikely that this contradiction occurs due to difference across the species, as it was shown that molecular mechanisms underlying olfaction in teleosts and mammals are similar (Saraiva et al., 2015).

In agreement with the ALMS mouse model where rhodopsin mislocalization is observed in the retina outer nuclear layer, we are also able to observe the same type of mislocalization in the zebrafish homozygous mutant retina.

Cardiac defects were previously shown to affect homozygous *Alms1*$^{Gt/Gt}$ mice (Shenje et al., 2014). Significantly the measured heart to body ratio was larger in the homozygotes compared to their wild type littermates. Additionally, impaired cardiomyocyte differentiation was observed in the homozygous mutant mice, as they remain proliferative for longer period of time. We report that cardiac defects do also exist in the *alms1* homozygous zebrafish mutants. *Alms1*$^{-/-}$ ventricles occupy larger volume compared to their wt siblings, indicating that *alms1*$^{-/-}$mutants have enlarged hearts. It was additionally observed that homozygous mutants display reduced heartbeat demonstrating that the heart function is compromised. This observation leads to the conclusion that a heart dilation phenotype exists in the *alms1* homozygous mutants, it cannot be however concluded that the observed phenotype is necessarily cardiomyopathy, as the heart muscle morphology was not assessed. In conclusion, these data show the importance of Alms1 in cardiac function.

The heart enlargement phenotype observed in the *alms1* homozygous mutants reminded us of the overgrown organ phenotype observed in Hippo pathway related mutants. Hippo correlation with organ size is widely known in *Drosophila melanogaster,* where mutations of key pathway components lead to increased organ size which occurs due to increased cell proliferation (Pan, 2010; F. X. Yu, Zhao, & Guan, 2015). Similarly, the mouse heart is overgrown in *Sv1*, *Mst1/2* and *Lats1/2* mutants due to cardiomyocyte proliferation (Heallen et al., 2011). It was additionally shown that ALMS1 interacts with Lats2 and AMOT, two components of the Hippo pathway. Combination of these findings led us form the hypothesis that the observed heart enlargement observed in the *alms1* zebrafish mutants derives from Hippo pathway deregulation. Analysis of the transcription product of the Hippo pathway, BIRC2 revealed upregulation of the Hippo activity during the specific developmental stage, suggesting that the proliferation of the cardiac cells is downregulated, not clearly confirming the correlation between the observed phenotype and the pathway activity. The expected result would be downregulation of the Hippo pathway, which would lead to increased proliferation. Our analysis reveals however a general deregulation of the pathway in *alms1* homozygous hearts.

In summary, analysis of the *alms1* zebrafish mutants revealed that homozygous larvae exhibit curly body, ciliogenesis in the olfactory pit is disrupted and larvae are also characterised by rhodopsin mislocalization in the outer nuclear layer of the retina, confirming the sensory role of Alms1. We furthermore observed compromised cardiac function in the homozygous mutants, manifested by enlarged heart size and reduced heartbeat at larval stages. We cannot confirm that the observed heart enlargement derives from the Hippo pathway deregulation, we did although observe upregulation of the pathway activity in the hearts of the *alms1* homozygous mutants at 6 dpf. In conclusion, the zebrafish ALMS model partially recapitulates the human phenotypes and could be a useful model to study phenotypes like retinal degeneration and heart defects related to ALMS.

# Figures

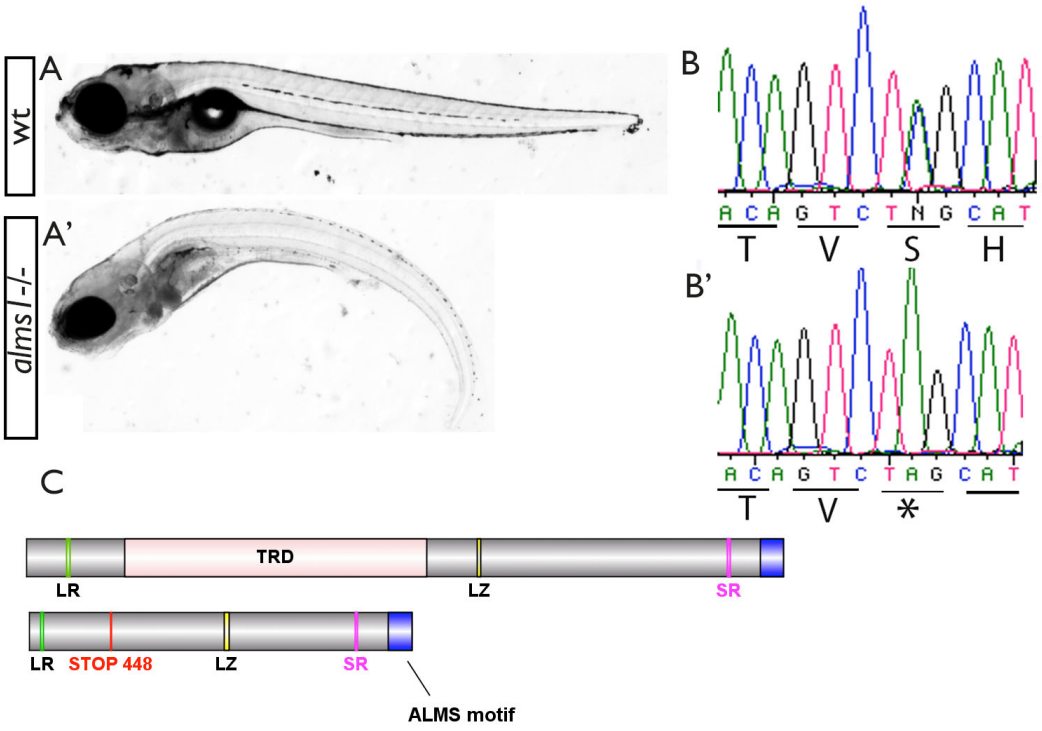


**Fig. 1 External phenotype of the *alms1* mutant**. **A, A'**. External phenotype of wt and *alms1*$^{-/-}$ larvae at 5 dpf. *alms1*$^{-/-}$ larvae appear with curly body axis. **B,B'**. Representative sequences from heterozygous (**B**) and homozygous *alms1* (**B'**) mutant larvae. The asterisk indicates the presence of a stop codon. **C**. Schematic representation of the protein domains of the human (upper scheme) and zebrafish Alms1 protein. Note the difference in length between the two species. The point mutation causing a premature stop codon at the amino acid 448 is indicated. LR: Leucine Rich, TRD: Tandem Repeat Domain, LZ: Leucine Zipper, SR: Serine Rich. The blue box represents the ALMS motif for both human and zebrafish proteins.

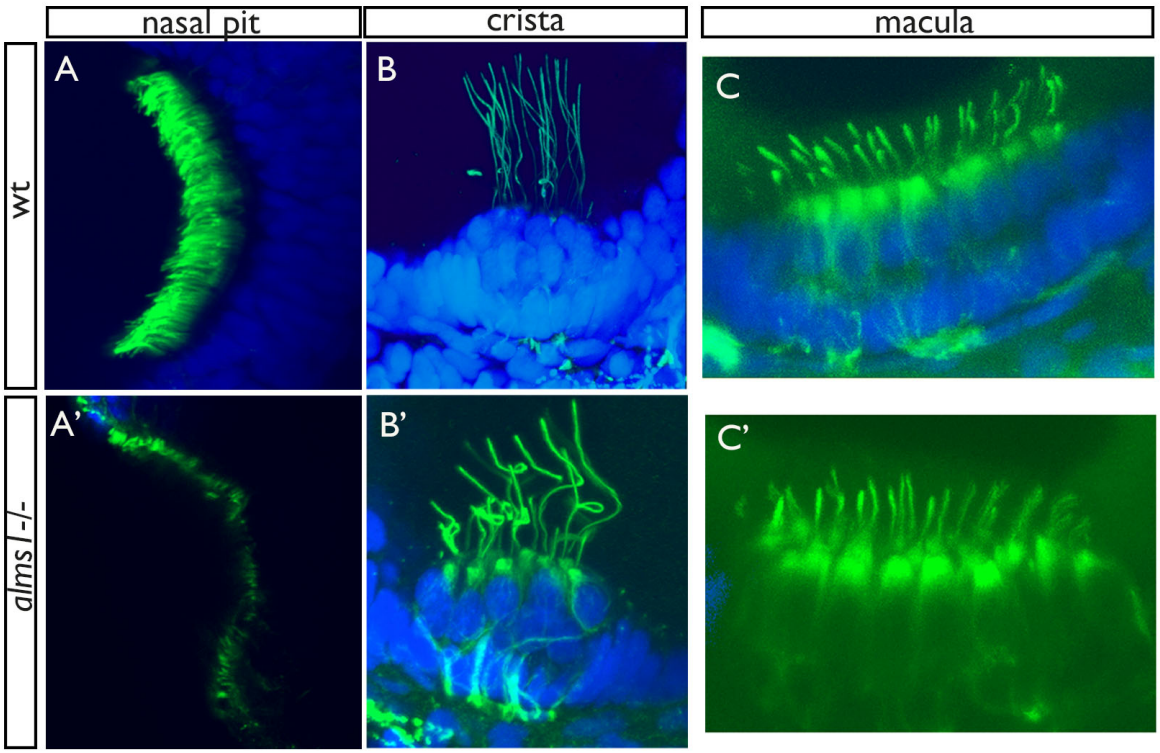


**Fig.2 Analysis of ciliogenesis at 5 dpf larvae**. **A, A'**. Shorter cilia in the olfactory pit of a 5 dpf *alms1*$^{-/-}$ larva. Ciliogenesis is not affected for the rest of the tissues including the cristae (**B,B'**) and the maculae (**C, C'**) of the ear. DAPI: blue and green: anti-acetylated tubulin. Scalebars are 5µm.

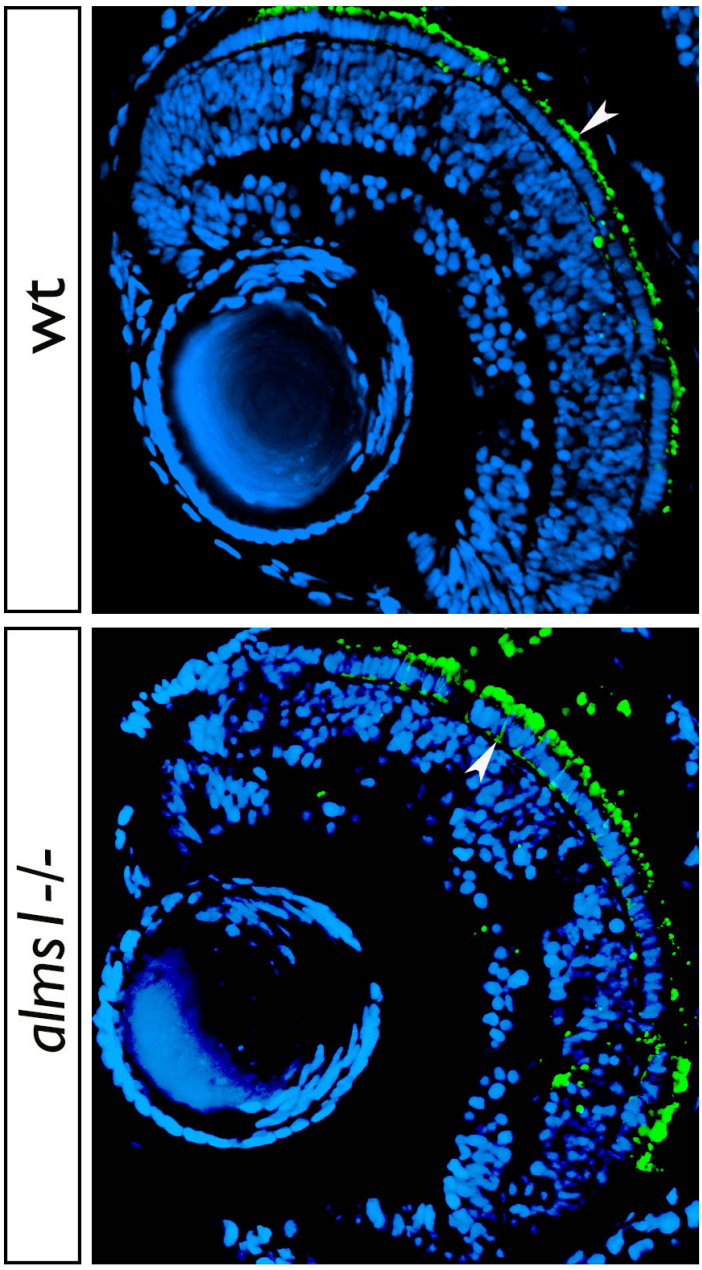


**Fig.3 Retina analysis of the *alms1* mutant**. **A-A'**. Rhodopsin mislocalization is observed in the retina of 5 dpf *alms1*$^{-/-}$ larvae as rhodopsin is mislocalised in the outer nuclear layer and is not restricted in the outer segment as indicated in the wt retina with an arrowhead. DAPI: blue, green: anti-zpr. Scalebars are 5µm.

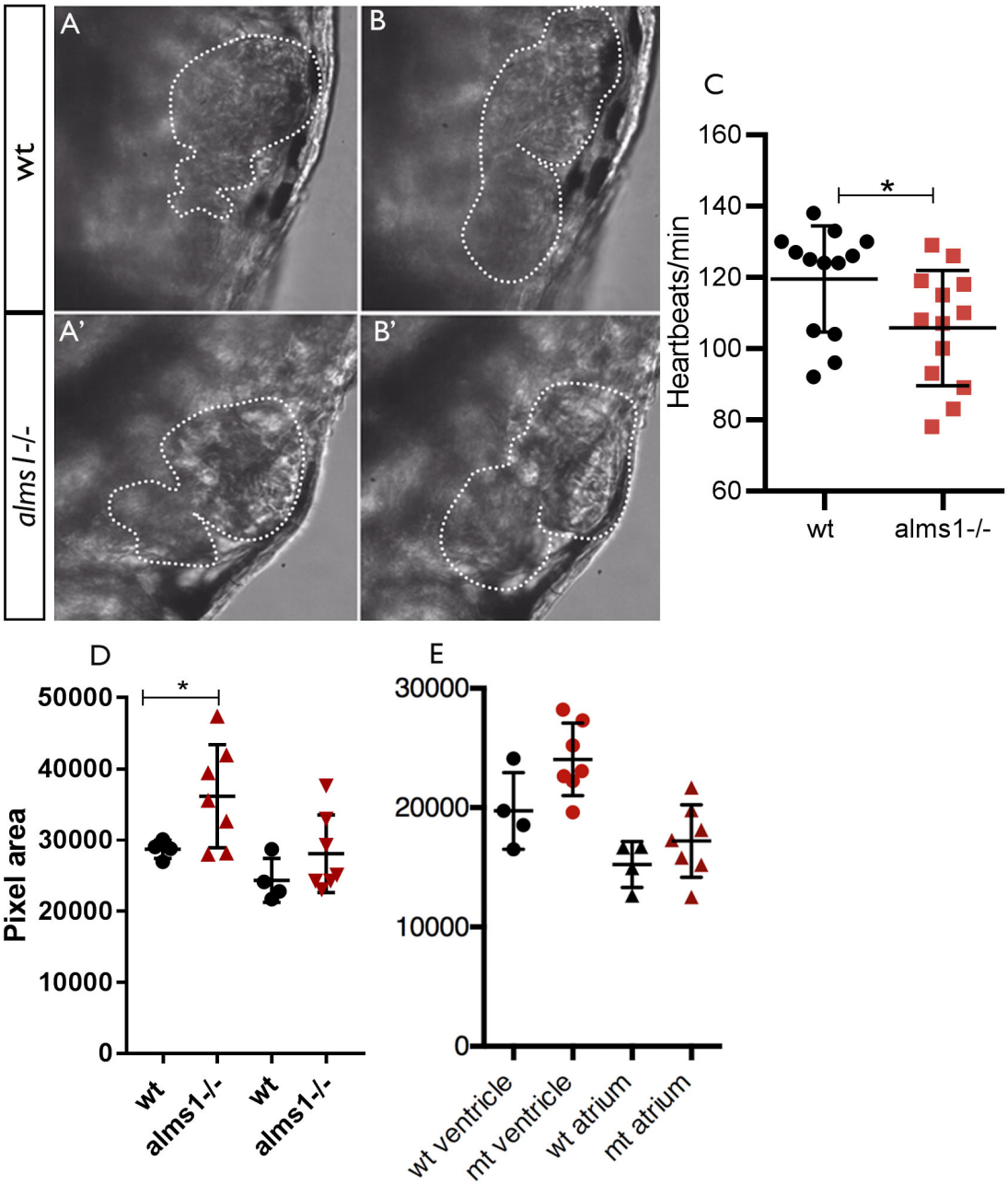


**Fig.4 Heart analysis of the *alms1* mutant**. **A-B'**. Images of the heart of wt and *alms1*$^{-/-}$ larvae at 6 dpf during cardiac systole (**A**, **A'**) and diastole (**B**, **B'**). The heart area during cardiac systole and diastole was measured based on a slow motion video of the beating heart. **C**. Quantification of the heartbeat rate per minute for wt and *alms1*$^{-/-}$ larvae at 5 dpf (n=13, 2 individual crosses, t-test, p=0.0336). **D**. Volume of the heart during cardiac diastole (n=4 wt larvae and 7 homozygous mutant larvae, t-test, ventricle p=0.0355 and atrium p=0.1267) and **E**. systole (n=4 wt larvae and 7 homozygous mutant larvae, t-test, ventricle p=0.16109 and atrium p=0.68) based on measurements of the outlined area as shown in **A-B'**.

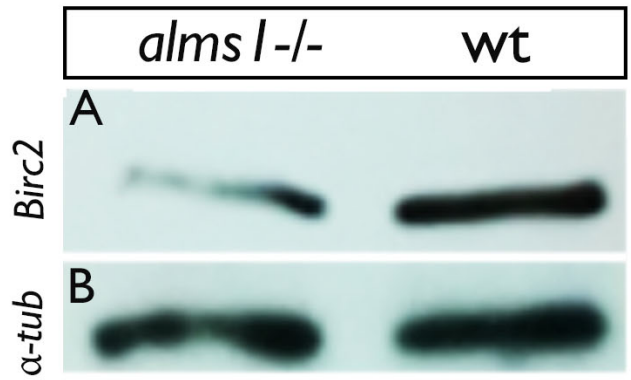


**Fig.5 Hippo pathway is upregulated in the heart of *alms1* mutants. A**. Expression levels of BIRC2 in wt and *alms1*$^{-/-}$ hearts. **A**'. α-tubulin was used as loading control (experiment was repeated two times)

# CHAPTER V

# ANALYSIS OF THE RAB23 AND TUBBY FUNCTION DURING ZEBRAFISH DEVELOPMENT

## Introduction

Mutations in *RAB23* are responsible for the manifestation of the Carpenter Syndrome (OMIM 201000), a genetic disorder characterised by obesity, polydactyly, craniosynostosis, syndactyly, congenital heart defects etc (D. Jenkins et al., 2007).

Rab23 belongs to the RAB family of small guanosine triphophatases that regulate trafficking including fusion and docking of membranes in eukaryotic cells (Evans, Ferguson, Wainwright, Parton, & Wicking, 2003; D. Jenkins et al., 2007). Binding and hydrolysis mediated by RAB proteins is connected to the recruitment of specific effectors on membranes which are important for membrane docking and fusion processes (Olkkonen & Stenmark, 1997). Rab23 was found to localise to the plasma membrane in BHK-21 cells and it is additionally associated with intracellular vesicular structures. It has been furthermore shown that RAB23 colocalizes with Patched (Ptch1) (Evans et al., 2003). It also contributes in lysosome and phagosome fusion (Smith et al., 2007). There is additional evidence of its localisation in primary cilia (Boehlke et al., 2010; Lim & Tang, 2015), where it is responsible for the ciliary trafficking of Kif17, a kinesin-2 family protein. Rab23 is required for the association of Kif17 with importin- β2 in order to enter cilia (Abdelhamed et al., 2015). Regarding the association of RAB23 with its cargoes, it has been shown that its depletion prevents ciliary dopamine receptors (DR1) from accessing the ciliary membrane, while it is able to drive non-ciliary GPCRs to cilia (Leaf & Von Zastrow, 2015). The activity of Rab23 is additionally dependent on IFT (Huangfu et al., 2003).

Interesting and well described is its role in the Hh pathway. Rab23 acts upstream of Gli transcription factors and downstream of Smoothened (Smo). The primary target of Rab23 is Gli2, while Rab23 and Gli3 have additive effects in patterning. Rab23 has also potentially a role in the production of Gli3 (Eggenschwiler, Bulgakov, Qin, Li, & Anderson, 2006).

*Rab23* mouse knockouts are represented by mutations in the mouse *open brain gene* (*opb*) for which two alleles exist; one spontaneously derived and one

generated by ENU mutagenesis. Early stop codons are introduced in the open reading frame of *opb* through single nucleotide substitutions resulting in truncated proteins of 39 and 79 aa. The mouse mutants die during the second half of gestation, they have open neural tube, polydactyly, defective somites and not fully developed eyes. The causing mutation was mapped to Rab23 (Eggenschwiler et al., 2001).

The role of Rab23 in the establishment of the left-right asymmetry has been additionally reported. Rab23 is required for the production of functional Nodal signals while dorsal forerunner cells specific knockdown of Rab23 in the zebrafish embryo causes laterality defects based on the expression of the laterality markers *lefty* and *spaw* (Fuller, O'Connell, Gordon, Mauti, & Eggenschwiler, 2014).

The correlation of Rab23 with Kif17 trafficking into cilia as well as its involvement in the Hh made us wonder if the zebrafish model phenotypes could resemble human phenotypes more closely compared to mouse mutants. *rab23* homozygous mutant zebrafish display curly body axis in confirmation of its ciliary role, while they additionally lack olfactory cilia which could be explained by the fact that Kif17 plays an olfactory cilia specific role (Zhao et al., 2012). A developmental delay in the retina was also observed, as rhodopsin was not equally distributed in the larval *rab23*$^{-/-}$ retina, a phenotype possibly associated with the poorly developed eyes of the mouse mutants. *rab23* homozygous mutants at 3 dpf do also display left-right asymmetry defects, based on defective heart looping, confirming the role of the protein in laterality establishment.

*TUBBY* (*Tub*) is a gene mutated in the naturally occurring mouse mutant that displays obesity, retinal and cochlear degeneration (Ohlemiller et al., 1995). The difference between *Tub* mutant mice and other naturally occurring mouse obesity models is that *Tub* homozygotes gain weight slower; resembling the human obesity disorders (Coleman, 1978). Regarding the correlation of TUB with human disease, it has been proposed as a candidate gene correlated with body composition and carbohydrate intake in middle aged women (van Vliet-Ostaptchouk et al., 2008). It has been furthermore reported that certain TUB polymorphisms are associated with higher Body Mass Index (BMI) in human individuals (Shiri-Sverdlov et al., 2006). TUB and TUBBY like proteins (TULPs) are characterised by a significant similarity in their sequences as they share the TUBBY domain at the C-terminal of the protein. In contrast, the N-terminus of the protein is diverse, possibly due to the diverse functions of the family members (Mukhopadhyay et al., 2010). The TUBBY domain additionally

interacts with specific phosphoinositides and more specifically phosphatidylinositol 4, 5-biphosphate, PIP2 (Santagata et al., 2001). Tandem affinity purification and mass spectrometry of the TUB family proteins revealed that TUB interacts with IFT-A through the N-terminus (Mukhopadhyay et al., 2010) and the IFT binding region overlaps with a nuclear targeting signal. Furthermore the N-terminus of TUB has been identified as phagocytosis promoting molecule in retinal pigmented epithelium cells and macrophages (Caberoy, Maiguel, Kim, & Li, 2010). The N-terminus has been also detected to bind DNA (Boggon, Shan, Santagata, Myers, & Shapiro, 1999).

Tub is expressed in the retina and brain regions including the hippocampus and the hypothalamus (Ikeda, Naggert, & Nishina, 2002). It was found to localise in the cytoplasm, the nucleus and the plasma membrane in stable transgenic cell lines (Beales et al., 1999). The family has been also shown to display a role in GPCR trafficking, as rhodopsin is not fully transported in connecting cilia in mouse photoreceptors, while metabolism regulation related GPCRs like SSTR3 and MCHR1 fail to localise to neuronal cilia (X. Sun et al., 2012).

The *tub* mutation in zebrafish reveals that homozygous mutants do not have morphological defects and they can survive to adulthood. Rhodopsin mislocalisation is already present in the homozygote retina at 5 dpf, confirming the role of *tub* in GPCR localisation. The fact that no external phenotypes present suggest that ciliogenesis is unaffected.

## Materials and Methods

Microscopy

5 dpf *rab23* and *tub* homozygous mutants and non-mutant sibling larvae were photographed as previously described after being mounted in 3% methylcellulose with the lateral side up.

Immunohistochemistry

Cilia analysis was performed as previously described at 5 dpf using mouse anti-acetylated tubulin (1:500 dilution) primary antibody and anti-mouse Alexa Fluor 488 (1:500 dilution) secondary antibody. Larvae were incubated overnight for both the primary and the secondary antibody.

Cryosections of 5 dpf retinae were stained with anti-zpr3 primary antibody (1:500 dilution) overnight followed by washes and overnight incubation in anti-mouse Alexa 488 secondary antibody (1:500 dilution) as previously described. Images were obtained using a Confocal FV1000 with a 40x oil lens.

Heart Looping

*rab23* wt and homozygous mutants were anaesthetised using 1mL Tricaine in 20mL embryo medium (working concentration) until they stop swimming. The heart looping was assessed under an AxioZoom V16 microscope and heart position (Left or Right) was manually scored.

## Results

**1.** *rab23*$^{-/-}$ zebrafish mutants exhibit curly body axis and heart looping defects

In order to investigate the role of Rab23 in zebrafish development we obtained the ENU generated mutant allele sa13880 from the Sanger zebrafish collection. Paralogue search in the Ensembl database did not identify any gene paralogues. The specific nonsense point mutation (Fig.23 B, B') occurs in exon 6 out of the total 7 exons and specifically in the amino acid 164 out of the total 237 aa (Fig.23 C). The appearance of a premature stop codon within the Rab23 family domain should result in an early-truncated Rab23 protein. This specific mutation excludes the C-terminal part of the protein, which harbours cysteine residues that are important for the prenylation of the protein. Prenylation is a critical step for Rab proteins in order to be associated with the cytoplasmic leaflet of membranes. We can thus conclude that the allele studied is most likely null, as the C-terminus of the protein is absent after the appearance of the premature stop codon within the Rab23-like domain. The phenotype of the *rab23*$^{-/-}$ mutants first became apparent at 3 dpf. The homozygous mutants display curly body (Fig.23 A'); reminiscent of the phenotype encountered very often in zebrafish cilia mutants. The appearance of phenotype in homozygous mutants was confirmed by Sanger sequencing at 3 dpf. The homozygous mutants can survive until 8 dpf, as they are unable to swim and feed properly. No other phenotype except the curly body is obvious during larval stages. Pigmentation is developing normally and the eye size is also unaffected. No phenotype is observed in the *rab23* heterozygous mutant larvae. The appearance of the curly body phenotype is of Mendelian ratio.

The positioning of the heart at 3 dpf larvae was also evaluated, since Rab23 has been closely linked to the regulation of organ laterality. At 3 dpf, wt zebrafish larvae should have their heart positioned at the right side of their body

(Fig.23 D). *rab23* homozygous mutants often loop their heart at the left compared to their wt siblings who are characterised by rightward looping of their hearts (Fig.23 D). Only 28% of the *rab23*$^{-/-}$ mutants displayed rightward looping of the heart ventricle, while 75% of their siblings looped their hearts at the right side. It is noteworthy that there is a small percentage of wt larvae that display incorrect heart looping, as previously reported (Leventea et al., 2016). Wild type zebrafish strains often appear with laterality defects in small percentages.

In conclusion, *rab23* homozygous mutant larvae appear with the classic curly body cilia mutant related phenotype, which first becomes apparent at 3 dpf and can survive until 8 dpf. The homozygous mutants additionally display laterality defects based on the incorrect cardiac looping at the left side of their body 3 dpf in contrast to their wt type siblings, which are characterised by rightward looping.

**2.** *rab23*$^{-/-}$ mutants lack olfactory cilia and are developmentally delayed

Ciliogenesis in the zebrafish tissues was examined at 5 dpf. Cilia were present in all organs analysed, including the ear sensory patches (Fig.24 B', C'), cristae and maculae, and the neuromasts, they were however absent in the nasal pit of the *rab23* homozygous mutant larvae (Fig.24 A'). The appearance of the olfactory neurons in the nasal pit was obvious, olfactory cilia were however absent in the nasal cavity. *rab23* wt larvae were characterised by unaffected ciliogenesis in all tissues examined (Fig.24 A-C). Cilia in the kidney are difficult to be visualised at this specific developmental point in wholemount preparations.

The localization of rhodopsin in the retina was additionally analysed at 5 dpf larvae. Rhodopsin was normally localised in the outer segments of the retina photoreceptors in the wt larvae (Fig.24 D), this localization was although defective in the *rab23*$^{-/-}$ mutants (Fig.24 D'). More specifically rhodopsin was present in the outer segments of the photoreceptors it was not however equally distributed in the outer surface of the photoreceptors, as its expression was mostly concentrated at the periphery and was less prominent in the centre of the retina. More generally, the rhodopsin staining at 5 dpf was reduced in the *rab23* homozygous mutants, indicating the existence of a developmental delay in the retina, possibly related to neuronal differentiation. The retina developmental delay is unlikely to be caused by a general delay in development, as the yolk of both wt and homozygous mutant larvae was of comparable size (Fig.23 A, A').

In summary, these data indicate that *rab23* homozygous mutants lack olfactory cilia in agreement with the role of Rab23 in Kif17 trafficking into the cilia, as Kif17 is required for olfactory cilia morphogenesis (Zhao et al., 2012).

**3.** The *tub* zebrafish mutant displays retinal defects

In order to investigate the role of Tub in zebrafish development we obtained the ENU generated mutant allele sa18104 from the Sanger zebrafish collection. Paralogue search using the Ensembl online database did not identify any gene paralogues. The specific nonsense mutation (Fig.25 B, B') occurs in exon 3 out of total 12 exons and more specifically in the amino acid 74 out of the 503 total aa (Fig.25 C). This mutation is causing the appearance of a premature stop codon and leads to a truncated Tub protein at the N-terminus, near the location of the nuclear targeting signal $K_{39}$KKR. Homozygous mutants did not display any external phenotype at larval stages (Fig.25 A') and they were raised to adulthood. No external defects were observed in the adult homozygous mutants. This indicates the absence of ciliogenesis defects.

As Tub is important for GPCR localization, analysis of rhodopsin localization was performed at 5 dpf (Fig.25 D, D'). As expected, rhodopsin is mislocalized in the outer nuclear layer of the retina instead of remaining in the outer segments of the photoreceptors. This observation is in agreement with the fact that *TUB* mutations cause blindness in human patients.

In conclusion, *tub* homozygous mutant zebrafish do not display external phenotypes and survive to adulthood. Rhodopsin mislocalization is additionally observed at larval stages in agreement with the blindness phenotype of the TUB mouse model.

## Discussion

*RAB23* is a causative gene for the Carpenter Syndrome, a pleiotropic disorder with craniosynostosis, obesity, limb defects etc. Rab23 mutations have been described in the *opb* (Gunther et al., 1994). Homozygous *opb* mice die during the second gestation half with phenotypes including open neural tube, polydactyly, defective somites and not fully developed eyes (Eggenschwiler et al., 2001). Analysis of the *rab23* mutant in zebrafish revealed that homozygous mutants are characterised by curly body axis, reminiscent of the zebrafish cilia mutant phenotype. This observation confirms the fact that *rab23* is a ciliary gene, as previously demonstrated *in vitro* (Ishikawa, Thompson, Yates, & Marshall, 2012). Analysis of ciliogenesis at 5 dpf did furthermore reveal that cilia

are absent in the nasal pit of the homozygous mutant larvae, but not in the rest of the tissues, suggesting a Rab23 specific role in the olfactory cilia. This finding could be explained based on the fact that a kinesin-2 motor protein, Kif17 is mislocalised in *Rab23* depleted cells (Lim & Tang, 2015). It has been also shown that Rab23 mediates the transport of Kif17 to the primary cilium (Lim & Tang, 2015). Cilia in the olfactory pit of Kif17 mutants are also shorter, while Kif17 is additionally required for cyclic-nucleotide-gated channel targeting into the immotile olfactory neuron cilia (P. M. Jenkins et al., 2006). A developmental delay in the retina was also observed, as rhodopsin was not as prominent compared to its expression in the control larvae, suggesting that neurons in the retina are not fully differentiated. This finding is in agreement with the incomplete development of the eye observed in the *opb* mutant mice. It has been additionally found that *rab23* homozygous mutants display laterality defects based on the defective heart looping at 3 dpf, consistently with the role of Rab23 in left right asymmetry (Fuller et al., 2014). Overall, the study of *rab23* mutations in the zebrafish model suggests that they are causing embryonic lethality as in the mouse model but the homozygous mutants can survive till larval stages. There is a difference observed in the genotype phenotype correlation between human and mice, as the mutation is lethal for the *opb* mouse model but human patients of the Carpenter syndrome are viable.

*Tub* is another gene analysed in this project. Mutations in *tub* have been associated with the maturity onset obesity phenotype in mice, accompanies by retinal and cochlear degeneration (Ohlemiller et al., 1995). No human disorder has been associated with *TUB* mutations, there is however evidence that *TUB* variants are implicated in body composition and feeding behaviour in humans (van Vliet-Ostaptchouk et al., 2008). Interestingly, some of the TUB phenotypes overlap with those of BBS, the association of these genes is however currently unknown. Analysis of a *tub* mutation at the N-terminus of the protein, close to its nuclear localisation signal revealed the absence of any obvious external phenotype in zebrafish homozygous mutants. It was also observed that rhodopsin, is mislocalised in the $tub^{-/-}$ retina, confirming the role of Tub in GPCR trafficking. It is possible that the mislocalisation precedes the photoreceptor cell death due to the *tub* mutation that should lead to defective RPE phagocytosis.

In summary, mutations in cilia related genes in the zebrafish model can give insight into their function as they are able to survive at least till larval stages. Some of the phenotypes observed in these cilia mutants are in agreement with those described in the *opb* and *Tub* mouse models.

# Figures

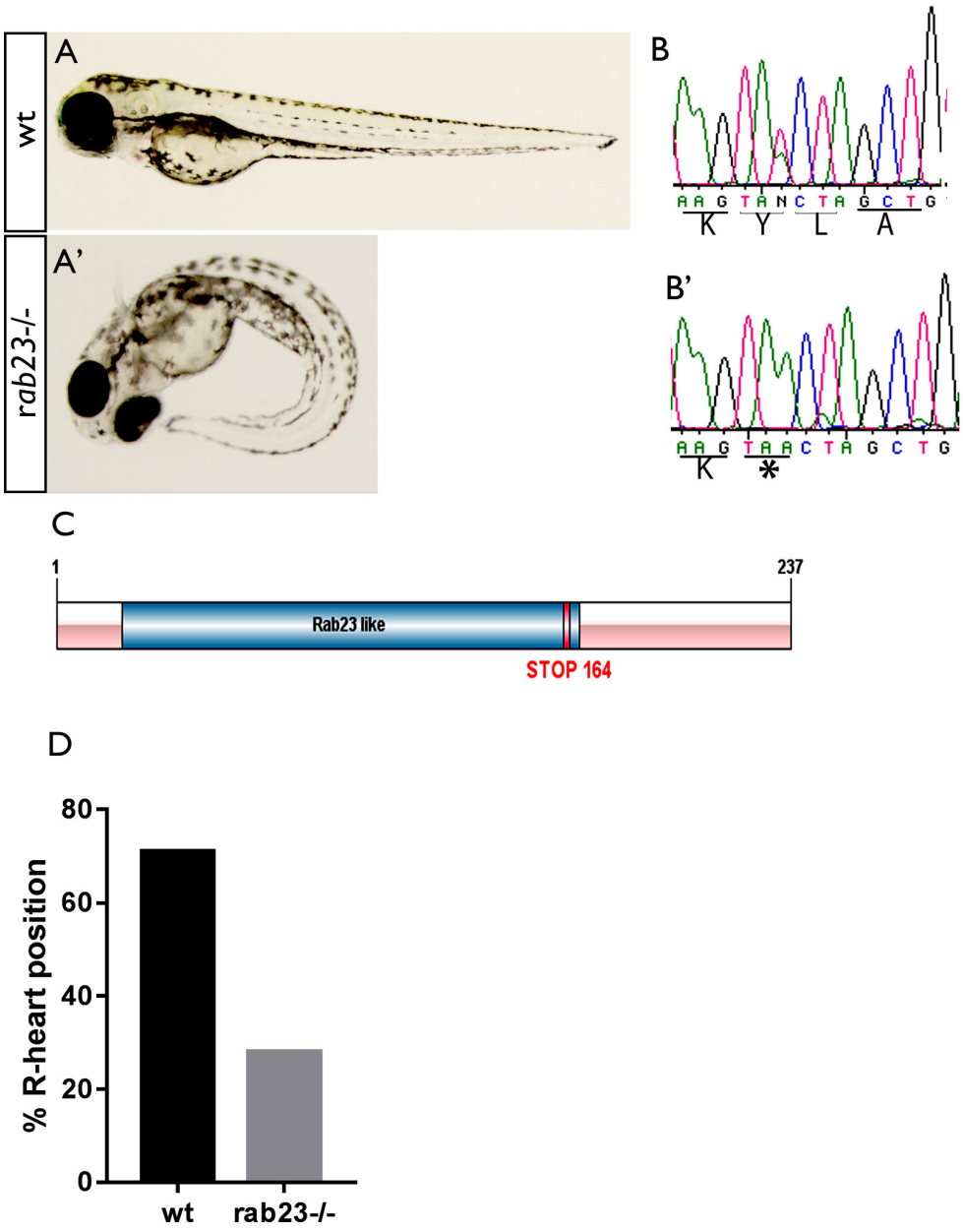


**Fig. 1 External phenotype of the *rab23* mutants and laterality defects during larval stages**. **A**. wt and **A'**. *rab23* $^{-/-}$larvae displaying curly at 5 dpf. **B,B'**. Representative sequences derived from heterozygous (**B**) and *rab23*$^{-/-}$ larvae. The asterisk indicates the presence of a stop codon in the amino acid sequence. **C**. Schematic representation of the Rab23 protein domain. The mutation point is indicated at the amino acid 164 within the Rab23 domain. **D**. Quantification of the heart looping of wt and *rab23*$^{-/-}$ larvae at 3 dpf (n=7 larvae). wt larvae have rightward (R) heart looping at this stage.

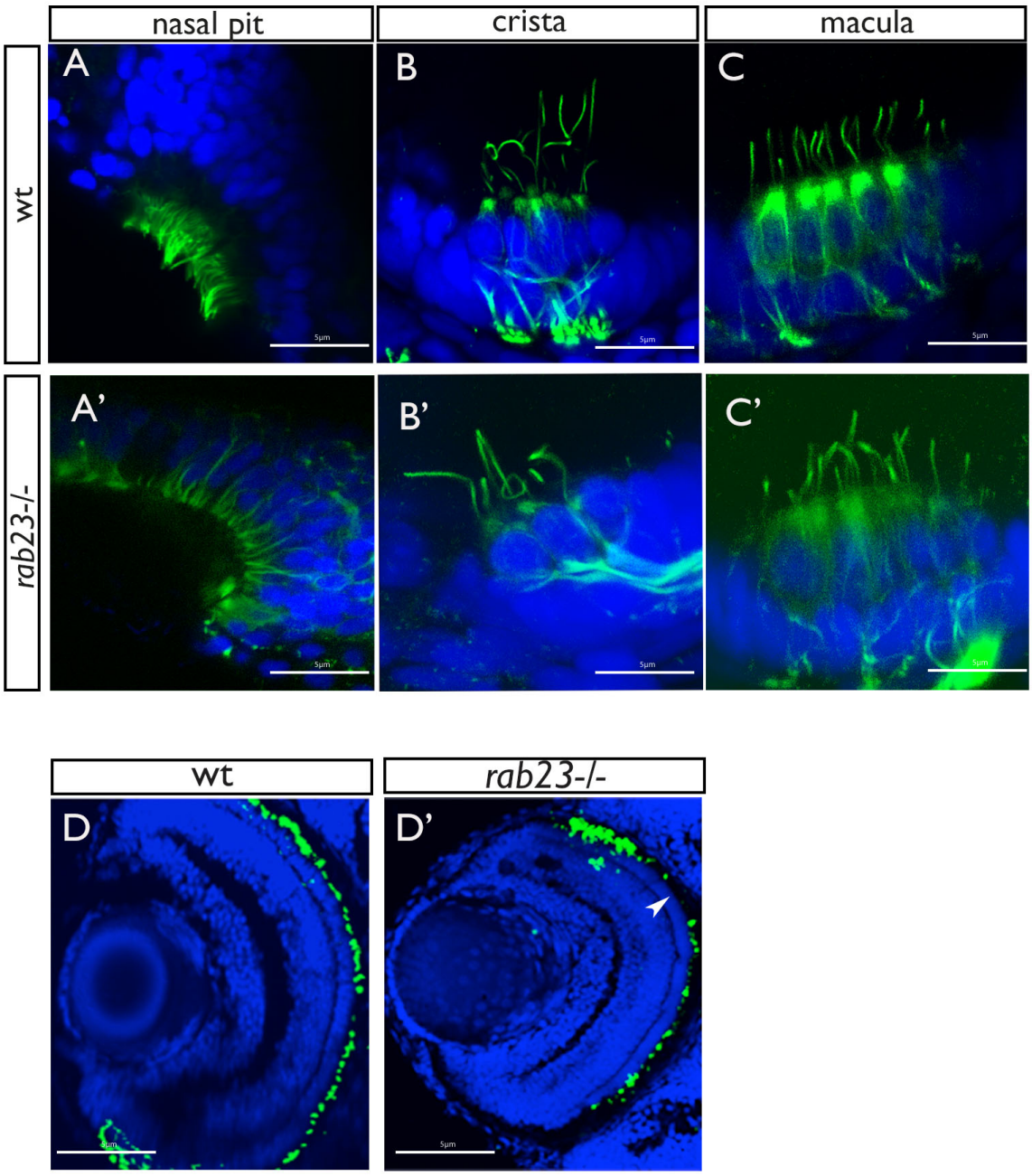


**Fig.2 Analysis of ciliogenesis in the *rab23* mutant**. **A, A'**. Absence of olfactory cilia in the nasal pit (green staining appears due to olfactory neurons being labelled by acetylated tubulin) of 5 dpf *rab23*$^{-/-}$larvae, while cilia is normally present in **B,B'**. ear cristae and **C, C'**. maculae.**D, D.** Cryosections of the larval retina at 5 dpf of wt (**D**) and *rab23*$^{-/-}$ zebrafish. Arrowhead is pointing at rhodopsin localization in the *rab23*$^{-/-}$ retina. DAPI: blue, green: anti-zpr3. Scalebars are 5µm.

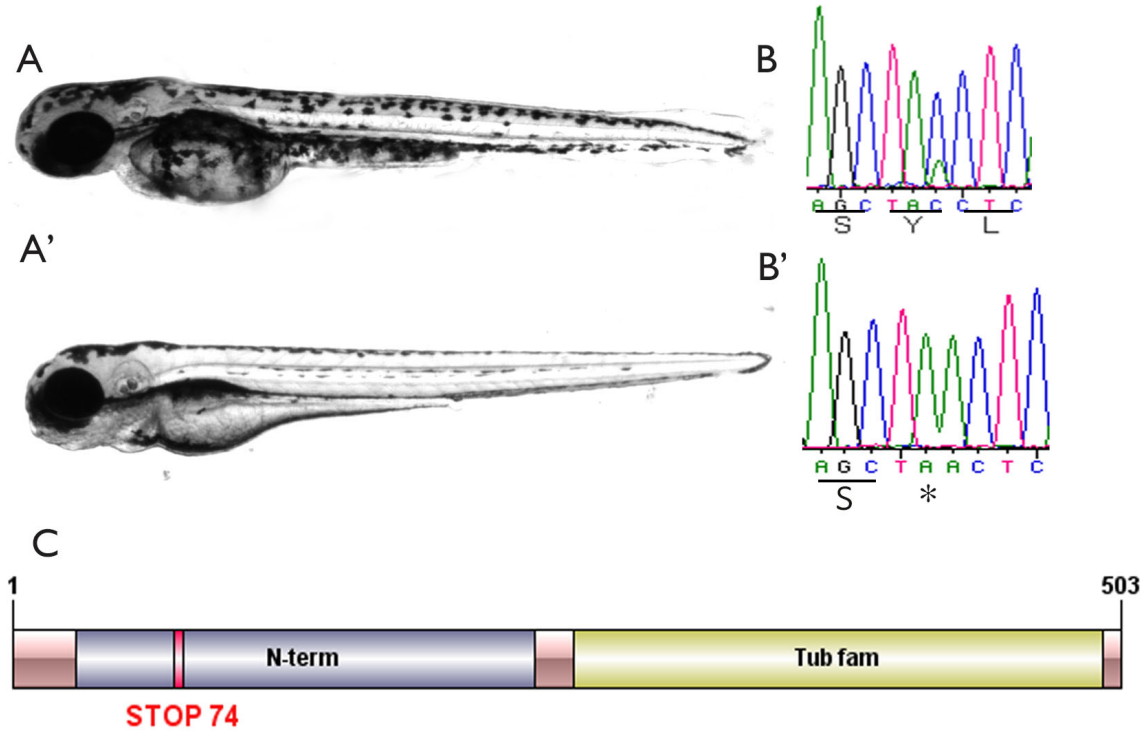


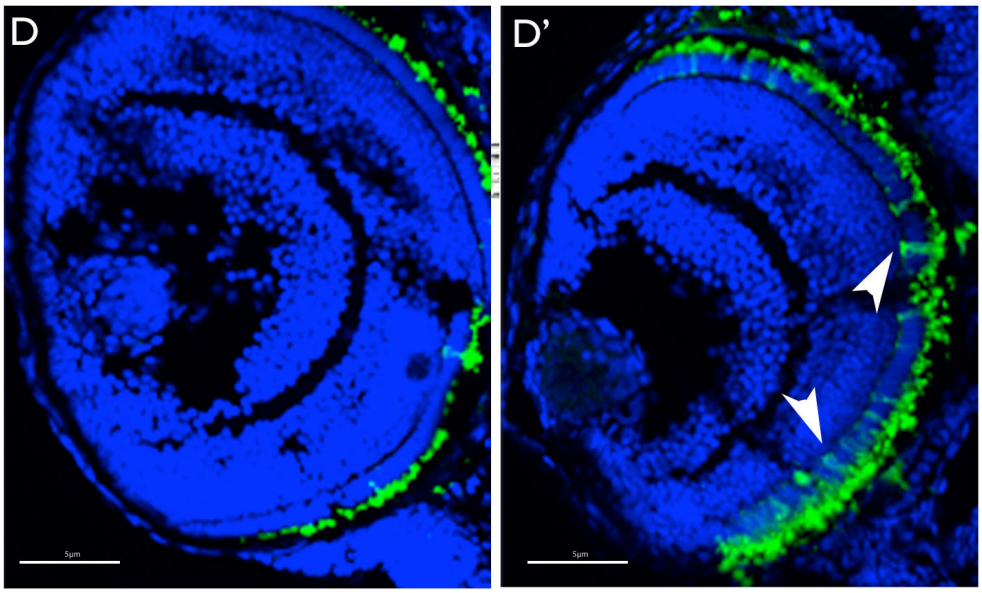


**Fig.3 External phenotype and retinal analysis of the *tubby* mutant. A, A'**. External phenotype of wt and *tubby*$^{-/-}$ at 5 dpf. **B,B'**. Representative sequences from heterozygous and homozygous mutant *tub* larvae. The asterisk indicates the presence of a stop codon. **C**. Schematic representation of the Tub protein. The position of the stop codon is indicated at 74 amino acids out of the total 503 amino acids of the protein. **D, D'**. Cryosections of wt (**D**) and *tub*$^{-/-}$ retinae at 5 dpf. The arrowhead indicates rhodopsin mislocalisation in the outer nuclear layer. DAPI: blue, green: anti-zpr3. Scalebars are 5µm.

# CHAPTER VI

# Summary, Conclusions and Future Directions

## Summary

In summary, the mutant zebrafish reported here recapitulate to a certain extent human phenotypes. These phenotypes differ from the ones reported in the morpholino experiments. While some of the zebrafish mutants described here exhibit expected phenotypes related to ciliopathy manifestations, other zebrafish mutants recapitulate rare phenotypes observed in BBS and JBTS patients, which have not been previously described in mouse models and give insight into novel functions of cilia genes (summarised phenotypes in Table 6).

## Conclusions and discussion of novel findings

This study provides, for the first time, evaluation of the zebrafish as a model to study human ciliopathies. It was specifically shown that zebrafish cannot fully recapitulate the human disease phenotypes, this model can be however useful in the study of tissue specific phenotypes including rhodopsin mislocalization in the retina, anosmia, skeletal and vestibular system defects as well as cardiac anomalies.

The *bbs2* and *bb9* zebrafish mutants

We show that the core Bbsome genes, *bbs2* and *bbs9*, have a role in skeletal morphogenesis, a previously unreported role in the mouse BBS models. It is worth mentioning that mouse BBS models fail to recapitulate polydactyly phenotypes found in human patients and this could possibly imply that the skeletal defects cannot be modelled in the mouse mutants. In such case, zebrafish could be an alternative for the study of skeletal and bone related phenotypes of the syndrome. We hypothesize that mutations in other Bbsome components would result in similar phenotypes to those observed in the two mutants analysed. This is based on the fact that the BBSome components belong to the same complex. In this study we identified that *bbs9*$^{-/-}$ mutants exhibit rhodopsin mislocalization at larval stages, in contrast to the *bbs2*$^{-/-}$ mutants, which are not characterised by retinal defects. This surprising observation led to the hypothesis that the *bbs2*$^{-/-}$ mutant retina can compensate for the photoreceptor loss with increased cell proliferation in the ONL where degeneration should be observed. Indeed, increased proliferation levels were

observed in the ONL of *bbs2* homozygous mutants during adulthood, indicating that there is a regeneration process in the homozygous mutant retina. The possibility that Bbs2 is not important for retina function should be excluded based on the retinal degeneration phenotype observed in the mouse *Bbs2* mutant (Nishimura et al., 2004).

The *cep290* zebrafish mutant

Surprisingly, this study revealed the role of Cep290 in otolith morphogenesis. *cep290*$^{-/-}$ mutants display a high frequency of three otoliths in their otic vesicle during early larval stages along with hyperactive swimming behaviour. The hyperactivity behaviour is particularly apparent during adulthood and can be attributed both to polarity defects in the inner ear epithelium and to the abnormal arrangement of crystals in the utricular otoliths. It is therefore shown for the first time that Cep290 is involved in otolith morphogenesis. We furthermore identified Coch, a human deafness related protein being reduced in adult *cep290*$^{-/-}$ sagittae, presumably attributing to the observed otolithic structure defects. Reduction of this specific protein in the otoliths in the absence of Cep290, suggests that Cep290 is important for the regulation of Coch secretion. We particularly assume that in the absence of Cep290, Coch cannot be secreted in the endolympatic fluid of the ear. The defective secretion has not been confirmed, we hypothesize however that the observed phenotypes could derive from Cep290 additional roles in other cell regions except the ciliary transition zone. It has been reported that Cep290 has a role in cell-cell and cell-matrix junctions (Schouteden, Serwas, Palfy, & Dammermann, 2015). We cannot also exclude the possibility of secretion of vesicles containing Coch through cilia, as it has been shown that cilia of the *Chamydomonas reinhardtii* secrete vesicles, known as ectosomes (Wood et al., 2013). This possibility could explain that absence of Cep290 in the ciliary transition zone affects secretion of Coch vesicles in the ear lumen. An additional possibility is that cilia motility is disrupted in the otic vesicle of the *cep290*$^{-/-}$ mutants, it has been however shown that cilia motility does not affect otolith formation and tether cells in the ear are those that are important for otolith nucleation and growth (Stooke-Vaughan, Huang, Hammond, Schier, & Whitfield, 2012).

The *alms1* and *rab23* zebrafish mutant

Analysis of an *alms1* mutant allele revealed the role of Alms1 in olfactory cilia morphogenesis. This finding is reminiscent of the importance of BBS proteins in olfactory cilia. Some of the BBS mouse mutants and a fraction of human patients exhibit anosmia defects (Katsanis et al., 2001). In contrast to our

finding, ALMS mouse models were shown to display unaffected olfactory cilia microtubule arrangement, this observation does not however exclude the possibility that olfaction is intact. Olfactory defects have not been reported in ALMS human patients until now. We additionally showed for the first time the association between Alms1 and the Hippo pathway. Absence of Alms1 results in upregulation of the pathway in the zebrafish heart during larval stages.

Similar to Alms1, a role for Rab23 has been observed in the olfactory cilia. This role possibly derives from the requirement of Rab23 for Kif17 trafficking (Lim & Tang, 2015) and is in contrast with *in vitro* studies suggesting unaffected ciliogenesis in the absence of Rab23 (Lim & Tang, 2015). In agreement with the olfactory cilia role of Rab23, *Kif17*$^{-/-}$ mutants have been shown to display defective olfactory cilia but no other ciliogenesis defects (Zhao & Malicki, 2011).

## Future directions

The investigation of the mechanism behind the bone morphogenesis defect observed in the *bbs* mutants would be crucial in order to identify a specific role for *Bbs* during bone development. More specifically, it would be useful to identify which cell type is particularly affected during the skeletal morphogenesis by the absence of Bbs2 and Bbs9. This finding would potentially establish a Bbs specific role in the regulation of osteogenesis. Additionally, in order to unravel the reason behind the absence of retinal degeneration defects in the *bbs2*$^{-/-}$ mutants it would be crucial to exclude the possibility that a hypomorphic allele was analysed.

Essential would also be the evaluation of the cilia motility in the otic vesicle of *cep290* homozygous mutants, as it is possible that compromised cilia motility is the underlying reason behind the otolith and associated behavioural defects. Interesting would be also the confirmation of secretion defects of Coch in the ear lumen due to the absence of Cep290. Accumulation of vesicles in the apical surface of cells in the ear maculae of the homozygous mutants would indicate that Coch is unable to be efficiently secreted in the ear lumen. Alternatively, in order to test the possibility that Coch is secreted through cilia; we would have to confirm the existence of secretory vesicles in cilia.

It would be finally worth investigating the exact role of Alms1 in the regulation of the Hippo pathway, whose dysregulation could be possibly the reason behind the heart enlargement defects observed in the *alms1* mutants.

| Mutant name | Curly body | Ciliogenesis defects | Retinal defects | Other |
|---|---|---|---|---|
| *bbs2*$^{sa2952}$ | - | - | - | + |
| *bbs9*$^{sa14425}$ | - | - | + | + |
| *cep290*$^{sa1383}$ | - | - | - | + |
| *alms1* $^{sa10311}$ | + | + | + | + |
| *rab23*$^{sa13880}$ | + | + | + | + |
| *tubby*$^{sa18104}$ | - | unknown | + | unknown |

Table 6. Phenotype summary of the mutants analyzed in this study. (+) indicates the existence of the phenotypes while (-) indicates absence of a specific phenotype.

# APPENDIX

BBS2 alignment

Similarity: 84.9%

```
homo              1 MLLPVFTLKLRHKISPRMVAIGRYDGTHPCLAAATQTGKVFIHNPHTRNQ
                    ||:|:|||||.|||:|||||||:|||.||||.||||.||||||||||.|
zebrafish         1 MLVPIFTLKLNHKINPRMVAIGKYDGIHPCLTAATQAGKVFIHNPHTRAQ

homo             51 HVSASRVFQSPLESDVSLLNINQAVSCLTAGVLNPELGYDALLVGTQTNL
                    ..:|.|:.||..:||:|||||||:|||||||.|.|:...|.||||:||||
zebrafish        51 RPTAHRLSQSTQDSDISLLNINQSVSCLTAGTLGPKSTGDTLLVGSQTNL

homo            101 LAYDVYNNSDLFYREVADGANAIVLGTLGDISSPLAIIGGNCALQGFNHE
                    |||||::|:|:||:||.|||||||||.||||.||||||||||||||::|
zebrafish       101 LAYDVHDNTDVFYKEVTDGANAIVLGKLGDIQSPLAIIGGNCALQGFDYE

homo            151 GSDLFWTVTGDNVNSLALCDFDGDGKKELLVGSEDFDIRVFKEDEIVAEM
                    |:||||||||||.||.|||||..|||.||||||||||||||||:|.||
zebrafish       151 GNDLFWTVTGDNVRSLVLCDFTADGKNELLVGSEDFDIRVFKEDELVTEM

homo            201 TETEIVTSLCPMYGSRFGYALSNGTVGVYDKTSRYWRIKSKNHAMSIHAF
                    .|.|.|||||.|:||||||||:||||||||:|:||||||||||||||||
zebrafish       201 AENETVTSLCHMHGSRFGYALANGTVGVYDRTARYWRIKSKNHAMSIHAF

homo            251 DLNSDGVNELITGWSNGKVDARSDRTGEVIFKDNFSSAIAGVVEGDYRMD
                    |||:|||.||||||||||:||||||||||||||||::||||||||||
zebrafish       251 DLNADGVVELITGWSNGKIDARSDRTGEVIFKDNFSSSVAGVVEGDYRMD

homo            301 GHIQLICCSVDGEIRGYLPGTAEMRGNLMDTSAEQDLIRELSQKKQNLLL
                    |.|||||.||:||:|||||.:.||:|||||:|.||||||||||:||||:|
zebrafish       301 GQIQLICTSVEGEVRGYLPASKEMKGNLMDSSIEQDLIRELSQRKQNLML

homo            351 ELRNYEENAKAELASPLNEADGHRGIIPANTRLHTTLSVSLGNETQTAHT
                    |||||||||||  ...|:|.:...|:|||||:|.|.|||...:|:|.||.
zebrafish       351 ELRNYEENAKA--LPGLSEGESKMGVIPANTQLQTALSVRRASESQKAHI

homo            401 ELRISTSNDTIIRAVLIFAEGIFTGESHVVHPSIHNLSSSICIPIVPPKD
                    ||.|||.|:|||||||||||||.|||||||||..|||..:.:||:||||
zebrafish       399 ELNISTPNETIIRAVLIFAEGIFEGESHVVHPSAQNLSGCVRVPIIPPKD

homo            451 VPVDLHLKAFVGYRSSTQFHVFESTRQLPRFSMYALTSLDP-ASEPISYV
                    :|||||:|||||.::|||||||.||||||||||.| ::|| |.||...|
zebrafish       449 IPVDLHIKAFVGGKTSTQFHVFEITRQLPRFSMYDL-NVDPSAPEPTGKV

homo            500 NFTIAERAQRVVVWLGQNFLLPEDTHIQNAPFQVCFTSLRNGGHLHIKIK
                    .|.|.:|.||||:||.|||||||..   ::| .|.|::||.||.|.|.::
zebrafish       498 TFCINDRPQRVVMWLNQNFLLPEGI---DSP-DVTFSALRGGGLLRISLQ

homo            550 LSGEITINTDDIDLAGDIIQSMASFFAIEDLQVEADFPVYFEELRKVLVK
                    .|||||:.|||||||||::||:|||.||||||.|:||||||:|||..|.:
zebrafish       544 TSGEITLRTDDIDLAGDLVQSLASFLAIEDLQAESDFPVYFKELRATLTE

homo            600 VDEYHSVHQKLSADMADHSNLIRSLLVGAEDARLMRDMKTMKSRYMELYD
                    |||:|||||||:|.||||||.||::||.|||||||.|.:.:||.||:||||
zebrafish       594 VDEFHSVHQKLTAAMADHSNYIRNMLVQAEDARLMGDWRNMKKRYIELYD

homo            650 LNRDLLNGYKIRCNNHTELLGNLKAVNQAIQRAGRLRVGKPKNQVITACR
                    |||||:|.||||.||||..||..||:||||||||||||||||:|||||||
zebrafish       644 LNRDLVNEYKIRSNNHNALLARLKSVNQAIQRAGRLRVGKPKSQVITACR

homo            700 DAIRSNNINTLFKIMRVGTASS    721
                    |||::||||.||||||.||.||
zebrafish       694 DAIKNNNINALFKIMRAGTTSS    715
```

BBS9 alignment

Similarity:70.2%

```
homo              1 MSLFKARDWWSTILGDKEEFDQGCLCLANVDNSGNGQDKIIVGSFMGYLR
                    ||||||||||:::||:.|||||||||:.:|||||.|.||||||||||.||
zebrafish         1 MSLFKARDWWASVLGEGEEFDQGCLCVGDVDNSGTGYDKIIVGSFMGMLR

homo             51 IFSPHPAKTGDGAQAEDLLLEVDLRDPVLQVEVGKFVSGTEMLHLAVLHS
                    ||||||||..:..:|:..||||.:.||::|||:||||||.:|.|||||||.
zebrafish        51 IFSPHPAKPDELTEADTQLLEVQMPDPIIQVELGKFVSCSESLHLAVLHP

homo            101 RKLCVYSVSGTLGNVEHGNQCQMKLMYEHNLQRTACNMTYGSFGGVKGRD
                    |||.||:|||||.|||||||:|.|::|:||||||||||||||.||||.|..
zebrafish       101 RKLSVYAVSGTAGNVEHGDQYQLRLVYEHNLQRTACNMTYGPFGGVTGHH

homo            151 LICIQSMDGMLMVFEQESYAFGRFLPGFLLPGPLAYSSRTDSFLTVSSCQ
                    .||||||||||.||||||||||||||||||||:|..|||||:||||.:
zebrafish       151 FICIQSMDGMLMFFEQESYAFGRFLPGFLLPGPLSYCIRTDSFITVSSTR

homo            201 QVESYKYQVLAFATDADKRQETEQQKLGSGKRLVVDWTLNIGEQALDICI
                    |||.|:|:.||.||||||.:|::.||...||||||..||||.:|||:||||||:
zebrafish       201 QVECYRYETLAVATDADTKQDSNQQSKSSGKRLTADWTLVLGEEALDICV

homo            251 VSFNQSASSVFVLGERNFFCLKDNGQIRFMKKLDWSPSCFLPYCSVSEGT
                    .:.:.:.||:|||||||.||||||||||||||::|||||||.||||||:
zebrafish       251 PNTSPAMSSIFVLGERNLFCLKDNGQIRFMKKLEFNPSCFLPYASVSEGS

homo            301 INTLIGNHNNMLHIYQDVTLKWATQLPHIPVAVRVGCLHDLKGVIVTLSD
                    .|.|:.||||||.:|||||||||.||..:||||||....:|||::|||||.
zebrafish       301 TNVLMCNHNNMLLVYQDVTLKWAAQLSCVPVAVRVANFLELKGLVVTLSS

homo            351 DGHLQCSYLGTDPSLFQAPNVQSRELNYDELDVEMKELQKIIKDVNKSQG
                    ||||||||:|||||.|.||.|.:||:||||:|.||||.||::|::..|:|.
zebrafish       351 DGHLQCSYMGTDPSFFTAPKVDAREVNYDEIDTEMKMLQRVIREATKTQD

homo            401 VWPMTEREDDLNVSVVVSPNFDSVSQATDVEVGTDLVPSVTVKVTLQNRV
                    :.|..|.|::|.::.|||.:.|.||.|...|:....|||||||.:::|.
zebrafish       401 ILPRAETEEELRLTAVVSSSLDEVSCAIIPEMNGMPVPSVTVKVKIKSRA

homo            451 ILQKAKLSVYVQPPLELTCDQFTFEFMTPDLTRTVSFSVYLKRSYTPSEL
                    ::|..|::|.|||||.:|.|||..:.|.......||||.:|...|.|:::
zebrafish       451 VVQNPKMTVCVQPPLAVTQDQFVLDSMGSGSELVVSFSAFLNGLYPPADM

homo            501 EGNAVVSYSRPTDRNPDGIPRVIQCKFRLPLKLICLPGQPSKTASHKITI
                    .|:..||||..|:.||.||||||.||||.|||:|:|.|....|.|.:||||:
zebrafish       501 SGDIAVSYSSATELNPSGIPRVSQCKFSLPLRLVCYPSSAIKNAKYKITV

homo            551 DTNKSPVSLLSLFPGFASQSDDDQVNVMGFHFLGGARITVLASKTSQRYR
                    ||||.||:|..:||.|:.:||::..:.:||..:.|:::.||||||||||
zebrafish       551 DTNKPPVNLNEVFPDFSEKSDNNDSSALGFQLITGSKVIVLASKTSQRYR

homo            601 IQSEQFEDLWLITNELILRLQEYFEKQGVKDFACSFSGSIPLQEYFELID
                    ||||.|||:||:..||:.|..::|...|||||..||:|.|||.||||.:|
zebrafish       601 IQSESFEDIWLVAKELVQRFDQHFASLGVKDFRNSFTGPIPLPEYFETVD

homo            651 HHFELRINGEKLEELLSERAVQFRAIQRRLLARFKDKTPAPLQHLDTLLD
                    ||||||:|.:|.::||||||||||||||.|||||||.|||:||||::
zebrafish       651 HHFELRVNAQKYQDLLSERAVQFRAIQRRLLTRFKDKTPGPLQNLDTLME

homo            701 GTYKQVIALADAVEENQGNLFQSFTRLKSATHLVILLIALWQKLSADQVA
                    |||:||:|||||.|:|:..|.|:|.||:|||||:|||::|||.|:::|..
zebrafish       701 GTYRQVLALADAAEDNRERLIQAFARLRSATHLLILLLSLWQGLNSEQTT

homo            751 ILEAAFLPLQEDTQELGWEETVDAAISHLLKTCLSKSSKEQALNLNS-QL
```

```
                    ||||..|||.:||.:|||||:||||:||||||||:|.|:||::|:: .|
zebrafish       751 ILEATLLPLLQDTPQLGWEESVDAAVSHLLKTCLSRSPKDQAISLSTGPL

homo            800 NIPKDTSQLKKHITLLCDRLSKGGRLCLSTDAAAPQTMVMPGGCTTIPES
                    .||||||:|||||.||||||.|||||.||::|..|..::||..|.||||.
zebrafish       801 TIPKDTSRLKKHIMLLCDRLGKGGRLSLSSEANVPTAVMMPAACETIPEP

homo            850 DL---EERSVEQDSTELFTNHRHLTAETPRPEVSPLQGVSE---------
                    .:   ||..::||:.: :...:..:........|..:...|
zebrafish       851 IIEQDEEAPLQQDAAK-YIKKKQSSKRVKSKSDSSKESSKEKKEKDPGKE

homo            888 --------------------------------------------------

zebrafish       900 STKETKKDSGKEKEAKVSTKESRRESTKEPKKESTKEPSKESSKDKESPR

homo            888 ----------------------------    887

zebrafish       950 EKEPSKEKTKVSRKSSVKAKEKKSEAGDG    978
```

Rab23 alignment

Similarity: 92%

```
homo              1 MLEEDMEVAIKMVVVGNGAVGKSSMIQRYCKGIFTKDYKKTIGVDFLERQ
                    ||||||||||:||||||||||||||||||||||||||||||||||||||||
zebrafish         1 MLEEDMEVAIKVVVVGNGAVGKSSMIQRYCKGIFTKDYKKTIGVDFLERQ

homo             51 IQVNDEDVRLMLWDTAGQEEFDAITKAYYRGAQACVLVFSTTDRESFEAV
                    |.||.||||||||||||||||||||||||||||||||||||||||||||:
zebrafish        51 IIVNGEDVRLMLWDTAGQEEFDAITKAYYRGAQACVLVFSTTDRESFEAI

homo            101 SSWREKVVAEVGDIPTVLVQNKIDLLDDSCIKNEEAEALAKRLKLRFYRT
                    |||:|||..|||||||||||||||||:.||||||.||||||||||||||
zebrafish       101 SSWKEKVEMEVGDIPTVLVQNKIDLLDDTVIKNEEAEGLAKRLKLRFYRT

homo            151 SVKEDLNVNEVFKYLAEKYLQKLKQQIAEDPELTHSSSNKIGVFNTSGGS
                    |||||||||||||||:||||:||||.||:.::.|:||||||||||:|..
zebrafish       151 SVKEDLNVNEVFKYLADKYLQRLKQQSAEETDIIHTSSNKIGVFNTTGSG

homo            201 HSGQNSSTLNGGDVINLRPNKQRTKKNRNPFSSCSIP    237
                    |..||||.|||.:::||||||||||.:|||.||.:.
zebrafish       201 HPNQNSSDLNGREIVNLRPNKQRTKKTKNPFGSCRLL    237
```

TUB alignment

Similarity: 75.1%

```
homo              1 MGARTPLPSFWVSFFAETGILFPGGTPWPMGSQHSKQHRKPGPLKRGHRR
                                                 |.|:||..
zebrafish         1 -----------------------------MSSKHSSD-------------

homo             51 DRRTTRRKYWKEGREIARVLDDEGRNLRQQKLDRQRALLEQKQKKKRQEP
                          |..    ...|||||.|||||||||||||||||||||||||
zebrafish         9 ---------WIP----YSTLDDEGTNLRQQKLDRQRALLEQKQKKKRQEP

homo            101 LMVQANADGRPRSRRARQSEEQAPLVESYLSSSGSTSYQVQEAD-----S
                    ||||:|.|||.|.||.|||||||||||||.:.||.|.||||:     :
zebrafish        46 LMVQSNLDGRSRVRRTRQSEEQAPLVESYLSGNSSTIYHVQEAEQEEVKA

homo            146 LASVQLGATRPTAPASAKRTKAAATAGGQGGAARKEKKGKHKGTSGPAAL
                    :|.||       ||.|||::| ..|:..|.|:|:|||||||..||||.
zebrafish        96 VAEVQ-------APRSAKKSK-PPTSTPQTGSAKKEKKGKHKGIDGPAAF

homo            196 AEDKSEAQGPVQILTVG----QSDHAQDAGETAAGGGERPSGQDLRATMQ
                    .::..|....:||||||    |...|:..|| |.|.......||||.||.
zebrafish       138 QDEGQELGNQIQILTVGHSPAQESEAEGQGE-AVGSTHSQGKQDLRVTML

homo            242 RKGISSSMSFDEDEEDEEENSSSSSQLNSNTRPSSATSRKSVREAASAPS
                    :|||||||:|||:|::::..|||||||||||||.||||:||.:||.||.:
zebrafish       187 KKGISSSMNFDEEEDEDDLVSSSSSQLNSNTRPGSATSKKSSKEATSAST

homo            292 PTAPEQPVDVEVQDLEEFALRPAPQGITIKCRITRDKKGMDRGMYPTYFL
                    |.|.|..:||:  |||||.|||||||:|:||||||||||||||||:|
zebrafish       237 PLANEPSIDVD--DLEEFTLRPAPQGVTVKCRITRDKKGMDRGMYPTYYL

homo            342 HLDREDGKKVFLLAGRKRKKSKTSNYLISVDPTDLSRGGDSYIGKLRSNL
                    ||:|||||||||||||||||||||||:|||||||||:|:||||||||
zebrafish       285 HLEREDGKKVFLLAGRKRKKSKTSNYLISIDPTDLSRGGESFIGKLRSNL

homo            392 MGTKFTVYDNGVNPQKASSSTLESGTLRQELAAVCYETNVLGFKGPRKMS
                    |||||||||:|:||.|.:|| ||:|.|||||||:||||||||||||||
zebrafish       335 MGTKFTVYDSGMNPVKTTSS-LEAGNLRQELAAICYETNVLGFKGPRKMS

homo            442 VIVPGMNMVHERVSIRPRNEHETLLARWQNKNTESIIELQNKTPVWNDDT
                    ||:|||||.|||||||||||:||||||||:|||:|||.||||||||||
zebrafish       384 VIIPGMNMDHERVSIRPRNEHESLLARWQNKSTESVIELHNKTPVWNDDT

homo            492 QSYVLNFHGRVTQASVKNFQIIHGNDPDYIVMQFGRVAEDVFTMDYNYPL
                    |||||||||||||||||||||.|||||||||||||||||||||||||:
zebrafish       434 QSYVLNFHGRVTQASVKNFQIIHDNDPDYIVMQFGRVAEDVFTMDYNYPM

homo            542 CALQAFAIALSSFDSKLACE    561
                    ||||||||||||||||||||
zebrafish       484 CALQAFAIALSSFDSKLACE    503
```

ALMS1 alignment

Similarity 23.9%

```
human              1 MEPEDLPWPGELEEEEEEEEEEEEEEEEAAAAAAANVDDVVVVEEVEEE
zebrafish          1 --------------------------------------------------
human             51 AGRELDSDSHYGPQHLESIDDEEDEEAKAWLQAHPGRILPPLSPPQHRYS
zebrafish          1 --------------------------------------------------
human            101 EGERTSLEKIVPLTCHVWQQIVYQGNSRTQISDTNVVCLETTAQRGSGDD
zebrafish          1 --------------------------------------------------
human            151 QKTESWHCLPQEMDSSQTLDTSQTRFNVRTEDTEVTDFPSLEEGILTQSE
zebrafish          1 --------------------------------------------------
human            201 NQVKEPNRDLFCSPLLVIQDSFASPDLPLLTCLTQDQEFAPDSLFHQSEL
zebrafish          1 --------------------------------------------------
human            251 SFAPLRGIPDKSEDTEWSSRPSEVSEALFQATAEVASDLASSRFSVSQHP
zebrafish          1 --------------------------------------------------
human            301 LIGSTAVGSQCPFLPSEQGNNEETISSVDELKIPKDCDRYDDLCSYMSWK
zebrafish          1 --------------------------------------------------
human            351 TRKDTQWPENNLADKDQVSVATSFDITDENIATKRSDHFDAARSYGQYWT
zebrafish          1 --------------------------------------------------
human            401 QEDSSKQAETYLTKGLQGKVESDVITLDGLNENAVVCSERVAELQRKPTR
zebrafish          1 --------------------------------------------------
human            451 ESEYHSSDLRMLRMSPDTVPKAPKHLKAGDTSKGGIAKVTQSNLKSGITT
zebrafish          1 --------------------------------------------------
human            501 TPVDSDIGSHLSLSLEDLSQLAVSSPLETTTGQHTDTLNQKTLADTHLTE
zebrafish          1 --------------------------------------------------
human            551 ETLKVTAIPEPADQKTATPTVLSSSHSHRGKPSIFYQQGLPDSHLTEEAL
zebrafish          1 --------------------------------------------------
human            601 KVSAAPGLADQTTGMSTLTSTSYSHREKPGTFYQQELPESNLTEEPLEVS
zebrafish          1 --------------------------------------------------
human            651 AAPGPVEQKTGIPTVSSTSHSHGEDLLFFYRQTLPDGHLTDQALKVSAVS
zebrafish          1 --------------------------------------------------
human            701 GPADQKTGTATVLSTPHSHREKPGIFYQQEFADSHQTEETLTKVSATPGP
zebrafish          1 --------------------------------------------------
human            751 ADQKTEIPAVQSSSYSQREKPSILYPQDLADSHLPEEGLKVSAVAGPADQ
zebrafish          1 --------------------------------------------------
human            801 KTGLPTVPSSAYSHREKLLVFYQQALLDSHLPEEALKVSAVSGPADGKTG
```

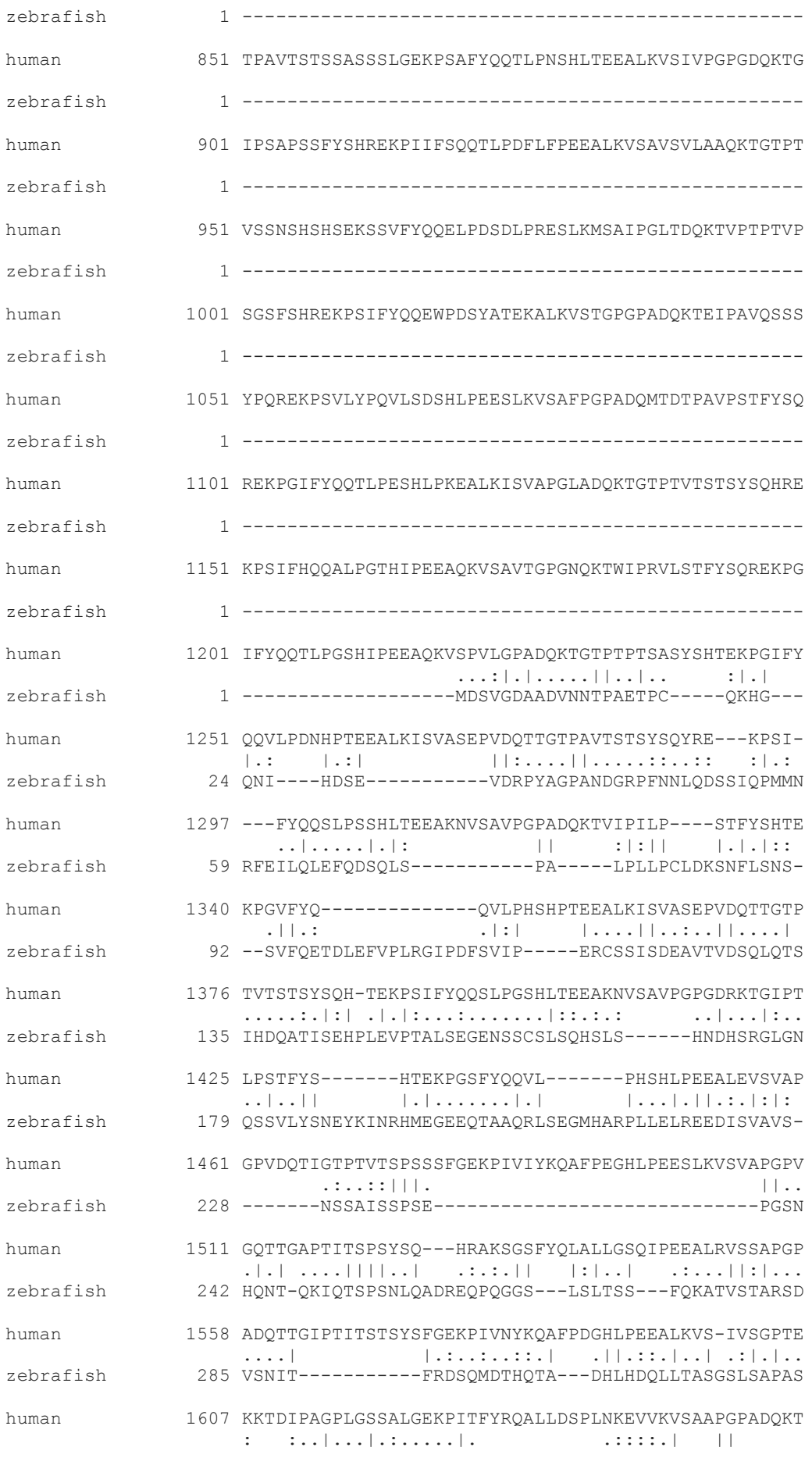
zebrafish 1 ----------
human 851 TPAVTSTSSASSSLGEKPSAFYQQTLPNSHLTEEALKVSIVPGPGDQKTG
zebrafish 1 ----------
human 901 IPSAPSSFYSHREKPIIFSQQTLPDFLFPEEALKVSAVSVLAAQKTGTPT
zebrafish 1 ----------
human 951 VSSNSHSHSEKSSVFYQQELPDSDLPRESLKMSAIPGLTDQKTVPTPTVP
zebrafish 1 ----------
human 1001 SGSFSHREKPSIFYQQEWPDSYATEKALKVSTGPGPADQKTEIPAVQSSS
zebrafish 1 ----------
human 1051 YPQREKPSVLYPQVLSDSHLPEESLKVSAFPGPADQMTDTPAVPSTFYSQ
zebrafish 1 ----------
human 1101 REKPGIFYQQTLPESHLPKEALKISVAPGLADQKTGTPTVTSTSYSQHRE
zebrafish 1 ----------
human 1151 KPSIFHQQALPGTHIPEEAQKVSAVTGPGNQKTWIPRVLSTFYSQREKPG
zebrafish 1 ----------
human 1201 IFYQQTLPGSHIPEEAQKVSPVLGPADQKTGTPTPTSASYSHTEKPGIFY
zebrafish 1 ----------MDSVGDAADVNNTPAETPC-----QKHG---
human 1251 QQVLPDNHPTEEALKISVASEPVDQTTGTPAVTSTSYSQYRE---KPSI-
zebrafish 24 QNI----HDSE----------VDRPYAGPANDGRPFNNLQDSSIQPMMN
human 1297 ---FYQQSLPSSHLTEEAKNVSAVPGPADQKTVIPILP----STFYSHTE
zebrafish 59 RFEILQLEFQDSQLS----------PA-----LPLLPCLDKSNFLSNS-
human 1340 KPGVFYQ----------QVLPHSHPTEEALKISVASEPVDQTTGTP
zebrafish 92 --SVFQETDLEFVPLRGIPDFSVIP-----ERCSSISDEAVTVDSQLQTS
human 1376 TVTSTSYSQH-TEKPSIFYQQSLPGSHLTEEAKNVSAVPGPGDRKTGIPT
zebrafish 135 IHDQATISEHPLEVPTALSEGENSSCSLSQHSLS------HNDHSRGLGN
human 1425 LPSTFYS-------HTEKPGSFYQQVL-------PHSHLPEEALEVSVAP
zebrafish 179 QSSVLYSNEYKINRHMEGEEQTAAQRLSEGMHARPLLELREEDISVAVS-
human 1461 GPVDQTIGTPTVTSPSSSFGEKPIVIYKQAFPEGHLPEESLKVSVAPGPV
zebrafish 228 -------NSSAISSPSE----------PGSN
human 1511 GQTTGAPTITSPSYSQ---HRAKSGSFYQLALLGSQIPEEALRVSSAPGP
zebrafish 242 HQNT-QKIQTSPSNLQADREQPQGGS---LSLTSS---FQKATVSTARSD
human 1558 ADQTTGIPTITSTSYSFGEKPIVNYKQAFPDGHLPEEALKVS-IVSGPTE
zebrafish 285 VSNIT----------FRDSQMDTHQTA---DHLHDQLLTASGSLSAPAS
human 1607 KKTDIPAGPLGSSALGEKPITFYRQALLDSPLNKEVVKVSAAPGPADQKT

```
zebrafish        321 R---LHGGNKSSDSAQSFTIA-----------GEDLIHV---PG------

human           1657 ETLPVHSTSYSNRGKPVIFYQQTLSDSHLPEEALKVPPV-PGPDAQKTET
                     :.....|:.|:.:......||...:.:....|||. |.|...|
zebrafish        348 ----LQRALLSSGGRLIGADGSFLSSQPVFQSTPAVPPTRPLPALTK---

human           1706 PSVSSSLYSYREKPIVFYQQALPDSELTQEALKVSAVPQPADQKTGLSTV
                     ||:..|    ::|.:.                ..:.:||....:|||..:
zebrafish        391 PSLIHS----KQKAVA---------------SAATLPQSNQSRTGLMPL

human           1756 -------TSSFYSHT--EKP-----NISYQQELPDSHLTEEALKVSNVPG
                           :||.||.|  .||     .:|:...:.:.|::...|.    |.
zebrafish        421 LDLSDQHSSSMYSQTTSSKPPKTEQTVSHAHSVSNEHISPAVLN----PT

human           1792 PADQKTGVSTVTSTSYSHREKPIVSYQRELPHFTEAGLKILRVPGPADQK
                     .||..   .:.|...||..||     :.::.|     |.:.||..
zebrafish        467 AADTS---RSDTQLFYSSTEK-----KDQVSH-----LALGRVQS-----

human           1842 TGINILPSNSYPQREHSVISYEQELPDLTEVTLKAIGVPGPADQKTGIQI
                          |||.||.|:..:..:.:.....: .|...||.|.:.:|....:
zebrafish        499 -----LPSLSYLQKVDAWKANQSSSRSFCD-NLALQGVDGVSLKKKAQDV

human           1892 AS------------------SSSYSNREKASIFHQQELPDVTEEALNVFV
                     .|                  :||.|.::.:|.......|...:|| ...|
zebrafish        543 GSDIFNQMDSRDKHQALCMNASSQSIQQLSSSHSGSVSPRRVDEA-GASV

human           1924 VPGQGDRKTEIPTVPLSYYSRREKPSVISQQELPDSHLTEEALKVSPVSI
                     ..||.   ::.|.:....:|  ...||::..:.....|:::|.......:
zebrafish        592 CKGQA---SDSPVIRSQSHS--SLSSVVTSIQRDTGTLSKQAPLTQSKDV

human           1974 PAEQKT-----GIPIGLSSSYSHSHKEKLKISTVHIPDDQKTEFPAATLS
                     ||..::     |...|:::|.:|.....:|:|            |..:|.
zebrafish        637 PATNQSSLISGGSNEGMNTSAAHMDTNAIKMS------------PFLSLG

human           2019 SYSQIEKPKISTVIGPNDQKTPSQTAFHSSYSQTVKPNILFQQQLPDRDQ
                     .:|.     :|:.:..:...:.||.::|.  .|:::.::          ..
zebrafish        675 RFSD-----VSSSVNLSSTLSSSQGSYHG--EQSMRASV---------GA

human           2069 SKGILKISA---VPELTDVNTGKPVSLSSSYFHREKSNIFS--PQELPGR
                     :..::.:..   .|..|...|..|        |..:.||..  |..|...
zebrafish        709 ASSVVSLEVDNYAPYWTSRPTSPP--------HTREFNIEDRIPLYLLNL

human           2114 HVTED---VLKVSTIPGPAGQKTVLPTALPSSFSHREKPDIFYQKDLPDR
                     .:.:.   :|...|..||..:....||
zebrafish        751 GIDQSPSTILNPFTRRGPIREPEFSPT----------------------

human           2161 HLTEDALKISSALG------QADQITGLQ--TVPSGTYSHGENHKLVSEH
                         |...|..::|      |..::..||  |..|.:....|:...||.|
zebrafish        778 ----DLCTIKGSIGTPTKSTQPSEVDSLQKETFSSSSQHSTESSASVSHH

human           2203 VQRLIDNLN--SSDSSV-------------SSNNVLLNSQADDRVVINKP
                     :.  :..|:  ::||||             |:::.....|..|.....:.
zebrafish        824 LS--VHELSQPATDSSVKVILTQADAAQLQSTSHPSTTLQQSDAAESERS

human           2238 ESAGFRDVGSEEIQDAEN----SAKTLKEIRTLLMEAENMALKRCNFPAP
                     .|....:.|..|:..|::    .:.||.|||.||..||::...|.:..:.
zebrafish        872 FSLPVPESGPREVVKADDDSLVGSGTLHEIRRLLGRAESLVSGRSSLTSS

human           2284 LARFR----DISDISFIQSKKVVCFKEPSSTGVSNGDLLHRQPFTEESPS
                     ....|    |.|.:|..::.:........|.|.:...||.|.
zebrafish        922 PGSHRLSESDTSLVSLGRNARGYHTDTSLSAGGNLSLLLTRS--------

human           2330 SRCIQKDIGTQTNLKCRRGIENWEFISSTTVRSPLQEAESKVSMALEETL
                         ..|...:.:|...:|.::   |..|||:      .:.:|::.||:|
zebrafish        964 ----SSDSALKGSLSSSQGPQH---IDLTTVK------PAALSLSREESL

human           2380 RQYQAAKSVMRSEPEGCSG-----------TIGNKIIIPMMTVIKSDSSS
                     :......:..|:||||||.           |.|.:|.:|.:.|....:..
zebrafish       1001 KARDLRVTPRRAEPEGCSAADPDKGKPTTTTSGTQINLPSIAVSVPQNEE
```

```
human          2419 DASDGNGSCSWDSNLPESLESVSDVLLNFFPYVSPKTSITDSREEEGVSE
                    |.|:       |:.:..|..|:|.|                |.|.|.:|:
zebrafish      1051 DTSE-------DAPIGSSENSLSHV----------------SAEAESLSD

human          2469 SEDGGGSSVDSLAAHVKNLLQCESSLNHAKEILRNAEEEESRVRAHAWNM
                    |     ||..||||.|..|||.||.::........|:.|:||.|  .|.:
zebrafish      1078 S-----SSESSLAARVAKLLQSESPVSMVTSRPSTADPEDSRAR--EWIL

human          2519 KFNLAHDCGYSISELNEDDRRKVEEIKAELFGHGRTTDLSKGLQSPRGMG
                    .......|  ...|||.:||:::||||.||..:.:.|..|.
zebrafish      1121 MKVSGRRC--ESLELNTEDRKRIEEIKRELLLNTKYTKWSS---------

human          2569 CKPEAVCSHIIIESHEKGCFRTLTSEHPQLDRHPCAFRSAG-PSEMTRGR
                                                |....|..|.| .|:.|:|
zebrafish      1160 -------------------------------DSEGSAQSSIGLESQQTKG-

human          2618 QNPSSCRAKHVNLSASLDQNNSHFKVWNSLQLKSHSPFQNFIPDEFKISK
                           :|.|      .|...::.:.||....:|.......|.|:.:
zebrafish      1179 ---------YVGL------RNMENRLSDQLQKAPSNPLSTVQDLEAKVHE

human          2668 -GLRMPFDEKMDPWLSELVEPAFVPPKEVDFHSSSQMPSPEPMKKFTTSI
                     .||..|..|              |...:...::.:.|||:
zebrafish      1214 IALREGFSTK--------------PFTSITISTTRRTPSPQ---------

human          2717 TFSSHRHSKCISNSSVVKVGVTEGSQCTGASVGVFNSHFTEEQNPPRDLK
                       |..||.......:..||
zebrafish      1241 ---SPPHSPVTGTLKITNVG------------------------------

human          2767 QKTSSPSSFKMHSNSQDKEVTILAEGRRQSQKLPVDFERSFQEEKPLERS
                    ....:|:..|  .:.::||    .||:.      :|.:::.::
zebrafish      1258 SANETPAGTK--DSDREKE----TEGQH------IDEKKTTED-------

human          2817 DFTGSHSEPSTRANCSNFKEIQISDNHTLISMGRPSSTLGVNRSSSRLGV

zebrafish      1289 --------------------------------------------------

human          2867 KEKNVTITPDLPSCIFLEQRELFEQSKAPRADDHVRKHHSPSPQHQDYVA
                    |::| |||                 .||.|.            .|.||
zebrafish      1289 KQEN-TIT-----------------DKAQRM------------SHIDY--

human          2917 PDLPSCIFLEQRELFEQCKAPYVDHQMRENHSPLPQGQDSIASDLPSPIS
                     ::.|..|
zebrafish      1307 -NVTSSTF-------------------------------------------

human          2967 LEQCQSKAPGVDDQMNKHHFPLPQGQDCVVEKNNQHKPKSHISNINVEAK
                                              ||    |||:|:|
zebrafish      1314 --------------------------------NN----KSHLSHI-----

human          3017 FNTVVSQSAPNHCTLAASASTPPSNRKALSCVHITLCPKTSSKLDSGTLD
                                              |:||.||..:::
zebrafish      1323 --------------------------------HVTLSPKPKNQI------

human          3067 ERFHSLDAASKARMNSEFNFDLH-----TVSSRSLEPTSKLLTSKPVAQD
                     ||      .|:..|...:..|.     :|:...|||..::.|
zebrafish      1335 -RF------EKSTQNISQDVALQRPIVPSVADPQLEPMHRIST-------

human          3112 QESLGFLGPKSSLDFQVVQPSLPDSNTITQDLKTIPSQNSQIVTSRQIQV
                          |...||.:::                :.:..||:..|::|
zebrafish      1371 ------LNHVSSYEYR----------------ERVQGQNTGRVSAR----

human          3162 NISDFEGHSNPEGTPVFADRLPEKMKTPLSAFSEKLSSDAVTQITTESPE
                        |.........|  ::||..|.:|        ||...
zebrafish      1395 ----FPARHTQSSAP--SNRLDMKSRT--------LSGQT----------

human          3212 KTLFSSEIFINAEDRGHEIIEPGNQKLRKAPVKFASSSSVQQVTFSRGTD
                                                          :.||.
zebrafish      1421 ---------------------------------------------AYGTA
```

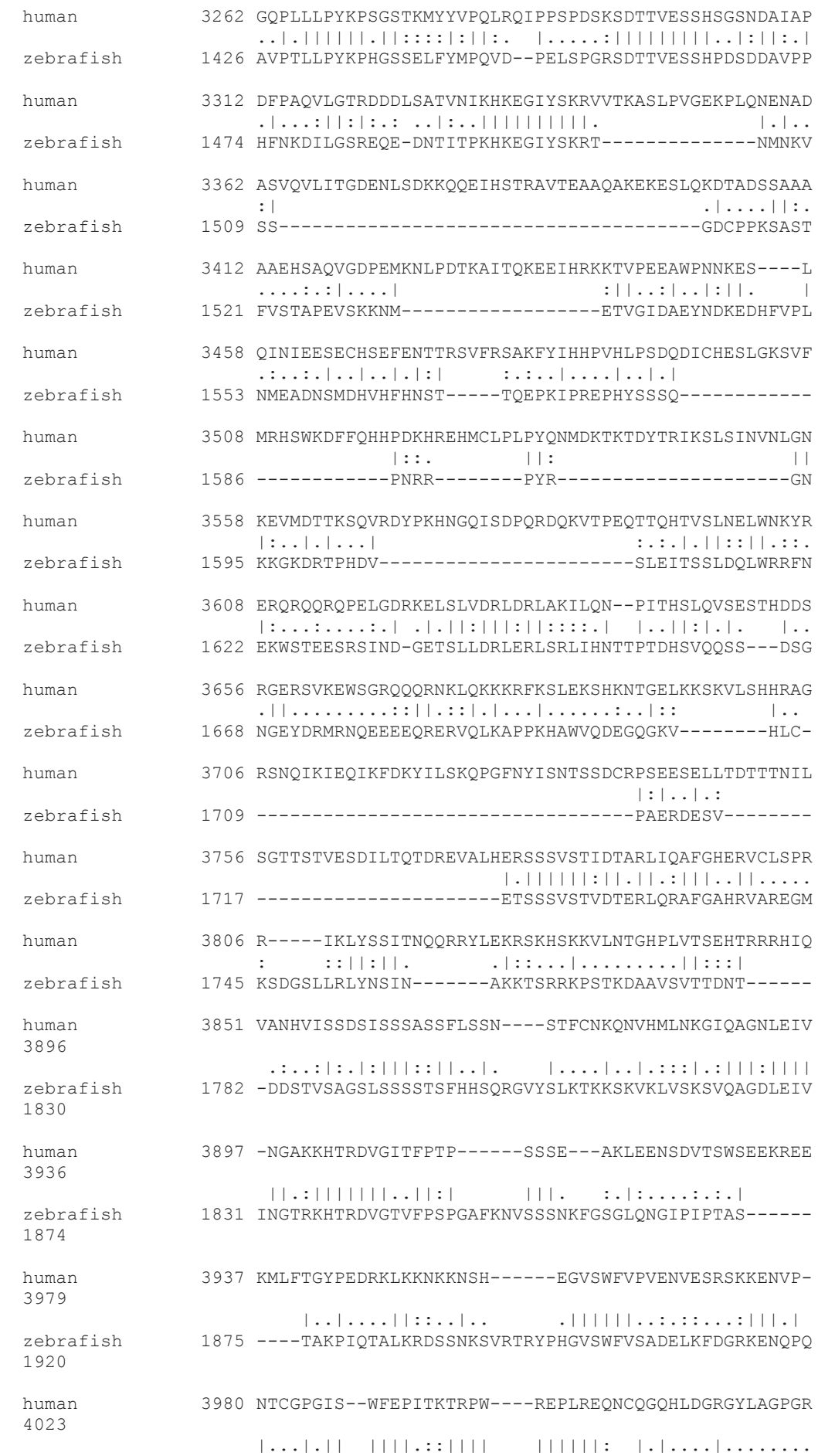
human 3262 GQPLLLPYKPSGSTKMYYVPQLRQIPPSPDSKSDTTVESSHSGSNDAIAP
zebrafish 1426 AVPTLLPYKPHGSSELFYMPQVD--PELSPGRSDTTVESSHPDSDDAVPP
human 3312 DFPAQVLGTRDDDLSATVNIKHKEGIYSKRVVTKASLPVGEKPLQNENAD
zebrafish 1474 HFNKDILGSREQE-DNTITPKHKEGIYSKRT--------------NMNKV
human 3362 ASVQVLITGDENLSDKKQQEIHSTRAVTEAAQAKEKESLQKDTADSSAAA
zebrafish 1509 SS-------------------------------------GDCPPKSAST
human 3412 AAEHSAQVGDPEMKNLPDTKAITQKEEIHRKKTVPEEAWPNNKES----L
zebrafish 1521 FVSTAPEVSKKNM------------------ETVGIDAEYNDKEDHFVPL
human 3458 QINIEESECHSEFENTTRSVFRSAKFYIHHPVHLPSDQDICHESLGKSVF
zebrafish 1553 NMEADNSMDHVHFHNST-----TQEPKIPREPHYSSSQ------------
human 3508 MRHSWKDFFQHHPDKHREHMCLPLPYQNMDKTKTDYTRIKSLSINVNLGN
zebrafish 1586 ------------PNRR--------PYR----------------------GN
human 3558 KEVMDTTKSQVRDYPKHNGQISDPQRDQKVTPEQTTQHTVSLNELWNKYR
zebrafish 1595 KKGKDRTPHDV-----------------------SLEITSSLDQLWRRFN
human 3608 ERQRQQRQPELGDRKELSLVDRLDRLAKILQN--PITHSLQVSESTHDDS
zebrafish 1622 EKWSTEESRSIND-GETSLLDRLERLSRLIHNTTPTDHSVQQSS---DSG
human 3656 RGERSVKEWSGRQQQRNKLQKKKRFKSLEKSHKNTGELKKSKVLSHHRAG
zebrafish 1668 NGEYDRMRNQEEEEQRERVQLKAPPKHAWVQDEGQGKV--------HLC-
human 3706 RSNQIKIEQIKFDKYILSKQPGFNYISNTSSDCRPSEESELLTDTTTNIL
zebrafish 1709 ----------------------------------PAERDESV--------
human 3756 SGTTSTVESDILTQTDREVALHERSSSVSTIDTARLIQAFGHERVCLSPR
zebrafish 1717 ----------------------ETSSSVSTVDTERLQRAFGAHRVAREGM
human 3806 R-----IKLYSSITNQQRRYLEKRSKHSKKVLNTGHPLVTSEHTRRRHIQ
zebrafish 1745 KSDGSLLRLYNSIN-------AKKTSRRKPSTKDAAVSVTTDNT------
human 3851 VANHVISSDSISSSASSFLSSN----STFCNKQNVHMLNKGIQAGNLEIV
3896
zebrafish 1782 -DDSTVSAGSLSSSSTSFHHSQRGVYSLKTKKSKVKLVSKSVQAGDLEIV
1830
human 3897 -NGAKKHTRDVGITFPTP------SSSE---AKLEENSDVTSWSEEKREE
3936
zebrafish 1831 INGTRKHTRDVGTVFPSPGAFKNVSSSNKFGSGLQNGIPIPTAS------
1874
human 3937 KMLFTGYPEDRKLKKNKKNSH------EGVSWFVPVENVESRSKKENVP-
3979
zebrafish 1875 ----TAKPIQTALKRDSSNKSVRTRYPHGVSWFVSADELKFDGRKENQPQ
1920
human 3980 NTCGPGIS--WFEPITKTRPW----REPLREQNCQGQHLDGRGYLAGPGR
4023

```
zebrafish       1921 NESEPSISQAWFEPYSRTRPWRESSREPLRER--QNQQEQERQTETRTAM

human           4024 EAG-RDLLKPFVRATLQESLQFHRPDFISRSGERIKRLKLIVQERKLQSM
                     |.. .|.....||.:|||:|:.|||:|:|||.||:|||.|:|:||:||::
zebrafish       1969 ETDISDKTSALVRLSLQEALELHRPEFVSRSRERMKRLGLLVEERRLQAI

human           4073 LQTERDALFNIDRERQGHQNRMCPLPKRVFLA--IQKNKPISKKEMIQRS
                     ...||:.|||.            |.|.|...|  :.:.:.:.:|||:|||
zebrafish       2019 FNREREELFNF------------PAPSRPLRAAPVPRKRVVPRKEMVQRS

human           4121 KRIYEQLPEVQKKREEEKRKSEYKSYRLRAQLYKKRVTNQLLGRKVPWD
                     :..|.:||||||:|||||::||:||||.|||:.|:|||::|||:.||.
zebrafish       2057 REKYAKLPEVQKRREEEKRRAEYRSYRLTAQLFNKKVTNRVLGRRAPWQ
```

# REFERENCES


Abdelhamed, Z. A., Natarajan, S., Wheway, G., Inglehearn, C. F., Toomes, C., Johnson, C. A., & Jagger, D. J. (2015). The Meckel-Gruber syndrome protein TMEM67 controls basal body positioning and epithelial branching morphogenesis in mice via the non-canonical Wnt pathway. *Dis Model Mech, 8*(6), 527-541. doi:10.1242/dmm.019083

Abu Safieh, L., Aldahmesh, M. A., Shamseldin, H., Hashem, M., Shaheen, R., Alkuraya, H., . . . Alkuraya, F. S. (2010). Clinical and molecular characterisation of Bardet-Biedl syndrome in consanguineous populations: the power of homozygosity mapping. *J Med Genet, 47*(4), 236-241. doi:10.1136/jmg.2009.070755

Aceto, J., Nourizadeh-Lillabadi, R., Maree, R., Dardenne, N., Jeanray, N., Wehenkel, L., . . . Muller, M. (2015). Zebrafish Bone and General Physiology Are Differently Affected by Hormones or Changes in Gravity. *PLoS One, 10*(6), e0126928. doi:10.1371/journal.pone.0126928

Afzelius, B. A. (2004). Cilia-related diseases. *J Pathol, 204*(4), 470-477. doi:10.1002/path.1652

Aizawa, H., Goto, M., Sato, T., & Okamoto, H. (2007). Temporally regulated asymmetric neurogenesis causes left-right difference in the zebrafish habenular structures. *Dev Cell, 12*(1), 87-98. doi:10.1016/j.devcel.2006.10.004

Alam, A., Adhi, M., Bano, R., Zubair, A., & Mushtaq, A. (2013). Meckel Gruber Syndrome: Second trimester diagnosis of a case in a non-consanguineous marriage. *Pak J Med Sci, 29*(1), 234-236. doi:10.12669/pjms.291.2930

Antal-Zimanyi, I., & Khawaja, X. (2009). The role of melanin-concentrating hormone in energy homeostasis and mood disorders. *J Mol Neurosci, 39*(1-2), 86-98. doi:10.1007/s12031-009-9207-6

Arsov, T., Silva, D. G., O'Bryan, M. K., Sainsbury, A., Lee, N. J., Kennedy, C., . . . Petrovsky, N. (2006). Fat aussie--a new Alstrom syndrome mouse showing a critical role for ALMS1 in obesity, diabetes, and spermatogenesis. *Mol Endocrinol, 20*(7), 1610-1622. doi:10.1210/me.2005-0494

Bahmad Jr, F., Costa, C. S., Teixeira, M. S., Barros Filho, J., Viana, L. M., & Marshall, J. (2014). Familial Alstrom syndrome: a rare cause of bilateral progressive hearing loss. *Braz J Otorhinolaryngol, 80*(2), 99-104.

Bang, P. I., Sewell, W. F., & Malicki, J. J. (2001). Morphology and cell type heterogeneities of the inner ear epithelia in adult and juvenile zebrafish (Danio rerio). *J Comp Neurol, 438*(2), 173-190.

Barisic, I., Boban, L., Loane, M., Garne, E., Wellesley, D., Calzolari, E., . . . Verellen-Dumoulin, C. (2015). Meckel-Gruber Syndrome: a population-based study on prevalence, prenatal diagnosis, clinical features, and survival in Europe. *Eur J Hum Genet, 23*(6), 746-752. doi:10.1038/ejhg.2014.174

Basten, S. G., & Giles, R. H. (2013). Functional aspects of primary cilia in signaling, cell cycle and tumorigenesis. *Cilia, 2*(1), 6. doi:10.1186/2046-2530-2-6

Basu, B., & Brueckner, M. (2008). Cilia multifunctional organelles at the center of vertebrate left-right asymmetry. *Curr Top Dev Biol, 85*, 151-174. doi:10.1016/S0070-2153(08)00806-5

Baxendale, S., & Whitfield, T. T. (2016). Methods to study the development, anatomy, and function of the zebrafish inner ear across the life course. *Methods Cell Biol, 134*, 165-209. doi:10.1016/bs.mcb.2016.02.007

Baye, L. M., Patrinostro, X., Swaminathan, S., Beck, J. S., Zhang, Y., Stone, E. M., . . . Slusarski, D. C. (2011). The N-terminal region of centrosomal protein 290 (CEP290) restores vision in a zebrafish model of human blindness. *Hum Mol Genet, 20*(8), 1467-1477. doi:10.1093/hmg/ddr025

Beales, P. L., Elcioglu, N., Woolf, A. S., Parker, D., & Flinter, F. A. (1999). New criteria for improved diagnosis of Bardet-Biedl syndrome: results of a population survey. *J Med Genet, 36*(6), 437-446.

Becker-Heck, A., Zohn, I. E., Okabe, N., Pollock, A., Lenhart, K. B., Sullivan-Brown, J., . . . Burdine, R. D. (2011). The coiled-coil domain containing protein CCDC40 is essential for motile cilia function and left-right axis formation. *Nat Genet, 43*(1), 79-84. doi:10.1038/ng.727

Berbari, N. F., Johnson, A. D., Lewis, J. S., Askwith, C. C., & Mykytyn, K. (2008). Identification of ciliary localization sequences within the third intracellular loop of

G protein-coupled receptors. *Mol Biol Cell, 19*(4), 1540-1547. doi:10.1091/mbc.E07-09-0942
Berbari, N. F., Lewis, J. S., Bishop, G. A., Askwith, C. C., & Mykytyn, K. (2008). Bardet-Biedl syndrome proteins are required for the localization of G protein-coupled receptors to primary cilia. *Proc Natl Acad Sci U S A, 105*(11), 4242-4246. doi:10.1073/pnas.0711027105
Bever, M. M., & Fekete, D. M. (2002). Atlas of the developing inner ear in zebrafish. *Dev Dyn, 223*(4), 536-543. doi:10.1002/dvdy.10062
Boehlke, C., Bashkurov, M., Buescher, A., Krick, T., John, A. K., Nitschke, R., . . . Kuehn, E. W. (2010). Differential role of Rab proteins in ciliary trafficking: Rab23 regulates smoothened levels. *J Cell Sci, 123*(Pt 9), 1460-1467. doi:10.1242/jcs.058883
Boggon, T. J., Shan, W. S., Santagata, S., Myers, S. C., & Shapiro, L. (1999). Implication of tubby proteins as transcription factors by structure-based functional analysis. *Science, 286*(5447), 2119-2125.
Borovina, A., Superina, S., Voskas, D., & Ciruna, B. (2010). Vangl2 directs the posterior tilting and asymmetric localization of motile primary cilia. *Nat Cell Biol, 12*(4), 407-412. doi:10.1038/ncb2042
Brancati, F., Dallapiccola, B., & Valente, E. M. (2010). Joubert Syndrome and related disorders. *Orphanet J Rare Dis, 5*, 20. doi:10.1186/1750-1172-5-20
Brancati, F., Travaglini, L., Zablocka, D., Boltshauser, E., Accorsi, P., Montagna, G., . . . Valente, E. M. (2008). RPGRIP1L mutations are mainly associated with the cerebello-renal phenotype of Joubert syndrome-related disorders. *Clin Genet, 74*(2), 164-170. doi:10.1111/j.1399-0004.2008.01047.x
Branchek, T. (1984). The development of photoreceptors in the zebrafish, brachydanio rerio. II. Function. *J Comp Neurol, 224*(1), 116-122. doi:10.1002/cne.902240110
Brand, M., Heisenberg, C. P., Jiang, Y. J., Beuchle, D., Lun, K., Furutani-Seiki, M., . . . Nusslein-Volhard, C. (1996). Mutations in zebrafish genes affecting the formation of the boundary between midbrain and hindbrain. *Development, 123*, 179-190.
Brockerhoff, S. E., & Fadool, J. M. (2011). Genetics of photoreceptor degeneration and regeneration in zebrafish. *Cell Mol Life Sci, 68*(4), 651-659. doi:10.1007/s00018-010-0563-8
Bujakowska, K. M., Zhang, Q., Siemiatkowska, A. M., Liu, Q., Place, E., Falk, M. J., . . . Pierce, E. A. (2015). Mutations in IFT172 cause isolated retinal degeneration and Bardet-Biedl syndrome. *Hum Mol Genet, 24*(1), 230-242. doi:10.1093/hmg/ddu441
Burnight, E. R., Wiley, L. A., Drack, A. V., Braun, T. A., Anfinson, K. R., Kaalberg, E. E., . . . Tucker, B. A. (2014). CEP290 gene transfer rescues Leber congenital amaurosis cellular phenotype. *Gene Ther, 21*(7), 662-672. doi:10.1038/gt.2014.39
Caberoy, N. B., Maiguel, D., Kim, Y., & Li, W. (2010). Identification of tubby and tubby-like protein 1 as eat-me signals by phage display. *Exp Cell Res, 316*(2), 245-257. doi:10.1016/j.yexcr.2009.10.008
Calzada, A. P., Lopez, I. A., Beltran Parrazal, L., Ishiyama, A., & Ishiyama, G. (2012). Cochlin expression in vestibular endorgans obtained from patients with Meniere's disease. *Cell Tissue Res, 350*(2), 373-384. doi:10.1007/s00441-012-1481-x
Cao, Y., Park, A., & Sun, Z. (2010). Intraflagellar transport proteins are essential for cilia formation and for planar cell polarity. *J Am Soc Nephrol, 21*(8), 1326-1333. doi:10.1681/ASN.2009091001
Cardenas-Rodriguez, M., & Badano, J. L. (2009). Ciliary biology: understanding the cellular and genetic basis of human ciliopathies. *Am J Med Genet C Semin Med Genet, 151C*(4), 263-280. doi:10.1002/ajmg.c.30227
Chang, B., Khanna, H., Hawes, N., Jimeno, D., He, S., Lillo, C., . . . Swaroop, A. (2006). In-frame deletion in a novel centrosomal/ciliary protein CEP290/NPHP6 perturbs its interaction with RPGR and results in early-onset retinal degeneration in the rd16 mouse. *Hum Mol Genet, 15*(11), 1847-1857. doi:10.1093/hmg/ddl107
Chatterjee, P., Padmanarayana, M., Abdullah, N., Holman, C. L., LaDu, J., Tanguay, R. L., & Johnson, C. P. (2015). Otoferlin deficiency in zebrafish results in defects in balance and hearing: rescue of the balance and hearing phenotype with full-length and truncated forms of mouse otoferlin. *Mol Cell Biol, 35*(6), 1043-1054. doi:10.1128/MCB.01439-14

Chen, J. N., van Bebber, F., Goldstein, A. M., Serluca, F. C., Jackson, D., Childs, S., . . . Fishman, M. C. (2001). Genetic steps to organ laterality in zebrafish. *Comp Funct Genomics, 2*(2), 60-68. doi:10.1002/cfg.74
Chen, J. N., van Eeden, F. J., Warren, K. S., Chin, A., Nusslein-Volhard, C., Haffter, P., & Fishman, M. C. (1997). Left-right pattern of cardiac BMP4 may drive asymmetry of the heart in zebrafish. *Development, 124*(21), 4373-4382.
Chih, B., Liu, P., Chinn, Y., Chalouni, C., Komuves, L. G., Hass, P. E., . . . Peterson, A. S. (2012). A ciliopathy complex at the transition zone protects the cilia as a privileged membrane domain. *Nat Cell Biol, 14*(1), 61-72. doi:10.1038/ncb2410
Clark, K. J., Boczek, N. J., & Ekker, S. C. (2011). Stressing zebrafish for behavioral genetics. *Rev Neurosci, 22*(1), 49-62. doi:10.1515/RNS.2011.007
Cognard, N., Scerbo, M. J., Obringer, C., Yu, X., Costa, F., Haser, E., . . . Marion, V. (2015). Comparing the Bbs10 complete knockout phenotype with a specific renal epithelial knockout one highlights the link between renal defects and systemic inactivation in mice. *Cilia, 4*, 10. doi:10.1186/s13630-015-0019-8
Cohen, M. M., Jr. (2008). Craniofacial sutures. Development, disease and treatment. Foreword. *Front Oral Biol, 12*, vii-ix.
Coleman, D. L. (1978). Obese and diabetes: two mutant genes causing diabetes-obesity syndromes in mice. *Diabetologia, 14*(3), 141-148.
Collin, G. B., Cyr, E., Bronson, R., Marshall, J. D., Gifford, E. J., Hicks, W., . . . Naggert, J. K. (2005). Alms1-disrupted mice recapitulate human Alstrom syndrome. *Hum Mol Genet, 14*(16), 2323-2333. doi:10.1093/hmg/ddi235
Collin, G. B., Marshall, J. D., King, B. L., Milan, G., Maffei, P., Jagger, D. J., & Naggert, J. K. (2012). The Alstrom syndrome protein, ALMS1, interacts with alpha-actinin and components of the endosome recycling pathway. *PLoS One, 7*(5), e37925. doi:10.1371/journal.pone.0037925
Coppieters, F., Lefever, S., Leroy, B. P., & De Baere, E. (2010). CEP290, a gene with many faces: mutation overview and presentation of CEP290base. *Hum Mutat, 31*(10), 1097-1108. doi:10.1002/humu.21337
Corbit, K. C., Aanstad, P., Singla, V., Norman, A. R., Stainier, D. Y., & Reiter, J. F. (2005). Vertebrate Smoothened functions at the primary cilium. *Nature, 437*(7061), 1018-1021. doi:10.1038/nature04117
Corbit, K. C., Shyer, A. E., Dowdle, W. E., Gaulden, J., Singla, V., Chen, M. H., . . . Reiter, J. F. (2008). Kif3a constrains beta-catenin-dependent Wnt signalling through dual ciliary and non-ciliary mechanisms. *Nat Cell Biol, 10*(1), 70-76. doi:10.1038/ncb1670
Couzens, A. L., Knight, J. D., Kean, M. J., Teo, G., Weiss, A., Dunham, W. H., . . . Gingras, A. C. (2013). Protein interaction network of the mammalian Hippo pathway reveals mechanisms of kinase-phosphatase interactions. *Sci Signal, 6*(302), rs15. doi:10.1126/scisignal.2004712
Craige, B., Tsao, C. C., Diener, D. R., Hou, Y., Lechtreck, K. F., Rosenbaum, J. L., & Witman, G. B. (2010). CEP290 tethers flagellar transition zone microtubules to the membrane and regulates flagellar protein content. *J Cell Biol, 190*(5), 927-940. doi:10.1083/jcb.201006105
Davis, R. E., Swiderski, R. E., Rahmouni, K., Nishimura, D. Y., Mullins, R. F., Agassandian, K., . . . Sheffield, V. C. (2007). A knockin mouse model of the Bardet-Biedl syndrome 1 M390R mutation has cilia defects, ventriculomegaly, retinopathy, and obesity. *Proc Natl Acad Sci U S A, 104*(49), 19422-19427. doi:10.1073/pnas.0708571104
Delling, M., Indzhykulian, A. A., Liu, X., Li, Y., Xie, T., Corey, D. P., & Clapham, D. E. (2016). Primary cilia are not calcium-responsive mechanosensors. *Nature, 531*(7596), 656-660. doi:10.1038/nature17426
Delous, M., Baala, L., Salomon, R., Laclef, C., Vierkotten, J., Tory, K., . . . Saunier, S. (2007). The ciliary gene RPGRIP1L is mutated in cerebello-oculo-renal syndrome (Joubert syndrome type B) and Meckel syndrome. *Nat Genet, 39*(7), 875-881. doi:10.1038/ng2039
DeMaria, S., Berke, A. P., Van Name, E., Heravian, A., Ferreira, T., & Ngai, J. (2013). Role of a ubiquitously expressed receptor in the vertebrate olfactory system. *J Neurosci, 33*(38), 15235-15247. doi:10.1523/JNEUROSCI.2339-13.2013
Doerre, G., & Malicki, J. (2002). Genetic analysis of photoreceptor cell development in the zebrafish retina. *Mech Dev, 110*(1-2), 125-138.
Doll, C. A., Burkart, J. T., Hope, K. D., Halpern, M. E., & Gamse, J. T. (2011). Subnuclear development of the zebrafish habenular nuclei requires ER translocon function. *Dev Biol, 360*(1), 44-57. doi:10.1016/j.ydbio.2011.09.003

Driever, W., Solnica-Krezel, L., Schier, A. F., Neuhauss, S. C., Malicki, J., Stemple, D. L., . . . Boggs, C. (1996). A genetic screen for mutations affecting embryogenesis in zebrafish. *Development, 123*, 37-46.
Drivas, T. G., Wojno, A. P., Tucker, B. A., Stone, E. M., & Bennett, J. (2015). Basal exon skipping and genetic pleiotropy: A predictive model of disease pathogenesis. *Sci Transl Med, 7*(291), 291ra297. doi:10.1126/scitranslmed.aaa5370
Eggenschwiler, J. T., Bulgakov, O. V., Qin, J., Li, T., & Anderson, K. V. (2006). Mouse Rab23 regulates hedgehog signaling from smoothened to Gli proteins. *Dev Biol, 290*(1), 1-12. doi:10.1016/j.ydbio.2005.09.022
Eggenschwiler, J. T., Espinoza, E., & Anderson, K. V. (2001). Rab23 is an essential negative regulator of the mouse Sonic hedgehog signalling pathway. *Nature, 412*(6843), 194-198. doi:10.1038/35084089
Eisen, J. S., & Smith, J. C. (2008). Controlling morpholino experiments: don't stop making antisense. *Development, 135*(10), 1735-1743. doi:10.1242/dev.001115
Endoh-Yamagami, S., Evangelista, M., Wilson, D., Wen, X., Theunissen, J. W., Phamluong, K., . . . Peterson, A. S. (2009). The mammalian Cos2 homolog Kif7 plays an essential role in modulating Hh signal transduction during development. *Curr Biol, 19*(15), 1320-1326. doi:10.1016/j.cub.2009.06.046
Essner, J. J., Amack, J. D., Nyholm, M. K., Harris, E. B., & Yost, H. J. (2005). Kupffer's vesicle is a ciliated organ of asymmetry in the zebrafish embryo that initiates left-right development of the brain, heart and gut. *Development, 132*(6), 1247-1260. doi:10.1242/dev.01663
Evans, T. M., Ferguson, C., Wainwright, B. J., Parton, R. G., & Wicking, C. (2003). Rab23, a negative regulator of hedgehog signaling, localizes to the plasma membrane and the endocytic pathway. *Traffic, 4*(12), 869-884.
Falk, N., Losl, M., Schroder, N., & Giessl, A. (2015). Specialized Cilia in Mammalian Sensory Systems. *Cells, 4*(3), 500-519. doi:10.3390/cells4030500
Farag, T. I., & Teebi, A. S. (1989). High incidence of Bardet Biedl syndrome among the Bedouin. *Clin Genet, 36*(6), 463-464.
Ferrans, V. J. (1989). Pathologic anatomy of the dilated cardiomyopathies. *Am J Cardiol, 64*(6), 9C-11C.
Ferrante, M. I., Zullo, A., Barra, A., Bimonte, S., Messaddeq, N., Studer, M., . . . Franco, B. (2006). Oral-facial-digital type I protein is required for primary cilia formation and left-right axis specification. *Nat Genet, 38*(1), 112-117. doi:10.1038/ng1684
Fisch, C., & Dupuis-Williams, P. (2011). [The rebirth of the ultrastructure of cilia and flagella]. *Biol Aujourdhui, 205*(4), 245-267. doi:10.1051/jbio/2011023
Fliegauf, M., Benzing, T., & Omran, H. (2007). When cilia go bad: cilia defects and ciliopathies. *Nat Rev Mol Cell Biol, 8*(11), 880-893. doi:10.1038/nrm2278
Forsythe, E., & Beales, P. L. (2013). Bardet-Biedl syndrome. *Eur J Hum Genet, 21*(1), 8-13. doi:10.1038/ejhg.2012.115
Fotiadis, D., Liang, Y., Filipek, S., Saperstein, D. A., Engel, A., & Palczewski, K. (2003). Atomic-force microscopy: Rhodopsin dimers in native disc membranes. *Nature, 421*(6919), 127-128. doi:10.1038/421127a
Fuller, K., O'Connell, J. T., Gordon, J., Mauti, O., & Eggenschwiler, J. (2014). Rab23 regulates Nodal signaling in vertebrate left-right patterning independently of the Hedgehog pathway. *Dev Biol, 391*(2), 182-195. doi:10.1016/j.ydbio.2014.04.012
Garcia-Gonzalo, F. R., Corbit, K. C., Sirerol-Piquer, M. S., Ramaswami, G., Otto, E. A., Noriega, T. R., . . . Reiter, J. F. (2011). A transition zone complex regulates mammalian ciliogenesis and ciliary membrane composition. *Nat Genet, 43*(8), 776-784. doi:10.1038/ng.891
Gascue, C., Tan, P. L., Cardenas-Rodriguez, M., Libisch, G., Fernandez-Calero, T., Liu, Y. P., . . . Badano, J. L. (2012). Direct role of Bardet-Biedl syndrome proteins in transcriptional regulation. *J Cell Sci, 125*(Pt 2), 362-375. doi:10.1242/jcs.089375
Gerdes, J. M., Liu, Y., Zaghloul, N. A., Leitch, C. C., Lawson, S. S., Kato, M., . . . Katsanis, N. (2007). Disruption of the basal body compromises proteasomal function and perturbs intracellular Wnt response. *Nat Genet, 39*(11), 1350-1360. doi:10.1038/ng.2007.12
Gilula, N. B., & Satir, P. (1972). The ciliary necklace. A ciliary membrane specialization. *J Cell Biol, 53*(2), 494-509.
Goetz, S. C., & Anderson, K. V. (2010). The primary cilium: a signalling centre during vertebrate development. *Nat Rev Genet, 11*(5), 331-344. doi:10.1038/nrg2774

Green, J. A., & Mykytyn, K. (2010). Neuronal ciliary signaling in homeostasis and disease. *Cell Mol Life Sci, 67*(19), 3287-3297. doi:10.1007/s00018-010-0425-4
Grimes, D. T., Boswell, C. W., Morante, N. F., Henkelman, R. M., Burdine, R. D., & Ciruna, B. (2016). Zebrafish models of idiopathic scoliosis link cerebrospinal fluid flow defects to spine curvature. *Science, 352*(6291), 1341-1344. doi:10.1126/science.aaf6419
Guemez-Gamboa, A., Coufal, N. G., & Gleeson, J. G. (2014). Primary cilia in the developing and mature brain. *Neuron, 82*(3), 511-521. doi:10.1016/j.neuron.2014.04.024
Gunther, T., Struwe, M., Aguzzi, A., & Schughart, K. (1994). Open brain, a new mouse mutant with severe neural tube defects, shows altered gene expression patterns in the developing spinal cord. *Development, 120*(11), 3119-3130.
Guo, D. F., Cui, H., Zhang, Q., Morgan, D. A., Thedens, D. R., Nishimura, D., . . . Rahmouni, K. (2016). The BBSome Controls Energy Homeostasis by Mediating the Transport of the Leptin Receptor to the Plasma Membrane. *PLoS Genet, 12*(2), e1005890. doi:10.1371/journal.pgen.1005890
Habbig, S., Bartram, M. P., Muller, R. U., Schwarz, R., Andriopoulos, N., Chen, S., . . . Schermer, B. (2011). NPHP4, a cilia-associated protein, negatively regulates the Hippo pathway. *J Cell Biol, 193*(4), 633-642. doi:10.1083/jcb.201009069
Haddon, C., & Lewis, J. (1996). Early ear development in the embryo of the zebrafish, Danio rerio. *J Comp Neurol, 365*(1), 113-128. doi:10.1002/(SICI)1096-9861(19960129)365:1<113::AID-CNE9>3.0.CO;2-6
Handel, M., Schulz, S., Stanarius, A., Schreff, M., Erdtmann-Vourliotis, M., Schmidt, H., . . . Hollt, V. (1999). Selective targeting of somatostatin receptor 3 to neuronal cilia. *Neuroscience, 89*(3), 909-926.
Hansen, A., & Zeiske, E. (1993). Development of the olfactory organ in the zebrafish, Brachydanio rerio. *J Comp Neurol, 333*(2), 289-300. doi:10.1002/cne.903330213
Hansen, A., & Zeiske, E. (1998). The peripheral olfactory organ of the zebrafish, Danio rerio: an ultrastructural study. *Chem Senses, 23*(1), 39-48.
Happe, H., van der Wal, A. M., Leonhard, W. N., Kunnen, S. J., Breuning, M. H., de Heer, E., & Peters, D. J. (2011). Altered Hippo signalling in polycystic kidney disease. *J Pathol, 224*(1), 133-142. doi:10.1002/path.2856
Havia, M., Kentala, E., & Pyykko, I. (2002). Hearing loss and tinnitus in Meniere's disease. *Auris Nasus Larynx, 29*(2), 115-119.
Haycraft, C. J., Banizs, B., Aydin-Son, Y., Zhang, Q., Michaud, E. J., & Yoder, B. K. (2005). Gli2 and Gli3 localize to cilia and require the intraflagellar transport protein polaris for processing and function. *PLoS Genet, 1*(4), e53. doi:10.1371/journal.pgen.0010053
Heallen, T., Zhang, M., Wang, J., Bonilla-Claudio, M., Klysik, E., Johnson, R. L., & Martin, J. F. (2011). Hippo pathway inhibits Wnt signaling to restrain cardiomyocyte proliferation and heart size. *Science, 332*(6028), 458-461. doi:10.1126/science.1199010
Hearn, T., Renforth, G. L., Spalluto, C., Hanley, N. A., Piper, K., Brickwood, S., . . . Wilson, D. I. (2002). Mutation of ALMS1, a large gene with a tandem repeat encoding 47 amino acids, causes Alstrom syndrome. *Nat Genet, 31*(1), 79-83. doi:10.1038/ng874
Hearn, T., Spalluto, C., Phillips, V. J., Renforth, G. L., Copin, N., Hanley, N. A., & Wilson, D. I. (2005). Subcellular localization of ALMS1 supports involvement of centrosome and basal body dysfunction in the pathogenesis of obesity, insulin resistance, and type 2 diabetes. *Diabetes, 54*(5), 1581-1587.
Heon, E., Kim, G., Qin, S., Garrison, J. E., Tavares, E., Vincent, A., . . . Sheffield, V. C. (2016). Mutations in C8ORF37 cause Bardet Biedl syndrome (BBS21). *Hum Mol Genet*. doi:10.1093/hmg/ddw096
Hervieu, G. (2003). Melanin-concentrating hormone functions in the nervous system: food intake and stress. *Expert Opin Ther Targets, 7*(4), 495-511. doi:10.1517/14728222.7.4.495
Heydet, D., Chen, L. X., Larter, C. Z., Inglis, C., Silverman, M. A., Farrell, G. C., & Leroux, M. R. (2013). A truncating mutation of Alms1 reduces the number of hypothalamic neuronal cilia in obese mice. *Dev Neurobiol, 73*(1), 1-13. doi:10.1002/dneu.22031
Hopp, K., Heyer, C. M., Hommerding, C. J., Henke, S. A., Sundsbak, J. L., Patel, S., . . . Harris, P. C. (2011). B9D1 is revealed as a novel Meckel syndrome (MKS) gene

by targeted exon-enriched next-generation sequencing and deletion analysis. *Hum Mol Genet, 20*(13), 2524-2534. doi:10.1093/hmg/ddr151
Hostelley, T. L., Lodh, S., & Zaghloul, N. A. (2016). Whole organism transcriptome analysis of zebrafish models of Bardet-Biedl Syndrome and Alstrom Syndrome provides mechanistic insight into shared and divergent phenotypes. *BMC Genomics, 17*(1), 318. doi:10.1186/s12864-016-2679-1
Hsiao, Y. C., Tuz, K., & Ferland, R. J. (2012). Trafficking in and to the primary cilium. *Cilia, 1*(1), 4. doi:10.1186/2046-2530-1-4
Huang, P., & Schier, A. F. (2009). Dampened Hedgehog signaling but normal Wnt signaling in zebrafish without cilia. *Development, 136*(18), 3089-3098. doi:10.1242/dev.041343
Huangfu, D., & Anderson, K. V. (2005). Cilia and Hedgehog responsiveness in the mouse. *Proc Natl Acad Sci U S A, 102*(32), 11325-11330. doi:10.1073/pnas.0505328102
Huangfu, D., Liu, A., Rakeman, A. S., Murcia, N. S., Niswander, L., & Anderson, K. V. (2003). Hedgehog signalling in the mouse requires intraflagellar transport proteins. *Nature, 426*(6962), 83-87. doi:10.1038/nature02061
Hudspeth, A. J. (2001). How the ear's works work: mechanoelectrical transduction and amplification by hair cells of the internal ear. *Harvey Lect, 97*, 41-54.
Iannicelli, M., Brancati, F., Mougou-Zerelli, S., Mazzotta, A., Thomas, S., Elkhartoufi, N., . . . Valente, E. M. (2010). Novel TMEM67 mutations and genotype-phenotype correlates in meckelin-related ciliopathies. *Hum Mutat, 31*(5), E1319-1331. doi:10.1002/humu.21239
Ichikawa, K., Shimomura, N., Yamada, M., & Ohkubo, N. (2003). Control of calcium carbonate polymorphism and morphology through biomimetic mineralization by means of nanotechnology. *Chemistry, 9*(14), 3235-3241. doi:10.1002/chem.200204534
Ikeda, A., Naggert, J. K., & Nishina, P. M. (2002). Genetic modification of retinal degeneration in tubby mice. *Exp Eye Res, 74*(4), 455-461. doi:10.1006/exer.2001.1139
Ishikawa, H., Thompson, J., Yates, J. R., 3rd, & Marshall, W. F. (2012). Proteomic analysis of mammalian primary cilia. *Curr Biol, 22*(5), 414-419. doi:10.1016/j.cub.2012.01.031
Izzi, C., Maffei, P., Milan, G., Tardanico, R., Foini, P., Marshall, J., . . . Scolari, F. (2011). The Case mid R: Familial occurrence of retinitis pigmentosa, deafness, and nephropathy. *Kidney Int, 79*(6), 691-692. doi:10.1038/ki.2010.514
Jaffe, K. M., Grimes, D. T., Schottenfeld-Roames, J., Werner, M. E., Ku, T. S., Kim, S. K., . . . Burdine, R. D. (2016). c21orf59/kurly Controls Both Cilia Motility and Polarization. *Cell Rep, 14*(8), 1841-1849. doi:10.1016/j.celrep.2016.01.069
Jagger, D., Collin, G., Kelly, J., Towers, E., Nevill, G., Longo-Guess, C., . . . Forge, A. (2011). Alstrom Syndrome protein ALMS1 localizes to basal bodies of cochlear hair cells and regulates cilium-dependent planar cell polarity. *Hum Mol Genet, 20*(3), 466-481. doi:10.1093/hmg/ddq493
Janssen, S., Ramaswami, G., Davis, E. E., Hurd, T., Airik, R., Kasanuki, J. M., . . . Hildebrandt, F. (2011). Mutation analysis in Bardet-Biedl syndrome by DNA pooling and massively parallel resequencing in 105 individuals. *Hum Genet, 129*(1), 79-90. doi:10.1007/s00439-010-0902-8
Jenkins, D., Seelow, D., Jehee, F. S., Perlyn, C. A., Alonso, L. G., Bueno, D. F., . . . Wilkie, A. O. (2007). RAB23 mutations in Carpenter syndrome imply an unexpected role for hedgehog signaling in cranial-suture development and obesity. *Am J Hum Genet, 80*(6), 1162-1170. doi:10.1086/518047
Jenkins, P. M., Hurd, T. W., Zhang, L., McEwen, D. P., Brown, R. L., Margolis, B., . . . Martens, J. R. (2006). Ciliary targeting of olfactory CNG channels requires the CNGB1b subunit and the kinesin-2 motor protein, KIF17. *Curr Biol, 16*(12), 1211-1216. doi:10.1016/j.cub.2006.04.034
Jenkins, P. M., McEwen, D. P., & Martens, J. R. (2009). Olfactory cilia: linking sensory cilia function and human disease. *Chem Senses, 34*(5), 451-464. doi:10.1093/chemse/bjp020
Jin, H., White, S. R., Shida, T., Schulz, S., Aguiar, M., Gygi, S. P., . . . Nachury, M. V. (2010). The conserved Bardet-Biedl syndrome proteins assemble a coat that traffics membrane proteins to cilia. *Cell, 141*(7), 1208-1219. doi:10.1016/j.cell.2010.05.015

Jones, C., Roper, V. C., Foucher, I., Qian, D., Banizs, B., Petit, C., . . . Chen, P. (2008). Ciliary proteins link basal body polarization to planar cell polarity regulation. *Nat Genet, 40*(1), 69-77. doi:10.1038/ng.2007.54
Katsanis, N., Ansley, S. J., Badano, J. L., Eichers, E. R., Lewis, R. A., Hoskins, B. E., . . . Lupski, J. R. (2001). Triallelic inheritance in Bardet-Biedl syndrome, a Mendelian recessive disorder. *Science, 293*(5538), 2256-2259. doi:10.1126/science.1063525
Kaushik, A. P., Martin, J. A., Zhang, Q., Sheffield, V. C., & Morcuende, J. A. (2009). Cartilage abnormalities associated with defects of chondrocytic primary cilia in Bardet-Biedl syndrome mutant mice. *J Orthop Res, 27*(8), 1093-1099. doi:10.1002/jor.20855
Kennedy, B., & Malicki, J. (2009). What drives cell morphogenesis: a look inside the vertebrate photoreceptor. *Dev Dyn, 238*(9), 2115-2138. doi:10.1002/dvdy.22010
Kermen, F., Franco, L. M., Wyatt, C., & Yaksi, E. (2013). Neural circuits mediating olfactory-driven behavior in fish. *Front Neural Circuits, 7*, 62. doi:10.3389/fncir.2013.00062
Khan, S. A., Muhammad, N., Khan, M. A., Kamal, A., Rehman, Z. U., & Khan, S. (2016). Genetics of human Bardet-Biedl syndrome, an updates. *Clin Genet, 90*(1), 3-15. doi:10.1111/cge.12737
Khodiyar, V. K., Howe, D., Talmud, P. J., Breckenridge, R., & Lovering, R. C. (2013). From zebrafish heart jogging genes to mouse and human orthologs: using Gene Ontology to investigate mammalian heart development. *F1000Res, 2*, 242. doi:10.12688/f1000research.2-242.v2
Kim, J., Krishnaswami, S. R., & Gleeson, J. G. (2008). CEP290 interacts with the centriolar satellite component PCM-1 and is required for Rab8 localization to the primary cilium. *Hum Mol Genet, 17*(23), 3796-3805. doi:10.1093/hmg/ddn277
Kimura, R. S. (1969). Distribution, structure, and function of dark cells in the vestibular labyrinth. *Ann Otol Rhinol Laryngol, 78*(3), 542-561.
Kindt, K. S., Finch, G., & Nicolson, T. (2012). Kinocilia mediate mechanosensitivity in developing zebrafish hair cells. *Dev Cell, 23*(2), 329-341. doi:10.1016/j.devcel.2012.05.022
Kishi, S., Slack, B. E., Uchiyama, J., & Zhdanova, I. V. (2009). Zebrafish as a genetic model in biological and behavioral gerontology: where development meets aging in vertebrates--a mini-review. *Gerontology, 55*(4), 430-441. doi:10.1159/000228892
Knorz, V. J., Spalluto, C., Lessard, M., Purvis, T. L., Adigun, F. F., Collin, G. B., . . . Hearn, T. (2010). Centriolar association of ALMS1 and likely centrosomal functions of the ALMS motif-containing proteins C10orf90 and KIAA1731. *Mol Biol Cell, 21*(21), 3617-3629. doi:10.1091/mbc.E10-03-0246
Kobayashi, D., & Takeda, H. (2012). Ciliary motility: the components and cytoplasmic preassembly mechanisms of the axonemal dyneins. *Differentiation, 83*(2), S23-29. doi:10.1016/j.diff.2011.11.009
Kok, F. O., Shin, M., Ni, C. W., Gupta, A., Grosse, A. S., van Impel, A., . . . Lawson, N. D. (2015). Reverse genetic screening reveals poor correlation between morpholino-induced and mutant phenotypes in zebrafish. *Dev Cell, 32*(1), 97-108. doi:10.1016/j.devcel.2014.11.018
Kramer-Zucker, A. G., Olale, F., Haycraft, C. J., Yoder, B. K., Schier, A. F., & Drummond, I. A. (2005). Cilia-driven fluid flow in the zebrafish pronephros, brain and Kupffer's vesicle is required for normal organogenesis. *Development, 132*(8), 1907-1921. doi:10.1242/dev.01772
Kreiling, J. A., Prabhat, Williams, G., & Creton, R. (2007). Analysis of Kupffer's vesicle in zebrafish embryos using a cave automated virtual environment. *Dev Dyn, 236*(7), 1963-1969. doi:10.1002/dvdy.21191
Kulaga, H. M., Leitch, C. C., Eichers, E. R., Badano, J. L., Lesemann, A., Hoskins, B. E., . . . Katsanis, N. (2004). Loss of BBS proteins causes anosmia in humans and defects in olfactory cilia structure and function in the mouse. *Nat Genet, 36*(9), 994-998. doi:10.1038/ng1418
Lancaster, M. A., Gopal, D. J., Kim, J., Saleem, S. N., Silhavy, J. L., Louie, C. M., . . . Gleeson, J. G. (2011). Defective Wnt-dependent cerebellar midline fusion in a mouse model of Joubert syndrome. *Nat Med, 17*(6), 726-731. doi:10.1038/nm.2380
Leaf, A., & Von Zastrow, M. (2015). Dopamine receptors reveal an essential role of IFT-B, KIF17, and Rab23 in delivering specific receptors to primary cilia. *Elife, 4*. doi:10.7554/eLife.06996

Leightner, A. C., Hommerding, C. J., Peng, Y., Salisbury, J. L., Gainullin, V. G., Czarnecki, P. G., . . . Harris, P. C. (2013). The Meckel syndrome protein meckelin (TMEM67) is a key regulator of cilia function but is not required for tissue planar polarity. *Hum Mol Genet, 22*(10), 2024-2040. doi:10.1093/hmg/ddt054
Leitch, C. C., Zaghloul, N. A., Davis, E. E., Stoetzel, C., Diaz-Font, A., Rix, S., . . . Katsanis, N. (2008). Hypomorphic mutations in syndromic encephalocele genes are associated with Bardet-Biedl syndrome. *Nat Genet, 40*(4), 443-448. doi:10.1038/ng.97
Leventea, E., Hazime, K., Zhao, C., & Malicki, J. (2016). Analysis of cilia structure and function in zebrafish. *Methods Cell Biol, 133*, 179-227. doi:10.1016/bs.mcb.2016.04.016
Li, C., Jensen, V. L., Park, K., Kennedy, J., Garcia-Gonzalo, F. R., Romani, M., . . . Leroux, M. R. (2016). MKS5 and CEP290 Dependent Assembly Pathway of the Ciliary Transition Zone. *PLoS Biol, 14*(3), e1002416. doi:10.1371/journal.pbio.1002416
Li, G., Vega, R., Nelms, K., Gekakis, N., Goodnow, C., McNamara, P., . . . Glynne, R. (2007). A role for Alstrom syndrome protein, alms1, in kidney ciliogenesis and cellular quiescence. *PLoS Genet, 3*(1), e8. doi:10.1371/journal.pgen.0030008
Lim, Y. S., & Tang, B. L. (2015). A role for Rab23 in the trafficking of Kif17 to the primary cilium. *J Cell Sci, 128*(16), 2996-3008. doi:10.1242/jcs.163964
Lodh, S., Hostelley, T. L., Leitch, C. C., O'Hare, E. A., & Zaghloul, N. A. (2016). Differential effects on beta-cell mass by disruption of Bardet-Biedl syndrome or Alstrom syndrome genes. *Hum Mol Genet, 25*(1), 57-68. doi:10.1093/hmg/ddv447
Loktev, A. V., Zhang, Q., Beck, J. S., Searby, C. C., Scheetz, T. E., Bazan, J. F., . . . Nachury, M. V. (2008). A BBSome subunit links ciliogenesis, microtubule stability, and acetylation. *Dev Cell, 15*(6), 854-865. doi:10.1016/j.devcel.2008.11.001
Lopez-Schier, H., & Hudspeth, A. J. (2006). A two-step mechanism underlies the planar polarization of regenerating sensory hair cells. *Proc Natl Acad Sci U S A, 103*(49), 18615-18620. doi:10.1073/pnas.0608536103
Louvi, A., & Grove, E. A. (2011). Cilia in the CNS: the quiet organelle claims center stage. *Neuron, 69*(6), 1046-1060. doi:10.1016/j.neuron.2011.03.002
Louw, J. J., Corveleyn, A., Jia, Y., Iqbal, S., Boshoff, D., Gewillig, M., . . . Devriendt, K. (2014). Homozygous loss-of-function mutation in ALMS1 causes the lethal disorder mitogenic cardiomyopathy in two siblings. *Eur J Med Genet, 57*(9), 532-535. doi:10.1016/j.ejmg.2014.06.004
Lundberg, Y. W., Xu, Y., Thiessen, K. D., & Kramer, K. L. (2015). Mechanisms of otoconia and otolith development. *Dev Dyn, 244*(3), 239-253. doi:10.1002/dvdy.24195
M'Hamdi, O., Redin, C., Stoetzel, C., Ouertani, I., Chaabouni, M., Maazoul, F., . . . Chaabouni, H. (2014). Clinical and genetic characterization of Bardet-Biedl syndrome in Tunisia: defining a strategy for molecular diagnosis. *Clin Genet, 85*(2), 172-177. doi:10.1111/cge.12129
Maffei, P., Munno, V., Marshall, J. D., Scandellari, C., & Sicolo, N. (2002). The Alstrom syndrome: is it a rare or unknown disease? *Ann Ital Med Int, 17*(4), 221-228.
Malicki, J., & Avidor-Reiss, T. (2014). From the cytoplasm into the cilium: bon voyage. *Organogenesis, 10*(1), 138-157. doi:10.4161/org.29055
Malicki, J., Neuhauss, S. C., Schier, A. F., Solnica-Krezel, L., Stemple, D. L., Stainier, D. Y., . . . Driever, W. (1996). Mutations affecting development of the zebrafish retina. *Development, 123*, 263-273.
Malicki, J., Pooranachandran, N., Nikolaev, A., Fang, X., & Avanesov, A. (2016). Analysis of the retina in the zebrafish model. *Methods Cell Biol, 134*, 257-334. doi:10.1016/bs.mcb.2016.04.017
Marshall, J. D., Beck, S., Maffei, P., & Naggert, J. K. (2007). Alstrom syndrome. *Eur J Hum Genet, 15*(12), 1193-1202. doi:10.1038/sj.ejhg.5201933
Marshall, J. D., Maffei, P., Collin, G. B., & Naggert, J. K. (2011). Alstrom syndrome: genetics and clinical overview. *Curr Genomics, 12*(3), 225-235. doi:10.2174/138920211795677912
Marshall, J. D., Muller, J., Collin, G. B., Milan, G., Kingsmore, S. F., Dinwiddie, D., . . . Naggert, J. K. (2015). Alstrom Syndrome: Mutation Spectrum of ALMS1. *Hum Mutat, 36*(7), 660-668. doi:10.1002/humu.22796

Marshall, W. F., Vucica, Y., & Rosenbaum, J. L. (2001). Kinetics and regulation of de novo centriole assembly. Implications for the mechanism of centriole duplication. *Curr Biol, 11*(5), 308-317.
Marszalek, J. R., Ruiz-Lozano, P., Roberts, E., Chien, K. R., & Goldstein, L. S. (1999). Situs inversus and embryonic ciliary morphogenesis defects in mouse mutants lacking the KIF3A subunit of kinesin-II. *Proc Natl Acad Sci U S A, 96*(9), 5043-5048.
Matsui, T., Ishikawa, H., & Bessho, Y. (2015). Cell collectivity regulation within migrating cell cluster during Kupffer's vesicle formation in zebrafish. *Front Cell Dev Biol, 3*, 27. doi:10.3389/fcell.2015.00027
May-Simera, H., & Kelley, M. W. (2012). Planar cell polarity in the inner ear. *Curr Top Dev Biol, 101*, 111-140. doi:10.1016/B978-0-12-394592-1.00006-5
May-Simera, H. L., Kai, M., Hernandez, V., Osborn, D. P., Tada, M., & Beales, P. L. (2010). Bbs8, together with the planar cell polarity protein Vangl2, is required to establish left-right asymmetry in zebrafish. *Dev Biol, 345*(2), 215-225. doi:10.1016/j.ydbio.2010.07.013
May-Simera, H. L., & Kelley, M. W. (2012). Cilia, Wnt signaling, and the cytoskeleton. *Cilia, 1*(1), 7. doi:10.1186/2046-2530-1-7
McEwen, D. P., Koenekoop, R. K., Khanna, H., Jenkins, P. M., Lopez, I., Swaroop, A., & Martens, J. R. (2007). Hypomorphic CEP290/NPHP6 mutations result in anosmia caused by the selective loss of G proteins in cilia of olfactory sensory neurons. *Proc Natl Acad Sci U S A, 104*(40), 15917-15922. doi:10.1073/pnas.0704140104
Menotti-Raymond, M., David, V. A., Schaffer, A. A., Stephens, R., Wells, D., Kumar-Singh, R., . . . Narfstrom, K. (2007). Mutation in CEP290 discovered for cat model of human retinal degeneration. *J Hered, 98*(3), 211-220. doi:10.1093/jhered/esm019
Miesfeld, J. B., & Link, B. A. (2014). Establishment of transgenic lines to monitor and manipulate Yap/Taz-Tead activity in zebrafish reveals both evolutionarily conserved and divergent functions of the Hippo pathway. *Mech Dev, 133*, 177-188. doi:10.1016/j.mod.2014.02.003
Mihai, C. M., Marshall, J. D., & Stoicescu, R. M. (2011). Bardet-Biedl syndrome with end-stage kidney disease in a four-year-old Romanian boy: a case report. *J Med Case Rep, 5*, 378. doi:10.1186/1752-1947-5-378
Mitchison, T., Wuhr, M., Nguyen, P., Ishihara, K., Groen, A., & Field, C. M. (2012). Growth, interaction, and positioning of microtubule asters in extremely large vertebrate embryo cells. *Cytoskeleton (Hoboken), 69*(10), 738-750. doi:10.1002/cm.21050
Mombaerts, P. (1999). Molecular biology of odorant receptors in vertebrates. *Annu Rev Neurosci, 22*, 487-509. doi:10.1146/annurev.neuro.22.1.487
Moore, S. J., Green, J. S., Fan, Y., Bhogal, A. K., Dicks, E., Fernandez, B. A., . . . Parfrey, P. S. (2005). Clinical and genetic epidemiology of Bardet-Biedl syndrome in Newfoundland: a 22-year prospective, population-based, cohort study. *Am J Med Genet A, 132A*(4), 352-360. doi:10.1002/ajmg.a.30406
Mukhopadhyay, S., Wen, X., Chih, B., Nelson, C. D., Lane, W. S., Scales, S. J., & Jackson, P. K. (2010). TULP3 bridges the IFT-A complex and membrane phosphoinositides to promote trafficking of G protein-coupled receptors into primary cilia. *Genes Dev, 24*(19), 2180-2193. doi:10.1101/gad.1966210
Mykytyn, K., Mullins, R. F., Andrews, M., Chiang, A. P., Swiderski, R. E., Yang, B., . . . Sheffield, V. C. (2004). Bardet-Biedl syndrome type 4 (BBS4)-null mice implicate Bbs4 in flagella formation but not global cilia assembly. *Proc Natl Acad Sci U S A, 101*(23), 8664-8669. doi:10.1073/pnas.0402354101
Mykytyn, K., Nishimura, D. Y., Searby, C. C., Shastri, M., Yen, H. J., Beck, J. S., . . . Sheffield, V. C. (2002). Identification of the gene (BBS1) most commonly involved in Bardet-Biedl syndrome, a complex human obesity syndrome. *Nat Genet, 31*(4), 435-438. doi:10.1038/ng935
Nachury, M. V., Loktev, A. V., Zhang, Q., Westlake, C. J., Peranen, J., Merdes, A., . . . Jackson, P. K. (2007). A core complex of BBS proteins cooperates with the GTPase Rab8 to promote ciliary membrane biogenesis. *Cell, 129*(6), 1201-1213. doi:10.1016/j.cell.2007.03.053
Nachury, M. V., Seeley, E. S., & Jin, H. (2010). Trafficking to the ciliary membrane: how to get across the periciliary diffusion barrier? *Annu Rev Cell Dev Biol, 26*, 59-87. doi:10.1146/annurev.cellbio.042308.113337

Nakayama, K., & Loomis, J. M. (1974). Optical velocity patterns, velocity-sensitive neurons, and space perception: a hypothesis. *Perception, 3*(1), 63-80.
Nasevicius, A., & Ekker, S. C. (2000). Effective targeted gene 'knockdown' in zebrafish. *Nat Genet, 26*(2), 216-220. doi:10.1038/79951
Nguyen, D., & Xu, T. (2008). The expanding role of mouse genetics for understanding human biology and disease. *Dis Model Mech, 1*(1), 56-66. doi:10.1242/dmm.000232
Nicolson, T., Rusch, A., Friedrich, R. W., Granato, M., Ruppersberg, J. P., & Nusslein-Volhard, C. (1998). Genetic analysis of vertebrate sensory hair cell mechanosensation: the zebrafish circler mutants. *Neuron, 20*(2), 271-283.
Nishimura, D. Y., Fath, M., Mullins, R. F., Searby, C., Andrews, M., Davis, R., . . . Sheffield, V. C. (2004). Bbs2-null mice have neurosensory deficits, a defect in social dominance, and retinopathy associated with mislocalization of rhodopsin. *Proc Natl Acad Sci U S A, 101*(47), 16588-16593. doi:10.1073/pnas.0405496101
Nonaka, S., Tanaka, Y., Okada, Y., Takeda, S., Harada, A., Kanai, Y., . . . Hirokawa, N. (1998). Randomization of left-right asymmetry due to loss of nodal cilia generating leftward flow of extraembryonic fluid in mice lacking KIF3B motor protein. *Cell, 95*(6), 829-837.
Norris, D. P., & Grimes, D. T. (2012). Mouse models of ciliopathies: the state of the art. *Dis Model Mech, 5*(3), 299-312. doi:10.1242/dmm.009340
Novarino, G., Akizu, N., & Gleeson, J. G. (2011). Modeling human disease in humans: the ciliopathies. *Cell, 147*(1), 70-79. doi:10.1016/j.cell.2011.09.014
Ocbina, P. J., Tuson, M., & Anderson, K. V. (2009). Primary cilia are not required for normal canonical Wnt signaling in the mouse embryo. *PLoS One, 4*(8), e6839. doi:10.1371/journal.pone.0006839
Ohlemiller, K. K., Hughes, R. M., Mosinger-Ogilvie, J., Speck, J. D., Grosof, D. H., & Silverman, M. S. (1995). Cochlear and retinal degeneration in the tubby mouse. *Neuroreport, 6*(6), 845-849.
Olkkonen, V. M., & Stenmark, H. (1997). Role of Rab GTPases in membrane traffic. *Int Rev Cytol, 176*, 1-85.
Olsen, O., Funke, L., Long, J. F., Fukata, M., Kazuta, T., Trinidad, J. C., . . . Bredt, D. S. (2007). Renal defects associated with improper polarization of the CRB and DLG polarity complexes in MALS-3 knockout mice. *J Cell Biol, 179*(1), 151-164. doi:10.1083/jcb.200702054
Oteiza, P., Koppen, M., Krieg, M., Pulgar, E., Farias, C., Melo, C., . . . Concha, M. L. (2010). Planar cell polarity signalling regulates cell adhesion properties in progenitors of the zebrafish laterality organ. *Development, 137*(20), 3459-3468. doi:10.1242/dev.049981
Pan, D. (2010). The hippo signaling pathway in development and cancer. *Dev Cell, 19*(4), 491-505. doi:10.1016/j.devcel.2010.09.011
Panizzi, J. R., Becker-Heck, A., Castleman, V. H., Al-Mutairi, D. A., Liu, Y., Loges, N. T., . . . Drummond, I. A. (2012). CCDC103 mutations cause primary ciliary dyskinesia by disrupting assembly of ciliary dynein arms. *Nat Genet, 44*(6), 714-719. doi:10.1038/ng.2277
Parelkar, S. V., Kapadnis, S. P., Sanghvi, B. V., Joshi, P. B., Mundada, D., & Oak, S. N. (2013). Meckel-Gruber syndrome: A rare and lethal anomaly with review of literature. *J Pediatr Neurosci, 8*(2), 154-157. doi:10.4103/1817-1745.117855
Park, P. S. (2014). Constitutively active rhodopsin and retinal disease. *Adv Pharmacol, 70*, 1-36. doi:10.1016/B978-0-12-417197-8.00001-8
Park, S. M., Park, S. W., Casaclang-Verzosa, G., Ommen, S. R., Pellikka, P. A., Miller, F. A., Jr., . . . Oh, J. K. (2009). Diastolic dysfunction and left atrial enlargement as contributing factors to functional mitral regurgitation in dilated cardiomyopathy: data from the Acorn trial. *Am Heart J, 157*(4), 762 e763-710. doi:10.1016/j.ahj.2008.12.018
Park, T. J., Mitchell, B. J., Abitua, P. B., Kintner, C., & Wallingford, J. B. (2008). Dishevelled controls apical docking and planar polarization of basal bodies in ciliated epithelial cells. *Nat Genet, 40*(7), 871-879. doi:10.1038/ng.104
Pedersen, L. B., & Akhmanova, A. (2014). Kif7 keeps cilia tips in shape. *Nat Cell Biol, 16*(7), 623-625. doi:10.1038/ncb2997
Pooranachandran, N., & Malicki, J. J. (2016). Unexpected Roles for Ciliary Kinesins and Intraflagellar Transport Proteins. *Genetics, 203*(2), 771-785. doi:10.1534/genetics.115.180943

Putoux, A., Attie-Bitach, T., Martinovic, J., & Gubler, M. C. (2012). Phenotypic variability of Bardet-Biedl syndrome: focusing on the kidney. *Pediatr Nephrol, 27*(1), 7-15. doi:10.1007/s00467-010-1751-3
Rachel, R. A., May-Simera, H. L., Veleri, S., Gotoh, N., Choi, B. Y., Murga-Zamalloa, C., . . . Swaroop, A. (2012). Combining Cep290 and Mkks ciliopathy alleles in mice rescues sensory defects and restores ciliogenesis. *J Clin Invest, 122*(4), 1233-1245. doi:10.1172/JCI60981
Rachel, R. A., Yamamoto, E. A., Dewanjee, M. K., May-Simera, H. L., Sergeev, Y. V., Hackett, A. N., . . . Swaroop, A. (2015). CEP290 alleles in mice disrupt tissue-specific cilia biogenesis and recapitulate features of syndromic ciliopathies. *Hum Mol Genet, 24*(13), 3775-3791. doi:10.1093/hmg/ddv123
Ramirez, N., Marrero, L., Carlo, S., & Cornier, A. S. (2004). Orthopaedic manifestations of Bardet-Biedl syndrome. *J Pediatr Orthop, 24*(1), 92-96.
Robinson, B. S., Huang, J., Hong, Y., & Moberg, K. H. (2010). Crumbs regulates Salvador/Warts/Hippo signaling in Drosophila via the FERM-domain protein Expanded. *Curr Biol, 20*(7), 582-590. doi:10.1016/j.cub.2010.03.019
Rohatgi, R., Milenkovic, L., & Scott, M. P. (2007). Patched1 regulates hedgehog signaling at the primary cilium. *Science, 317*(5836), 372-376. doi:10.1126/science.1139740
Rosenbaum, J. (2002). Intraflagellar transport. *Curr Biol, 12*(4), R125.
Ross, A. J., May-Simera, H., Eichers, E. R., Kai, M., Hill, J., Jagger, D. J., . . . Beales, P. L. (2005). Disruption of Bardet-Biedl syndrome ciliary proteins perturbs planar cell polarity in vertebrates. *Nat Genet, 37*(10), 1135-1140. doi:10.1038/ng1644
Rothschild, S. C., Lahvic, J., Francescatto, L., McLeod, J. J., Burgess, S. M., & Tombes, R. M. (2013). CaMK-II activation is essential for zebrafish inner ear development and acts through Delta-Notch signaling. *Dev Biol, 381*(1), 179-188. doi:10.1016/j.ydbio.2013.05.028
Sang, L., Miller, J. J., Corbit, K. C., Giles, R. H., Brauer, M. J., Otto, E. A., . . . Jackson, P. K. (2011). Mapping the NPHP-JBTS-MKS protein network reveals ciliopathy disease genes and pathways. *Cell, 145*(4), 513-528. doi:10.1016/j.cell.2011.04.019
Santagata, S., Boggon, T. J., Baird, C. L., Gomez, C. A., Zhao, J., Shan, W. S., . . . Shapiro, L. (2001). G-protein signaling through tubby proteins. *Science, 292*(5524), 2041-2050. doi:10.1126/science.1061233
Saraiva, L. R., Ahuja, G., Ivandic, I., Syed, A. S., Marioni, J. C., Korsching, S. I., & Logan, D. W. (2015). Molecular and neuronal homology between the olfactory systems of zebrafish and mouse. *Sci Rep, 5*, 11487. doi:10.1038/srep11487
Scholey, J. M. (2012). Kinesin-2 motors transport IFT-particles, dyneins and tubulin subunits to the tips of Caenorhabditis elegans sensory cilia: relevance to vision research? *Vision Res, 75*, 44-52. doi:10.1016/j.visres.2012.06.015
Schou, K. B., Pedersen, L. B., & Christensen, S. T. (2015). Ins and outs of GPCR signaling in primary cilia. *EMBO Rep, 16*(9), 1099-1113. doi:10.15252/embr.201540530
Schouteden, C., Serwas, D., Palfy, M., & Dammermann, A. (2015). The ciliary transition zone functions in cell adhesion but is dispensable for axoneme assembly in C. elegans. *J Cell Biol, 210*(1), 35-44. doi:10.1083/jcb.201501013
Schulte-Merker, S., & Stainier, D. Y. (2014). Out with the old, in with the new: reassessing morpholino knockdowns in light of genome editing technology. *Development, 141*(16), 3103-3104. doi:10.1242/dev.112003
Sheffield, V. C. (2010). The blind leading the obese: the molecular pathophysiology of a human obesity syndrome. *Trans Am Clin Climatol Assoc, 121*, 172-181; discussion 181-172.
Shenje, L. T., Andersen, P., Halushka, M. K., Lui, C., Fernandez, L., Collin, G. B., . . . Judge, D. P. (2014). Mutations in Alstrom protein impair terminal differentiation of cardiomyocytes. *Nat Commun, 5*, 3416. doi:10.1038/ncomms4416
Shetty, B. P., Alva, N., Patil, S., & Shetty, R. (2012). Meckel-Gruber syndrome (dysencephalia splanchnocystica). *J Contemp Dent Pract, 13*(5), 713-715.
Shiri-Sverdlov, R., Custers, A., van Vliet-Ostaptchouk, J. V., van Gorp, P. J., Lindsey, P. J., van Tilburg, J. H., . . . Wijmenga, C. (2006). Identification of TUB as a novel candidate gene influencing body weight in humans. *Diabetes, 55*(2), 385-389.
Singla, V., & Reiter, J. F. (2006). The primary cilium as the cell's antenna: signaling at a sensory organelle. *Science, 313*(5787), 629-633. doi:10.1126/science.1124534
Smith, A. C., Heo, W. D., Braun, V., Jiang, X., Macrae, C., Casanova, J. E., . . . Brumell, J. H. (2007). A network of Rab GTPases controls phagosome maturation and is

modulated by Salmonella enterica serovar Typhimurium. *J Cell Biol, 176*(3), 263-268. doi:10.1083/jcb.200611056
Sollner, C., Burghammer, M., Busch-Nentwich, E., Berger, J., Schwarz, H., Riekel, C., & Nicolson, T. (2003). Control of crystal size and lattice formation by starmaker in otolith biomineralization. *Science, 302*(5643), 282-286. doi:10.1126/science.1088443
Stooke-Vaughan, G. A., Huang, P., Hammond, K. L., Schier, A. F., & Whitfield, T. T. (2012). The role of hair cells, cilia and ciliary motility in otolith formation in the zebrafish otic vesicle. *Development, 139*(10), 1777-1787. doi:10.1242/dev.079947
Stooke-Vaughan, G. A., Obholzer, N. D., Baxendale, S., Megason, S. G., & Whitfield, T. T. (2015). Otolith tethering in the zebrafish otic vesicle requires Otogelin and alpha-Tectorin. *Development, 142*(6), 1137-1145. doi:10.1242/dev.116632
Stowe, T. R., Wilkinson, C. J., Iqbal, A., & Stearns, T. (2012). The centriolar satellite proteins Cep72 and Cep290 interact and are required for recruitment of BBS proteins to the cilium. *Mol Biol Cell, 23*(17), 3322-3335. doi:10.1091/mbc.E12-02-0134
Su, X., Driscoll, K., Yao, G., Raed, A., Wu, M., Beales, P. L., & Zhou, J. (2014). Bardet-Biedl syndrome proteins 1 and 3 regulate the ciliary trafficking of polycystic kidney disease 1 protein. *Hum Mol Genet, 23*(20), 5441-5451. doi:10.1093/hmg/ddu267
Sun, X., Haley, J., Bulgakov, O. V., Cai, X., McGinnis, J., & Li, T. (2012). Tubby is required for trafficking G protein-coupled receptors to neuronal cilia. *Cilia, 1*(1), 21. doi:10.1186/2046-2530-1-21
Sun, Z., Amsterdam, A., Pazour, G. J., Cole, D. G., Miller, M. S., & Hopkins, N. (2004). A genetic screen in zebrafish identifies cilia genes as a principal cause of cystic kidney. *Development, 131*(16), 4085-4093. doi:10.1242/dev.01240
Sung, C. H., & Leroux, M. R. (2013). The roles of evolutionarily conserved functional modules in cilia-related trafficking. *Nat Cell Biol, 15*(12), 1387-1397. doi:10.1038/ncb2888
Szymanska, K., Hartill, V. L., & Johnson, C. A. (2014). Unraveling the genetics of Joubert and Meckel-Gruber syndromes. *J Pediatr Genet, 3*(2), 65-78. doi:10.3233/PGE-14090
Szymanska, K., & Johnson, C. A. (2012). The transition zone: an essential functional compartment of cilia. *Cilia, 1*(1), 10. doi:10.1186/2046-2530-1-10
Tanimoto, M., Ota, Y., Inoue, M., & Oda, Y. (2011). Origin of inner ear hair cells: morphological and functional differentiation from ciliary cells into hair cells in zebrafish inner ear. *J Neurosci, 31*(10), 3784-3794. doi:10.1523/JNEUROSCI.5554-10.2011
Tappeiner, C., Balmer, J., Iglicki, M., Schuerch, K., Jazwinska, A., Enzmann, V., & Tschopp, M. (2013). Characteristics of rod regeneration in a novel zebrafish retinal degeneration model using N-methyl-N-nitrosourea (MNU). *PLoS One, 8*(8), e71064. doi:10.1371/journal.pone.0071064
Tayeh, M. K., Yen, H. J., Beck, J. S., Searby, C. C., Westfall, T. A., Griesbach, H., . . . Slusarski, D. C. (2008). Genetic interaction between Bardet-Biedl syndrome genes and implications for limb patterning. *Hum Mol Genet, 17*(13), 1956-1967. doi:10.1093/hmg/ddn093
Tissir, F., & Goffinet, A. M. (2010). Planar cell polarity signaling in neural development. *Curr Opin Neurobiol, 20*(5), 572-577. doi:10.1016/j.conb.2010.05.006
Tobin, J. L., Di Franco, M., Eichers, E., May-Simera, H., Garcia, M., Yan, J., . . . Beales, P. L. (2008). Inhibition of neural crest migration underlies craniofacial dysmorphology and Hirschsprung's disease in Bardet-Biedl syndrome. *Proc Natl Acad Sci U S A, 105*(18), 6714-6719. doi:10.1073/pnas.0707057105
Tsujikawa, M., & Malicki, J. (2004). Intraflagellar transport genes are essential for differentiation and survival of vertebrate sensory neurons. *Neuron, 42*(5), 703-716.
van Vliet-Ostaptchouk, J. V., Onland-Moret, N. C., Shiri-Sverdlov, R., van Gorp, P. J., Custers, A., Peeters, P. H., . . . van der Schouw, Y. T. (2008). Polymorphisms of the TUB gene are associated with body composition and eating behavior in middle-aged women. *PLoS One, 3*(1), e1405. doi:10.1371/journal.pone.0001405
Varshney, G. K., Pei, W., LaFave, M. C., Idol, J., Xu, L., Gallardo, V., . . . Burgess, S. M. (2015). High-throughput gene targeting and phenotyping in zebrafish using CRISPR/Cas9. *Genome Res, 25*(7), 1030-1042. doi:10.1101/gr.186379.114

Veleri, S., Bishop, K., Dalle Nogare, D. E., English, M. A., Foskett, T. J., Chitnis, A., . . . Swaroop, A. (2012). Knockdown of Bardet-Biedl syndrome gene BBS9/PTHB1 leads to cilia defects. *PLoS One, 7*(3), e34389. doi:10.1371/journal.pone.0034389

Vierkotten, J., Dildrop, R., Peters, T., Wang, B., & Ruther, U. (2007). Ftm is a novel basal body protein of cilia involved in Shh signalling. *Development, 134*(14), 2569-2577. doi:10.1242/dev.003715

Wallingford, J. B., & Mitchell, B. (2011). Strange as it may seem: the many links between Wnt signaling, planar cell polarity, and cilia. *Genes Dev, 25*(3), 201-213. doi:10.1101/gad.2008011

Waters, A. M., & Beales, P. L. (2011). Ciliopathies: an expanding disease spectrum. *Pediatr Nephrol, 26*(7), 1039-1056. doi:10.1007/s00467-010-1731-7

Weatherbee, S. D., Niswander, L. A., & Anderson, K. V. (2009). A mouse model for Meckel syndrome reveals Mks1 is required for ciliogenesis and Hedgehog signaling. *Hum Mol Genet, 18*(23), 4565-4575. doi:10.1093/hmg/ddp422

Wei, Q., Zhang, Y., Li, Y., Zhang, Q., Ling, K., & Hu, J. (2012). The BBSome controls IFT assembly and turnaround in cilia. *Nat Cell Biol, 14*(9), 950-957. doi:10.1038/ncb2560

Whitfield, T. T., Granato, M., van Eeden, F. J., Schach, U., Brand, M., Furutani-Seiki, M., . . . Nusslein-Volhard, C. (1996). Mutations affecting development of the zebrafish inner ear and lateral line. *Development, 123*, 241-254.

Wood, C. R., Huang, K., Diener, D. R., & Rosenbaum, J. L. (2013). The cilium secretes bioactive ectosomes. *Curr Biol, 23*(10), 906-911. doi:10.1016/j.cub.2013.04.019

Yang, T. T., Su, J., Wang, W. J., Craige, B., Witman, G. B., Tsou, M. F., & Liao, J. C. (2015). Superresolution Pattern Recognition Reveals the Architectural Map of the Ciliary Transition Zone. *Sci Rep, 5*, 14096. doi:10.1038/srep14096

Yen, H. J., Tayeh, M. K., Mullins, R. F., Stone, E. M., Sheffield, V. C., & Slusarski, D. C. (2006). Bardet-Biedl syndrome genes are important in retrograde intracellular trafficking and Kupffer's vesicle cilia function. *Hum Mol Genet, 15*(5), 667-677. doi:10.1093/hmg/ddi468

Yu, F. X., Zhao, B., & Guan, K. L. (2015). Hippo Pathway in Organ Size Control, Tissue Homeostasis, and Cancer. *Cell, 163*(4), 811-828. doi:10.1016/j.cell.2015.10.044

Yu, X., Lau, D., Ng, C. P., & Roy, S. (2011). Cilia-driven fluid flow as an epigenetic cue for otolith biomineralization on sensory hair cells of the inner ear. *Development, 138*(3), 487-494. doi:10.1242/dev.057752

Yuan, S., Zhao, L., Brueckner, M., & Sun, Z. (2015). Intraciliary calcium oscillations initiate vertebrate left-right asymmetry. *Curr Biol, 25*(5), 556-567. doi:10.1016/j.cub.2014.12.051

Zaghloul, N. A., & Katsanis, N. (2009). Mechanistic insights into Bardet-Biedl syndrome, a model ciliopathy. *J Clin Invest, 119*(3), 428-437. doi:10.1172/JCI37041

Zaghloul, N. A., Liu, Y., Gerdes, J. M., Gascue, C., Oh, E. C., Leitch, C. C., . . . Katsanis, N. (2010). Functional analyses of variants reveal a significant role for dominant negative and common alleles in oligogenic Bardet-Biedl syndrome. *Proc Natl Acad Sci U S A, 107*(23), 10602-10607. doi:10.1073/pnas.1000219107

Zhang, Q., Nishimura, D., Vogel, T., Shao, J., Swiderski, R., Yin, T., . . . Sheffield, V. C. (2013). BBS7 is required for BBSome formation and its absence in mice results in Bardet-Biedl syndrome phenotypes and selective abnormalities in membrane protein trafficking. *J Cell Sci, 126*(Pt 11), 2372-2380. doi:10.1242/jcs.111740

Zhang, Q., Yu, D., Seo, S., Stone, E. M., & Sheffield, V. C. (2012). Intrinsic protein-protein interaction-mediated and chaperonin-assisted sequential assembly of stable bardet-biedl syndrome protein complex, the BBSome. *J Biol Chem, 287*(24), 20625-20635. doi:10.1074/jbc.M112.341487

Zhao, C., & Malicki, J. (2007). Genetic defects of pronephric cilia in zebrafish. *Mech Dev, 124*(7-8), 605-616. doi:10.1016/j.mod.2007.04.004

Zhao, C., & Malicki, J. (2011). Nephrocystins and MKS proteins interact with IFT particle and facilitate transport of selected ciliary cargos. *EMBO J, 30*(13), 2532-2544. doi:10.1038/emboj.2011.165

Zhao, C., Omori, Y., Brodowska, K., Kovach, P., & Malicki, J. (2012). Kinesin-2 family in vertebrate ciliogenesis. *Proc Natl Acad Sci U S A, 109*(7), 2388-2393. doi:10.1073/pnas.1116035109

Zhou, Q., Li, L., Zhao, B., & Guan, K. L. (2015). The hippo pathway in heart development, regeneration, and diseases. *Circ Res, 116*(8), 1431-1447. doi:10.1161/CIRCRESAHA.116.303311

Zilber, Y., Babayeva, S., Seo, J. H., Liu, J. J., Mootin, S., & Torban, E. (2013). The PCP effector Fuzzy controls cilial assembly and signaling by recruiting Rab8 and Dishevelled to the primary cilium. *Mol Biol Cell, 24*(5), 555-565. doi:10.1091/mbc.E12-06-0437

Zimmerman, K., & Yoder, B. K. (2015). SnapShot: Sensing and Signaling by Cilia. *Cell, 161*(3), 692-692 e691. doi:10.1016/j.cell.2015.04.015